Schweizerische Eidgenossenschaft
Confédération suisse
Confederazione Svizzera
Confederaziun svizra

Federal Department of the Environment,
Transport, Energy and Communications DETEC

Swiss Federal Office of Energy
Energy Research and Cleantech

Final report from 8 June 2026

ADCAP

Demonstrator for carbon capture from flue gas and exhaust gas streams using solid adsorbents



Source: Demonstrator Pilot Plant Unit, EPFL

Publisher:
Swiss Federal Office of Energy SFOE
Energy Research and Cleantech
CH-3003 Berne
www.energy-research.ch

Co-financing:
Canton of Valais
Place St-Théodule 15, 1951 Sion
https://www.vs.ch

Subsidy recipients:
EPFL Valais-Wallis c/o EPFL
Bâtiment CE 3.316, Station 1
1015 Lausanne

HES-SO Valais Wallis. School of Engineering
Rue de l'Industrie 23
1950 Sion

Casale SA
Via G. Pocobelli 6
6900 Lugano

GAZNAT SA
Av. Général-Guisan 28
1800 Vevey

Authors:
Prof. Dr. Wendy Lee Queen, EPFL, wendy.queen@epfl.ch
Dr. Jordi Espin Marti, jordiespinmarti@gmail.com
Dr. Anita Justin, anita.justin@kaust.edu.sa
Dr. Mehrdad Asgari, ma2000@cam.ac.uk
Sanjay Venkatachalam, EPFL, sanjay.venkatachalam@epfl.ch
Pratap Narayan Soni. EPFL, pratap.soni@epfl.ch
Anne Belin, EPFL, anne.belin@epfl.ch

SFOE project coordinators:
Men Wirz, Men.Wirz@bfe.admin.ch
Elena-Lavinia Niederhäuser, elena-lavinia.niederhaeuser@bfe.admin.ch

SFOE contract number: SI/502432-01

The authors bear the entire responsibility for the content of this report and for the conclusions drawn therefrom.

Summary

Over the past decades, rising CO_2 emissions have become a major societal concern due to the adverse effects of increasing atmospheric greenhouse gas concentrations on the environment, motivating the development of large-scale carbon capture technologies. The most mature capture systems to date are liquid amine–based scrubbers; however, despite their proven performance, CO_2 capture with liquid alkanolamines remains highly energy intensive, typically requiring ≥ 4 MJ per kilogram of CO_2 captured.[1,2] This high energy penalty has constrained large-scale deployment and has driven growing interest in alternative capture approaches. In this context, solid adsorbents have emerged as promising candidates owing to their lower heat capacities and potential for substantially reduced regeneration energy.

The objective of this project was to demonstrate adsorption-based CO_2 capture using solid adsorbents at the kilogram scale and to identify the optimal combination of adsorbent and process configuration that minimizes energy demand and capture cost while maintaining high separation performance. It was hypothesized that, through appropriate material selection and process optimization, energy consumption could be reduced below 1 MJ kg^{-1} CO_2 while sustaining CO_2 productivities above 200 kg CO_2 m^{-3} h^{-1}, thereby enabling meaningful reductions in both the fixed and variable costs of carbon capture plants. To achieve this, an integrated framework combining dynamic process modelling, pilot-scale validation, techno-economic analysis, and life-cycle assessment was developed and applied over the course of the project.

A range of solid adsorbents, including zeolites, silicas, and metal–organic frameworks, with and without amine functionalization, were developed, scaled, and evaluated. In parallel, a dedicated pilot plant was designed and commissioned to operate under gas compositions and temperatures representative of industrial exhaust streams, enabling systematic assessment of key performance indicators such as CO_2 purity, recovery, productivity, and energy consumption. Dynamic process models were developed and validated against experimental breakthrough data, providing confidence for extrapolation to industrial-scale scenarios. Among the process configurations investigated, temperature–vacuum swing adsorption consistently emerged as the most favorable, achieving CO_2 purities exceeding 95 percent and recoveries around or above 90 percent at industrially relevant scales.

For zeolite 13X, industrial-scale simulations yielded capture costs of approximately 50 CHF t^{-1} CO_2 under dry flue-gas conditions with full waste-heat integration. When humid flue gas and pre-drying requirements were considered, capture costs increased moderately to approximately 60 CHF t^{-1} CO_2, while reduced waste-heat availability increased costs further to around 70–75 CHF t^{-1} CO_2, indicating competitiveness with state-of-the-art solvent-based capture technologies. In parallel, amine-functionalized composite adsorbents based on KIT-6 silica and MIL-101(Cr) metal–organic frameworks were successfully developed and scaled, and their integration into optimized adsorption cycles demonstrated that high purity and recovery can be achieved with energy consumptions meeting DOE-relevant targets. Life-cycle assessment revealed that, while adsorption-based capture offers favorable operational environmental performance, adsorbent synthesis, particularly solvent-intensive processing steps for MOF-based systems, dominates the overall environmental footprint. However, solvent recovery and alternative drying strategies can reduce the carbon footprint by up to approximately 80 percent, highlighting clear pathways toward environmentally competitive material production.

The influence of flue-gas humidity was explicitly examined, showing that pre-drying introduces a moderate but manageable cost penalty without undermining the overall viability of adsorption-based capture. Overall, the results indicate that adsorption-based CO_2 capture, and temperature–vacuum swing adsorption in particular, can reach a level of technical, energetic, environmental, and economic maturity that supports progression toward integrated demonstration and large-scale deployment.

The immediate priorities for progression are tonne-scale production of advanced adsorbents in collaboration with industrial manufacturers and integrated demonstration at a Swiss municipal solid waste incineration facility, where favourable flue gas composition and available waste heat provide the most competitive conditions. Most importantly, confirmation of long-term sorbent durability under realistic flue gas conditions - including humidity, SO_x, and NO_x - remains the key outstanding technical challenge to be addressed before large-scale deployment. Beyond incineration, the modular nature of the technology supports adaptation to other hard-to-abate sectors including cement, steel, and the chemical industry, directly contributing to Switzerland's target of capturing 12 million tonnes of CO_2 per year by 2050. The detailed steps, milestones, and industrial partnerships required to bring the technology from its current development stage to market readiness are outlined in the Technology Roadmap (Section 6.3).

Zusammenfassung

In den vergangenen Jahrzehnten sind steigende CO_2-Emissionen aufgrund der nachteiligen Auswirkungen zunehmender atmosphärischer Treibhausgaskonzentrationen auf die Umwelt zu einer zentralen gesellschaftlichen Herausforderung geworden. Dies hat die Entwicklung großskaliger Technologien zur CO_2-Abscheidung vorangetrieben. Die bislang technologisch am weitesten entwickelten Abscheidesysteme sind flüssige, aminhaltige Wäscher. Trotz ihrer nachgewiesenen Leistungsfähigkeit ist die CO_2-Abscheidung mit flüssigen Alkanolaminen jedoch mit einem sehr hohen Energiebedarf verbunden und erfordert typischerweise ≥ 4 MJ pro Kilogramm abgeschiedenem CO_2 für die Regeneration.[1,2] Diese hohe energetische Belastung hat den großtechnischen Einsatz eingeschränkt und das wachsende Interesse an alternativen Abscheidekonzepten gefördert. Vor diesem Hintergrund haben sich feste Adsorbentien als vielversprechende Kandidaten etabliert, da sie geringere Wärmekapazitäten aufweisen und das Potenzial besitzen, den Regenerationsenergiebedarf deutlich zu reduzieren.

Ziel dieses Projekts war es, die CO_2-Abscheidung mittels Adsorption an festen Adsorbentien im Kilogrammmaßstab zu demonstrieren und die optimale Kombination aus Adsorbens und Prozesskonfiguration zu identifizieren, um den Energiebedarf und die Abscheidekosten zu minimieren, ohne dabei die Trennleistung zu beeinträchtigen. Es wurde die Hypothese aufgestellt, dass durch eine geeignete Materialauswahl und Prozessoptimierung der Energieverbrauch auf unter 1 MJ kg^{-1} CO_2 gesenkt werden kann, während gleichzeitig CO_2-Produktivitäten von über 200 kg CO_2 m^{-3} h^{-1} aufrechterhalten werden. Dadurch könnten sowohl die fixen als auch die variablen Kosten von CO_2-Abscheideanlagen signifikant reduziert werden. Zur Umsetzung dieses Ziels wurde im Verlauf des Projekts ein integrierter Ansatz entwickelt und angewendet, der die dynamische Prozessmodellierung, die Validierung im Pilotmaßstab, die techno-ökonomische Analyse sowie die Lebenszyklusanalyse miteinander kombiniert.

Eine Vielzahl fester Adsorbentien, darunter Zeolithe, Siliken und metallorganische Gerüstverbindungen (MOFs), sowohl mit als auch ohne Amin-Funktionalisierung, wurde entwickelt, skaliert und evaluiert. Parallel dazu wurde eine dedizierte Pilotanlage konzipiert und in Betrieb genommen, die unter Gaszusammensetzungen und Temperaturen arbeitet, die für industrielle Abgasströme repräsentativ sind. Dies ermöglichte eine systematische Bewertung zentraler Leistungskennzahlen wie CO_2-Reinheit, Rückgewinnungsgrad, Produktivität und Energieverbrauch. Dynamische Prozessmodelle wurden entwickelt und anhand experimenteller Durchbruchsdaten validiert, wodurch eine zuverlässige Extrapolation auf industrielle Szenarien möglich wurde. Unter den untersuchten Prozesskonfigurationen erwies sich die Temperatur-Vakuum-Wechseladsorption (Temperature–Vacuum Swing Adsorption) durchgängig als die vorteilhafteste Variante und erreichte CO_2-Reinheiten von über 95 % sowie Rückgewinnungsgrade von etwa oder über 90 % bei industriell relevanten Maßstäben.

Für Zeolith 13X ergaben Simulationen im industriellen Maßstab bei trockenen Rauchgasbedingungen und vollständiger Abwärmenutzung Abscheidungskosten von etwa 50 CHF pro Tonne CO_2. Unter Berücksichtigung von feuchtem Rauchgas und Vor-Trocknungsanforderungen stiegen die Abscheidungskosten moderat auf etwa 60 CHF pro Tonne CO_2, während eine geringere Verfügbarkeit von Abwärme die Kosten weiter auf etwa 70–75 CHF pro Tonne CO_2 erhöhte, was auf eine Wettbewerbsfähigkeit mit modernsten lösungsmittelbasierten Abscheidungstechnologien hindeutet. Parallel dazu wurden aminfunktionalisierte Verbundadsorbentien auf Basis von KIT-6-Silika und der metallorganischen Gerüstverbindung MIL-101(Cr) erfolgreich entwickelt und skaliert. Deren Integration in optimierte Adsorptionszyklen zeigte, dass hohe CO_2-Reinheiten und Rückgewinnungsgrade bei Energieverbräuchen erreicht werden können, die den relevanten Zielvorgaben des DOE entsprechen. Die Lebenszyklusanalyse ergab, dass die adsorptionsbasierte CO_2-Abscheidung zwar günstige ökologische Eigenschaften im Betrieb aufweist, die Herstellung der Adsorbentien – insbesondere lösungsmittelintensive Prozessschritte bei MOF-basierten Systemen – jedoch den dominierenden Beitrag zur gesamten Umweltbilanz leistet. Durch die Implementierung von Lösungsmittelrückgewinnung und alternativen Trocknungsstrategien konnte der CO_2-Fußabdruck

jedoch um bis zu etwa 80 % reduziert werden, was klare Ansatzpunkte für eine ökologisch wettbewerbsfähige Materialproduktion aufzeigt.

Der Einfluss der Feuchte im Abgas wurde explizit untersucht. Dabei zeigte sich, dass eine vorgeschaltete Trocknung zwar eine moderate, aber beherrschbare Kostensteigerung verursacht, die grundsätzliche wirtschaftliche und technische Tragfähigkeit der adsorptionsbasierten CO_2-Abscheidung jedoch nicht beeinträchtigt. Insgesamt belegen die Ergebnisse, dass die adsorptionsbasierte CO_2-Abscheidung – insbesondere die Temperatur-Vakuum-Wechseladsorption – einen Reifegrad in technischer, energetischer, ökologischer und ökonomischer Hinsicht erreicht hat, der den Übergang zu integrierten Demonstrationsanlagen und einem großskaligen Einsatz rechtfertigt.

Die unmittelbaren Prioritäten für den weiteren Fortschritt sind die Produktion fortschrittlicher Adsorptionsmittel im Tonnenmaßstab in Zusammenarbeit mit industriellen Herstellern sowie eine integrierte Demonstration in einer Schweizer Kehrichtverbrennungsanlage, wo die günstige Zusammensetzung der Rauchgase und die verfügbare Abwärme die wettbewerbsfähigsten Bedingungen bieten. Vor allem aber bleibt der Nachweis der langfristigen Beständigkeit der Sorptionsmittel unter realistischen Rauchgasbedingungen – einschließlich Feuchtigkeit, SO_x und NO_x – die wichtigste noch zu bewältigende technische Herausforderung vor einem großtechnischen Einsatz. Über die Kehrichtverbrennung hinaus ermöglicht der modulare Aufbau der Technologie eine Anpassung an andere Sektoren, in denen Emissionsminderungen besonders schwierig sind, darunter die Zement-, Stahl- und Chemieindustrie, und trägt so direkt zum Ziel der Schweiz bei, bis 2050 jährlich 12 Millionen Tonnen CO_2 abzuscheiden. Die detaillierten Schritte, Meilensteine und Industriepartnerschaften, die erforderlich sind, um die Technologie von ihrem derzeitigen Entwicklungsstand zur Marktreife zu bringen, sind in der Technologie-Roadmap (Abschnitt 6.3) dargelegt.

Résumé

Au cours des dernières décennies, l'augmentation des émissions de CO_2 est devenue une préoccupation sociétale majeure en raison des effets néfastes de la hausse des concentrations atmosphériques de gaz à effet de serre sur l'environnement, ce qui a motivé le développement de technologies de captage du carbone à grande échelle. Les systèmes de captage les plus matures à ce jour sont les laveurs à base d'amines liquides ; toutefois, malgré leurs performances avérées, le captage du CO_2 par des alcanolamines liquides demeure très énergivore, nécessitant généralement ≥ 4 MJ par kilogramme de CO_2 capté pour la régénération.[1,2] Cette forte pénalité énergétique a limité le déploiement à grande échelle et a suscité un intérêt croissant pour des approches alternatives de captage. Dans ce contexte, les adsorbants solides sont apparus comme des candidats prometteurs en raison de leurs capacités calorifiques plus faibles et de leur potentiel de réduction substantielle de l'énergie de régénération.

L'objectif de ce projet était de démontrer le captage du CO_2 par adsorption à l'aide d'adsorbants solides à l'échelle du kilogramme et d'identifier la combinaison optimale d'adsorbant et de configuration de procédé permettant de minimiser la demande énergétique et le coût de captage tout en maintenant des performances de séparation élevées. Il a été émis l'hypothèse que, grâce à une sélection appropriée des matériaux et à une optimisation du procédé, la consommation énergétique pourrait être réduite en dessous de 1 MJ kg^{-1} CO_2 tout en maintenant des productivités en CO_2 supérieures à 200 kg CO_2 m^{-3} h^{-1}, permettant ainsi des réductions significatives des coûts fixes et variables des installations de captage du carbone. Pour atteindre cet objectif, un cadre intégré combinant la modélisation dynamique des procédés, la validation à l'échelle pilote, l'analyse technico-économique et l'analyse du cycle de vie a été développé et appliqué tout au long du projet.

Une gamme d'adsorbants solides, comprenant des zéolithes, des silices et des structures métallo-organiques (MOF), avec ou sans fonctionnalisation amine, a été développée, mise à l'échelle et évaluée. En parallèle, une unité pilote dédiée a été conçue et mise en service pour fonctionner sous des compositions gazeuses et des températures représentatives des effluents industriels, permettant une évaluation systématique des indicateurs clés de performance tels que la pureté du CO_2, le taux de récupération, la productivité et la consommation énergétique. Des modèles dynamiques de procédé ont été développés et validés à partir de données expérimentales de percée, apportant la confiance nécessaire pour l'extrapolation à des scénarios industriels. Parmi les configurations de procédé étudiées, l'adsorption par variation de température et de pression (temperature–vacuum swing adsorption) s'est systématiquement révélée la plus favorable, atteignant des puretés de CO_2 supérieures à 95 % et des récupérations proches ou supérieures à 90 % à des échelles industrielles pertinentes.

Pour la zéolite 13X, des simulations à l'échelle industrielle ont abouti à des coûts de captage d'environ 50 CHF par tonne de CO_2 dans des conditions de gaz de combustion secs avec une intégration totale de la chaleur résiduelle. Lorsque l'on a pris en compte les gaz de combustion humides et les besoins de préséchage, les coûts de captage ont augmenté modérément pour atteindre environ 60 CHF par tonne de CO_2, tandis que la disponibilité réduite de la chaleur résiduelle a fait grimper les coûts à environ 70–75 CHF par tonne de CO_2, ce qui indique une compétitivité par rapport aux technologies de captage à base de solvants de pointe. En parallèle, des adsorbants composites fonctionnalisés aux amines, à base de silice KIT-6 et de structures métallo-organiques MIL-101(Cr), ont été développés et mis à l'échelle avec succès, et leur intégration dans des cycles d'adsorption optimisés a démontré que des puretés et des taux de récupération élevés peuvent être atteints avec des consommations énergétiques conformes aux objectifs pertinents du DOE. L'analyse du cycle de vie a révélé que, bien que le captage par adsorption présente de bonnes performances environnementales en phase d'exploitation, la synthèse des adsorbants, en particulier les étapes de traitement intensives en solvants pour les systèmes à base de MOF, domine l'empreinte environnementale globale. Toutefois, la mise en œuvre de la récupération des solvants et de stratégies alternatives de séchage a permis de réduire l'empreinte carbone jusqu'à environ 80 %, mettant en évidence des voies claires vers une production de matériaux compétitive sur le plan environnemental.

L’influence de l’humidité des gaz de combustion a été examinée explicitement, montrant que le pré-séchage introduit une pénalité de coût modérée mais maîtrisable, sans compromettre la viabilité globale du captage par adsorption. Dans l’ensemble, les résultats démontrent que le captage du CO_2 par adsorption, et en particulier l’adsorption par variation de température et de pression, a atteint un niveau de maturité technique, énergétique, environnementale et économique suffisant pour justifier une progression vers des démonstrations intégrées et un déploiement à grande échelle.

Les priorités immédiates pour faire avancer le projet sont la production à l'échelle de la tonne d'adsorbants de pointe, en collaboration avec des fabricants industriels, et une démonstration intégrée dans une usine suisse d'incinération des déchets municipaux, où la composition favorable des gaz de combustion et la chaleur résiduelle disponible offrent les conditions les plus compétitives. Plus important encore, la confirmation de la durabilité à long terme des sorbants dans des conditions réelles de gaz de combustion – notamment en termes d’humidité, de SO_x et de NO_x – reste le principal défi technique à relever avant tout déploiement à grande échelle. Au-delà de l’incinération, la nature modulaire de cette technologie permet son adaptation à d’autres secteurs où la réduction des émissions est difficile, notamment le ciment, l’acier et l’industrie chimique, contribuant ainsi directement à l’objectif de la Suisse de capter 12 millions de tonnes de CO_2 par an d’ici 2050. Les étapes détaillées, les jalons et les partenariats industriels nécessaires pour faire passer cette technologie de son stade actuel de développement à la maturité commerciale sont présentés dans la feuille de route technologique (section 6.3).

Main findings («Take-Home Messages»)

1. *A temperature–vacuum swing adsorption process was successfully demonstrated at kilogram scale with Zeolite 13X as an adsorbent*. A custom-built pilot plant achieved CO_2 purities above 95% and recoveries at or above 90% under industrially representative flue gas conditions, confirming technical readiness for scale-up. Industrial-scale simulations yield capture costs of 50-75 CHF/t CO_2 for a feed flue gas with 12% CO_2, within IEA benchmarks for post-combustion capture. Life-cycle assessment estimates a net carbon capture efficiency of 89.5%.

2. *Two key adsorbent materials were scaled to kilogram quantities, including KIT-6 and MIL-101(Cr), without loss of performance*. The resulting amine-based composites (KIT-6 silica-amine and MIL-101(Cr)-amine) retained their CO_2 capacity, crystallinity, and cyclic stability, confirming their potential suitability for their further scaling and deployment. Furthermore, life-cycle assessments suggests that improvements in adsorbent synthesis, such as recovering and reusing the solvent, can reduce the environmental footprint of material production by up to 80% from 0.45 kg CO_2/g of material synthesized to 0.093 kg CO_2/g of material synthesized with solvent recovery.

3. *The technology assessed in this work directly supports Switzerland's climate commitments*. Under the Climate and Innovation Act (2025), federal agreement with waste treatment operators, Switzerland must operate CO_2 capture at a minimum capacity of 100,000 t CO_2/year by 2030, as part of a national target to capture 12 million tonnes of CO_2 per year by 2050 from hard-to-abate sectors including waste incineration, cement, and industry. This project provides the process models, scalable adsorbents, and techno-economic framework required to support this need.

Principales conclusions (« Messages clés »)

1. Un procédé d'adsorption par alternance température-vide a été mis en œuvre avec succès à l'échelle du kilogramme en utilisant de la zéolite 13X comme adsorbant. Une installation pilote sur mesure a permis d'atteindre des puretés de CO_2 supérieures à 95 % et des taux de récupération égaux ou supérieurs à 90 % dans des conditions de gaz de combustion représentatives de l'industrie, confirmant ainsi la maturité technique du procédé pour une mise à l'échelle. Des simulations à l'échelle industrielle indiquent des coûts de captage compris entre 50 et 75 CHF/t de CO_2 pour des gaz de combustion contenant 12 % de CO_2, ce qui s'inscrit dans les références de l'AIE pour le captage post-combustion. L'analyse du cycle de vie estime l'efficacité nette de captage du carbone à 89,5 %.

2. Deux adsorbants clés, le KIT-6 et le MIL-101(Cr), ont été produits à l'échelle du kilogramme sans perte de performance. Les composites à base d'amine ainsi obtenus (silice-amine KIT-6 et MIL-101(Cr)-amine) ont conservé leur capacité de fixation du CO_2, leur cristallinité et leur stabilité cyclique, confirmant leur aptitude potentielle à une production à plus grande échelle et à leur déploiement. De plus, les analyses du cycle de vie suggèrent que des améliorations dans la synthèse des adsorbants, telles que la récupération et la réutilisation du solvant, peuvent réduire l'empreinte environnementale de la production de matériaux jusqu'à 80 %, passant de 0,45 kg de CO_2 par gramme de matériau synthétisé à 0,093 kg de CO_2 par gramme de matériau synthétisé avec récupération du solvant.

3. La technologie évaluée dans le cadre de ces travaux soutient directement les engagements climatiques de la Suisse. En vertu de la loi sur le climat et l'innovation (2025) et de l'accord fédéral conclu avec les opérateurs de traitement des déchets, la Suisse doit exploiter des installations de captage du CO_2 d'une capacité minimale de 100 000 t de CO_2 par an d'ici 2030, dans le cadre d'un objectif national visant à capter 12 millions de tonnes de CO_2 par an d'ici 2050 dans les secteurs où la réduction des émissions est difficile, notamment l'incinération des déchets, la cimenterie et l'industrie. Ce projet fournit les modèles de procédés, les adsorbants évolutifs et le cadre technico-économique nécessaires pour répondre à ce besoin.

Wichtigste Ergebnisse („Kernaussagen“)

1. Ein Temperatur-Vakuum-Wechseladsorptionsverfahren wurde im Kilogramm-Maßstab mit Zeolith 13X als Adsorptionsmittel erfolgreich demonstriert. Eine speziell angefertigte Pilotanlage erzielte unter industriell repräsentativen Rauchgasbedingungen CO_2-Reinheiten von über 95 % und Rückgewinnungsraten von 90 % oder mehr, was die technische Bereitschaft für eine Skalierung bestätigt. Simulationen im industriellen Maßstab ergeben Abscheidungskosten von 50–75 CHF/t CO_2 für ein Einsatzrauchgas mit 12 % CO_2, was innerhalb der IEA-Benchmarks für die Abscheidung nach der Verbrennung liegt. Eine Lebenszyklusanalyse schätzt die Netto-Kohlenstoffabscheidungseffizienz auf 89,5 %.

2. Zwei wichtige Adsorptionsmittel – KIT-6 und MIL-101(Cr) – wurden ohne Leistungseinbußen auf Kilogramm-Mengen hochskaliert. Die daraus resultierenden aminbasierten Verbundstoffe (KIT-6-Silica-Amin und MIL-101(Cr)-Amin) behielten ihre CO_2-Kapazität, Kristallinität und zyklische Stabilität bei, was ihre potenzielle Eignung für eine weitere Skalierung und den Einsatz bestätigt. Darüber hinaus deuten Lebenszyklusanalysen darauf hin, dass Verbesserungen bei der Adsorptionsmittelsynthese, wie beispielsweise die Rückgewinnung und Wiederverwendung des Lösungsmittels, den ökologischen Fußabdruck der Materialproduktion um bis zu 80 % reduzieren können – von 0,45 kg CO_2/g synthetisiertem Material auf 0,093 kg CO_2/g synthetisiertem Material bei Lösungsmittelrückgewinnung.

3. Die in dieser Arbeit bewertete Technologie unterstützt direkt die Klimaschutzverpflichtungen der Schweiz. Gemäß dem Klima- und Innovationsgesetz (2025) und einer Vereinbarung des Bundes mit Abfallentsorgungsbetreibern muss die Schweiz bis 2030 eine CO_2-Abscheidung mit einer Mindestkapazität von 100.000 t CO_2/Jahr betreiben, als Teil des nationalen Ziels, bis 2050 jährlich 12 Millionen Tonnen CO_2 aus schwer zu reduzierenden Sektoren wie Abfallverbrennung, Zementindustrie und Industrie abzuscheiden. Dieses Projekt liefert die Prozessmodelle, skalierbaren Adsorptionsmittel und den technisch-wirtschaftlichen Rahmen, die zur Erfüllung dieser Anforderung erforderlich sind.

Contents

Summary ***3***

Zusammenfassung ***5***

Résumé ***7***

Main findings («Take-Home Messages») ***9***

Principales conclusions (« Messages clés ») ***10***

Wichtigste Ergebnisse („Kernaussagen“) ***11***

1 Introduction ***15***

1.1 Context and motivation *15*

1.2 Project objectives *17*

2 Approach, method, results and discussion ***18***

2.1 WP1 Design of the CO_2 separation demonstrator *18*

2.2 WP2 Design, scale-up and structuring of adsorbents for CO_2 capture *26*

2.3 WP3 Technoeconomic assessment to investigate for the viability of CO_2 capture process *49*

3 Conclusion and Outlook ***89***

4 Publications and other communications ***91***

5 References ***94***

6 Appendix ***97***

6.1 WP2 Adsorbent Design, Scale Up and Synthesis *97*

6.2 WP3 Technoeconomic assessment to investigate for the viability of CO2 capture process *105*

6.3 Technology Roadmap *119*

6.3.1. Outline 119

6.3.2. Involvement of industrial partners 119

6.3.3. Identification of potential application fields 121

6.3.4. IP protection and licensing 122

6.3.5. Remaining technical challenges 122

6.3.6. Required research and development activities 123

6.3.7. Validation by industrial partners 125

6.3.8. References 125

List of abbreviations

ACC – Annualized Capture Cost

BDC – 1,4-Benzenedicarboxylate

BDE – 1,3-Butadiendiepoxide

BET – Brunauer–Emmett–Teller

BMC – Bare Module Cost

CAPEX – Capital Expenditure

CCE – Carbon Capture Efficiency

CCUS – Carbon Capture, Utilisation and Storage

CEPCI – Chemical Engineering Plant Cost Index

DMF – Dimethylformamide

DMSO – Dimethyl Sulfoxide

DOE – Department of Energy (U.S.)

DSC – Differential Scanning Calorimetry

EPFL – École Polytechnique Fédérale de Lausanne

ESI-MS – Electrospray Ionisation Mass Spectrometry

FAT – Factory Acceptance Test

FU – Functional Unit

gPROMS – General PROcess Modelling System

GPTMS – (3-Glycidyloxypropyl)trimethoxysilane

GSA – Global System Analysis

HPR-20 – Hiden Precision Residual Gas Analyser, Model 20

IEA – International Energy Agency

IEAGHG – IEA Greenhouse Gas R&D Programme

KIT – Karlsruhe Institute of Technology

KPI – Key Performance Indicator

LCA – Life Cycle Assessment

LDF – Linear Driving Force

MEA – Monoethanolamine

MFC – Mass Flow Controller

MIL – Matériaux de l'Institut Lavoisier

MOF – Metal–Organic Framework

MSWI – Municipal Solid Waste Incineration

NMR – Nuclear Magnetic Resonance

OPEX – Operating Expenditure

PEI – Polyethyleneimine

PID – Proportional–Integral–Derivative

PLC – Programmable Logic Controller

PSA – Pressure Swing Adsorption

PSE – Process Systems Engineering

PXRD – Powder X-Ray Diffraction

RH – Relative Humidity

RT – Room Temperature

SA-TSA – Steam-Assisted Temperature Swing Adsorption

SAXS – Small-Angle X-Ray Scattering

SBA – Santa Barbara Amorphous

SFOE – Swiss Federal Office of Energy

TAC – Total Annualized Cost

TAEA – Tris(2-aminoethyl)amine

TCSA – Temperature Concentration Swing Adsorption

TEA – Techno-Economic Assessment

TEG – Triethylene Glycol

TEPA – Tetraethylenepentamine

TEOS – Tetraethyl Orthosilicate

TGA – Thermogravimetric Analysis

TMPTE – Trimethylolpropane Triglycidyl Ether

TRL – Technology Readiness Level

TSA – Temperature Swing Adsorption

TVSA – Temperature Vacuum Swing Adsorption

VSA – Vacuum Swing Adsorption

VPSA – Vacuum Pressure Swing Adsorption

1 Introduction

1.1 Context and motivation

Over the last two decades, pronounced climatic changes have been observed, with half of this period comprising the hottest years on record.[3] These changes have manifested in severe environmental impacts, including Arctic glacier melting,[4] rising sea levels,[5] and increasingly frequent extreme weather events.[6] Since the 1970s, global anthropogenic CO_2 emissions have increased by approximately 70 %, largely driven by the combustion of fossil fuels, which continue to supply 70–80 % of global energy demand. Large point sources, such as coal-fired power plants, alone account for more than 40 % of global CO_2 emissions.[7]

Carbon dioxide capture therefore plays a central role in climate-change mitigation strategies. Liquid amine scrubbers represent the most established CO_2 capture technology;[8] however, their large-scale deployment is constrained by high regeneration energy requirements, often consuming nearly 30 % of a power plant's energy output.[9] In addition, liquid amines suffer from operational drawbacks such as corrosion, volatility, and chemical degradation, leading to declining performance over time. Conventional alkanolamine-based capture processes typically require ≥ 4 MJ per kilogram of CO_2 captured.[1,2]

Solid adsorbents have emerged as promising alternatives due to their lower heat capacities compared to aqueous amine solutions, offering the potential for substantially reduced regeneration energy penalties.[10] In particular, amine-functionalized solids, where amines are incorporated into porous supports such as silicas, carbons, and metal–organic frameworks (MOFs), have demonstrated high CO_2 capacities and selectivities.[11] Despite their promise, these materials face challenges related to amine degradation and loss during repeated adsorption–desorption cycles, which limit long-term stability. Addressing these limitations through material and process optimization is therefore essential.

Within this project, solid adsorbents are being developed and evaluated for post-combustion CO_2 capture. Amines are incorporated directly into porous supports to exploit the favorable thermodynamics of solid–gas systems. Using SBA-15 silica as an initial platform, reasonable low-pressure CO_2 uptake (~1.5 mmol g^{-1}) was achieved; however, desorption at elevated temperatures revealed significant degradation of primary amines, forming urea species that severely reduced cyclic performance. To mitigate this, chemical modification strategies were implemented to reduce the fraction of primary amines, leading to markedly improved cyclability and stable CO_2 capacities (Figure 1) of approximately 1.2 mmol g^{-1}.

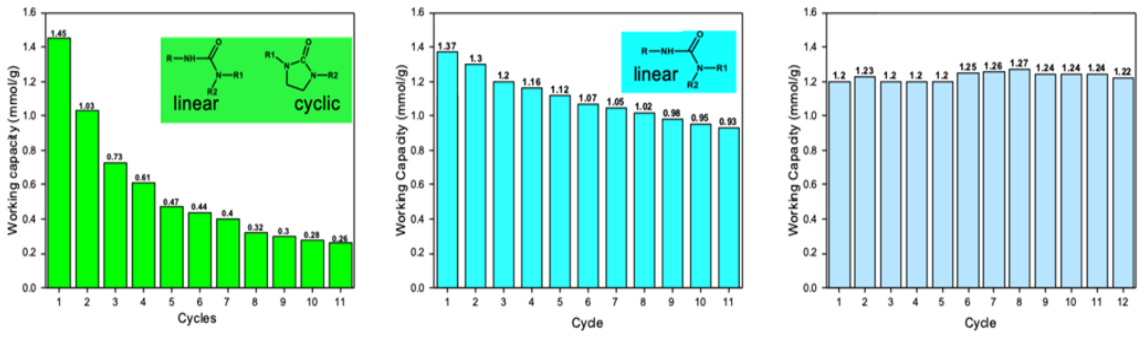


Figure 1: The CO_2 adsorption capacity drops with adsorption desorption cycling, diminishing the materials desorption capacity, when desorption is carried out at (left) 150 ºC and (middle) 120 ºC due to the formation of linear and cyclic ureas. However, when we modify the amines we see that we can stabilize the materials allowing

them to desorb CO_2 over many cycles without the formation of any urea species (right) when the desorption is carried out at 120 ºC.

To further enhance performance, larger-pore silicas were explored. KIT-6, with a pore volume roughly 40 % higher than SBA-15, enabled increased amine loading and delivered a stable cyclic capacity of approximately 1.5 mmol CO_2 per gram when infused with modified polyethyleneimine (Figure 2).

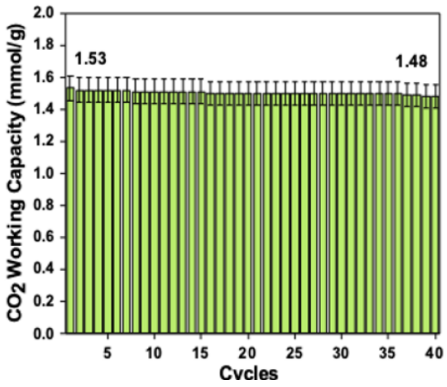


Figure 2: The CO_2 adsorption capacity of KIT-6/PEI is around 1.5 mmol per gram with a desorption temperature of 120 ºC. Adsorption was carried out at 40 ºC, a temperature that is relevant to post-combustion flue gas.

In parallel, MOF-based amine composites were developed, leveraging their high surface areas and tunable pore environments. Specifically, alkylamines, including tris(2-aminoethyl)amine (TAEA) and tetraethylene pentamine (TEPA) were crosslinked with epoxides, such as trimethylolpropane triglycidyl ether (TMPTE) and 1,3-butadiene diepoxide (BDE), within the pores of the metal–organic framework (MOF) Cr-BDC (also MIL-101(Cr), where BDC = 1,4-benzenedicarboxylate), producing four distinct MOF-polymer composites. These composites were then evaluated for their efficacy in postcombustion carbon capture and found to have promising CO_2 capacity, CO_2/N_2 selectivity, and kinetic breakthrough times, and cyclability (Figure 3). Details of the work was published in *Advanced Materials* in 2025.[12]

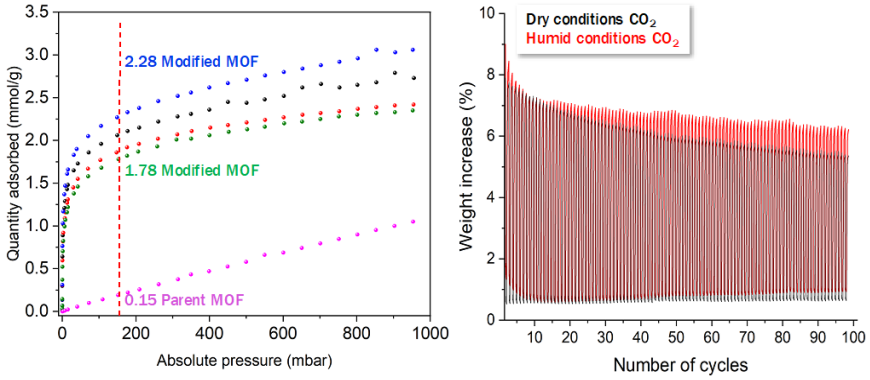


Figure 3: (left) The CO_2 adsorption capacity of the Cr-BDC MOF modified with amines. The modified materials offer capacities > 2 mmol per gram. (right) Moreover, the materials were cycled with adsorption at 40 °C and desorption at 120 °C. We tested several materials over 250 cycles and observe a ~20% decrease in cyclable capacity after 250 cycles in humid gas mixtures containing CO_2 (15%) and N_2 (85%). While we cannot elucidate the precise quantity of water and CO_2 adsorbed simultaneously in the composite under humid conditions, we do note that the cyclability is improved in wet conditions over dry ones.

While adsorbent design and optimization have continued throughout the SFOE project, the focus shifted toward scale-up, shaping, and process integration. Fine powders were transformed into mechanically robust forms suitable for fixed-bed operation as needed for performance validation in a continuous pilot-scale CO_2 capture unit. This step is critical to bridging laboratory-scale results with real-world operating conditions and assessing the broader applicability of these materials.

1.2 Project objectives

The overarching aim is to develop and demonstrate efficient CO_2 capture using amine-decorated solid adsorbents. Specific objectives include:

1. Scaling up two advanced adsorbents (amine-functionalized KIT-6 and MOF/amine composites).
2. Structuring these materials via extrusion, microdroplet formation, or tableting.
3. Demonstrating continuous adsorption–desorption operation over extended periods.
4. Evaluating performance using both simulated gas mixtures and real emission streams.
5. Benchmarking against commercial adsorbents, particularly zeolite 13X, across PSA, VSA, TVSA, and hybrid processes.
6. Identifying optimal material–process combinations through detailed process modeling and simulation.
7. Performing techno-economic assessments and comparative analyses.
8. Demonstrating capture of several kilograms of CO_2 per day in a pilot unit.
9. Exploring additional adsorbent classes, where feasible, and integrating the most promising system into a demonstrator.

Overall, the project seeks to determine whether solid adsorbents can compete with conventional liquid amine scrubbers in terms of energy efficiency, operational stability, and cost, while identifying the key parameters governing their large-scale implementation.

2 Approach, method, results and discussion

2.1 WP1 Design of the CO_2 separation demonstrator

In this project, our primary goal was to design and build a pilot-scale unit capable of testing CO_2 capture materials under realistic post-combustion flue-gas conditions. This required creating a system that is both versatile, robust and capable to simulate industrial gas mixtures and operate continuously with minimal supervision.

The resulting pilot plant is highly adaptable and allows us to test a wide range of CO_2 separation strategies; including temperature swing (TSA), vacuum swing (VSA) and pressure swing adsorption (PSA), as well as combinations of these approaches. It was engineered for automated operations with several automatic safety mechanisms that shut down the system if any abnormalities occur. Figure 4a and 4b shows the process and instrument automated panel of the CO_2 demonstration unit, and Figure 5 shows the actual device and mass spectrometer.

Key Features of the Pilot Plant:

- Multi-Bed System: Three adsorption beds (1.2 m long, 2.54 cm diameter) allow simultaneous adsorption–desorption cycling or stand-alone experiments. The third bed is designed to integrate with an upstream membrane unit in collaboration with EPFL Profesosr, Kumar Agrawal.
- Flexible Gas Handling: Six mass-flow controllers enable preparation of customized synthetic gas mixtures (CO_2, N_2, O_2, Ar, and acidic trace contaminants like So_x and NO_x). The system is compatible with both clean mixtures and industrial flue gas cylinders, with flow rates from 0.2 to 10 L/min.
- Humidity Control: Precise humidity adjustment is achieved using a humidity generator and heated gas lines to prevent condensation.
- Pressure & Vacuum Control: The plant can operate between 1 and 39 bar for PSA studies, and vacuum levels down to 30–50 mbar for VSA processes.
- Thermal Management: Beds are equipped with heating/cooling jackets and monitored by five internal thermocouples to study heat release during adsorption and to finely control TSA conditions.
- Flow Direction Flexibility: Four rotary valves allow gas flow to be switched between top-down and bottom-up operation to explore different process designs.
- Compression Capability: The system currently compresses gas to 6 bar. For CO_2 storage studies up to 50 bar, we plan to couple it with a high-pressure compressor from a neighboring research unit.
- Vacuum & Protection Systems: Dedicated vacuum pumps, a water-condensation trap, and automated valve control ensure safe and stable operations.
- Real-Time Gas Analysis: A high-precision Hiden HPR-20 mass spectrometer continuously monitors outlet gas composition (CO_2, N_2, O_2, Ar, NO_X, SO_X, and water). This allows us to quantify essential performance indicators such as purity, recovery, productivity, and energy requirements.
- Centralized, User-Friendly Control: All components are managed through an intuitive Programmable Logic Controller (PLC) interface that enables full automation of the process.

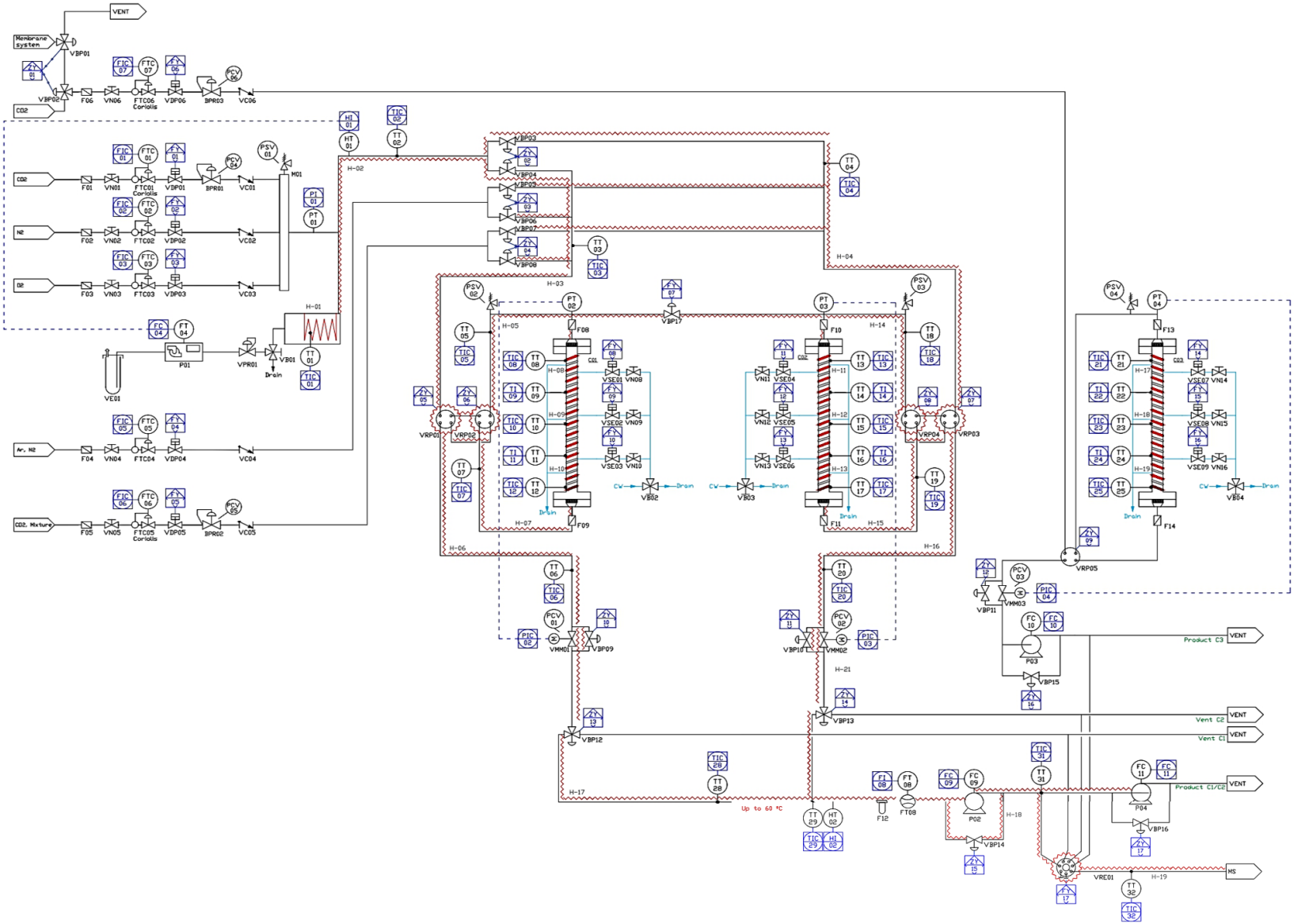


Figure 4a: Schematic of the demonstrator unit for CO_2 capture.

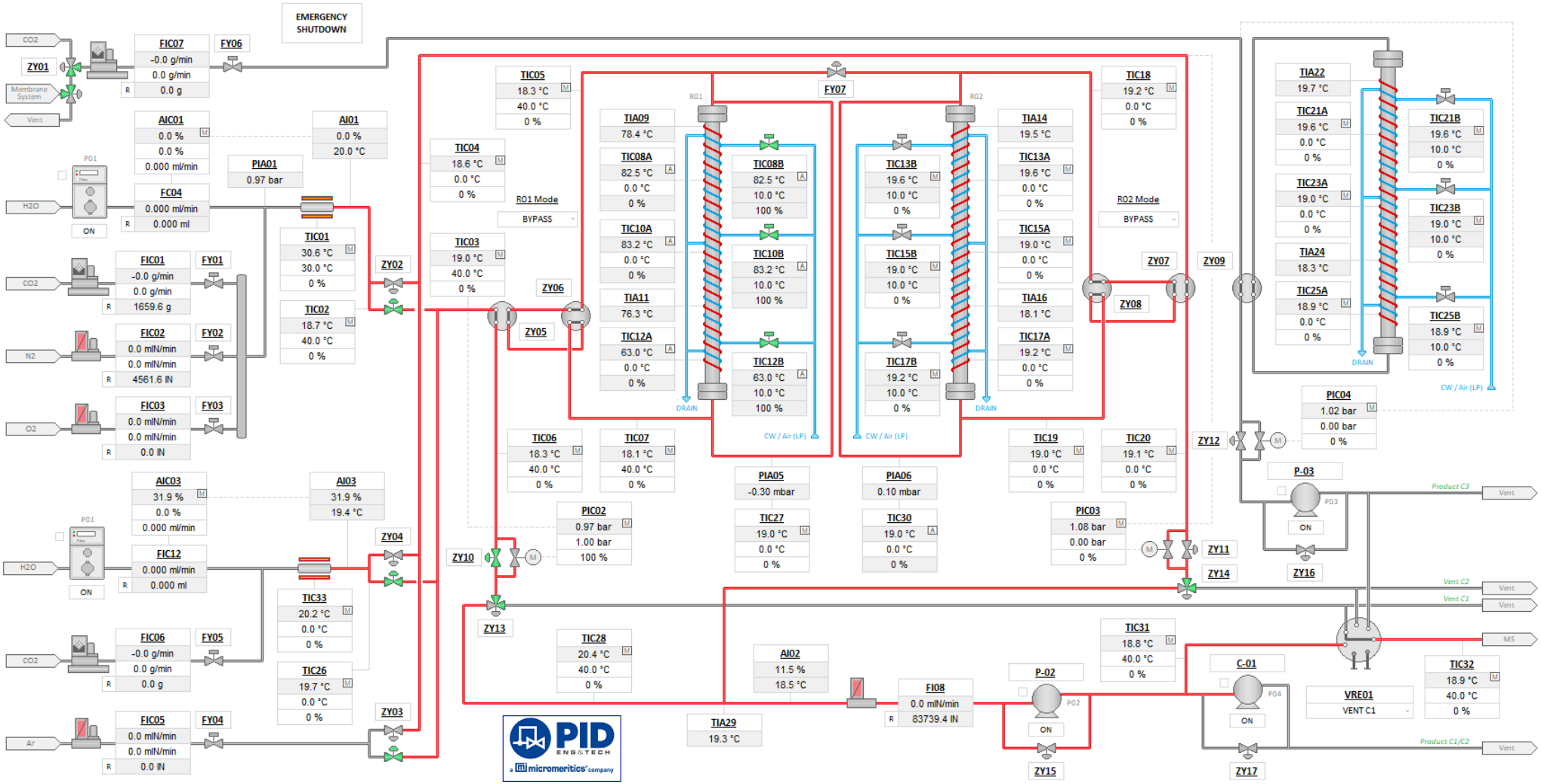


Figure 4b: Programmable Logic Controller (PLC) image that controls the pilot plant from a PC.



Figure 5: (left) Picture of the pilot plant by PID Eng&Tech facilities. (right) HPR-20 R&D mass spectrometer from Hiden.

During the installation and training phase, several key activities were carried out to validate and understand the operation of the demonstrator:

- Adsorbent Preparation & Activation: The pilot plant was commissioned using structured zeolite 13X. This includes preparation of the adsorption beds, determining optimal filling amounts, and performing in situ activation at 300 °C under vacuum for 12 hours.
- Breakthrough and Adsorption Measurements: CO_2/N_2 adsorption experiments at 40 °C were conducted to demonstrate separation. Using the mass spectrometer, CO_2 and N_2 breakthrough profiles were observed, confirming proper detection and gas-flow functionality.
- Regeneration Testing (TSA & TVSA): Two regeneration strategies were evaluated: (1) TSA: Heating above 120 °C using CO_2 or N_2 as the carrier gas; (2) TVSA: Applying vacuum together with moderate heating.
- Both approaches demonstrated successful breakthrough of CO_2. Refer to Figure 7 for the results of the TSA and TVSA breakthrough experiments.
- Software & Process-Control Training: The team received detailed instruction on the Programmable Logic Controller (PLC), including planning automated cycling programs, extracting sensor data, optimizing valve sequences, and safely managing long unattended runs.

Throughout this period, we documented the commissioning with breakthrough plots, temperature/pressure traces, operational notes, and photographs of key steps such as column packing, valve configurations, MS calibration, and compressor operation.



Figure 6: Image of the unpacked and installed pilot plant unit.

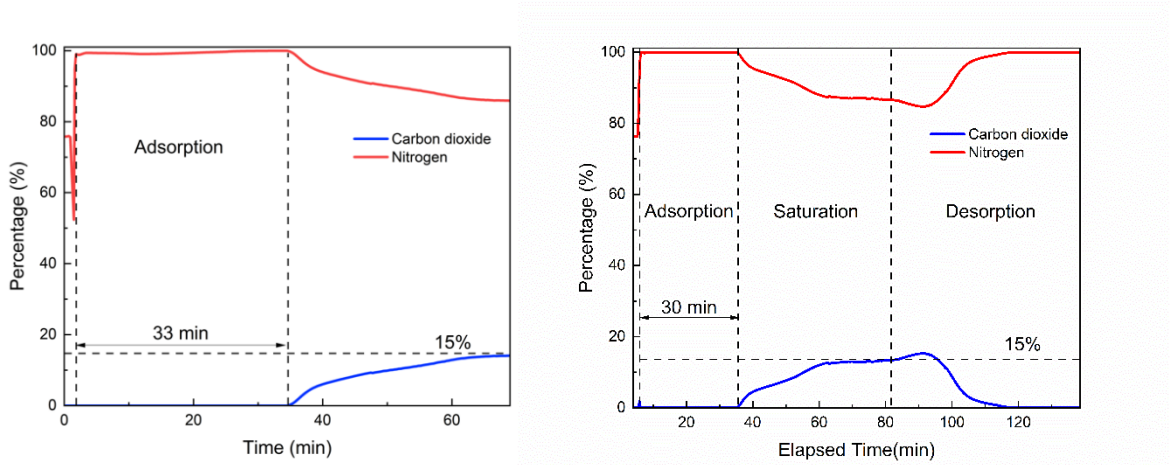


Figure 7: (left) TVSA measurement with a dry flue gas mixture consisting of 15 % CO_2 and 85 % N_2. Desorption was carried under vacuum followed by heating at 200 °C. Flow of N_2 was 3116 mL/ min and CO_2 was at 1 g/min. Breakthrough time of 33 minutes was observed. (right) TSA experiment with a dry flue gas mixture consisting of 15 % CO_2 and 85 % N_2. Desorption was carried under N_2 at 200 °C. Flow of N_2 was 3116 mL/min and CO_2 was at 1 g/min. Breakthrough time of 30 minutes was observed.

Humidity control

Since industrial exhaust gases often contain moisture, it was essential to test how well the system could add, control, and remove humidity during repeated operation.

The demonstrator controls humidity using a combination of a pump and an evaporator, with heating coils along the gas lines to prevent condensation. The pump delivers water at a defined rate (mL/min), either set manually or automatically adjusted by the system to reach a desired RH. The evaporator heats the water to generate vapor, which is then mixed with the gas stream (CO_2/N_2) to produce humidified mixtures. Among the several parameters influencing humidity generation: pump flow rate, pump pressure, evaporator temperature, line temperature, and gas flow rate; the gas mixture flow rates (N_2: 3116 mL/min; CO_2: 543 mL/min, yielding a 85:15 ratio) and line temperature (40 °C) were kept constant.

Two operating modes were tested:

- **Manual mode:** The user sets a specific pump flow rate, and the resulting RH is achieved.
- **Automatic mode:** The user inputs the target RH and evaporator temperature, and the device adjusts the pump flow rate accordingly to achieve the target RH.

Initially, both modes were tested to examine how quickly the system could reach the desired RH and whether it could maintain it stably. As shown in Figure 8, fluctuations in RH (ranging from 0 to 40 %) were observed, primarily caused by variations in pump pressure and, consequently, the water flow rate. To address this, an additional pump accessory was introduced to improve flow stability (Figure 9).

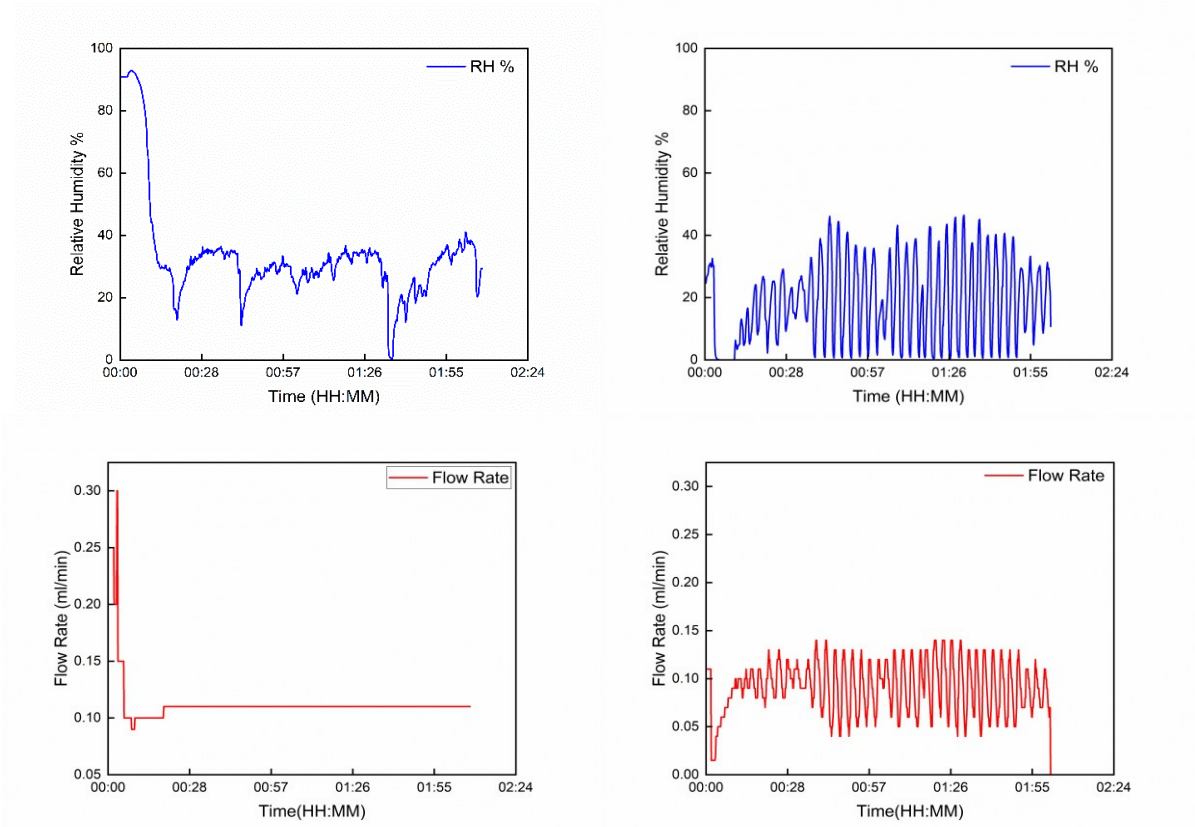


Figure 8: Variations of relative humidity (RH, in blue) with time for the manual (left) and automatic (right) operating modes of pump, along with the corresponding pump flow rate (in red). The gas mixture flow rates (N_2: 3116 mL/min, CO_2: 543 mL/min) and line temperature (40 °C) were kept constant.

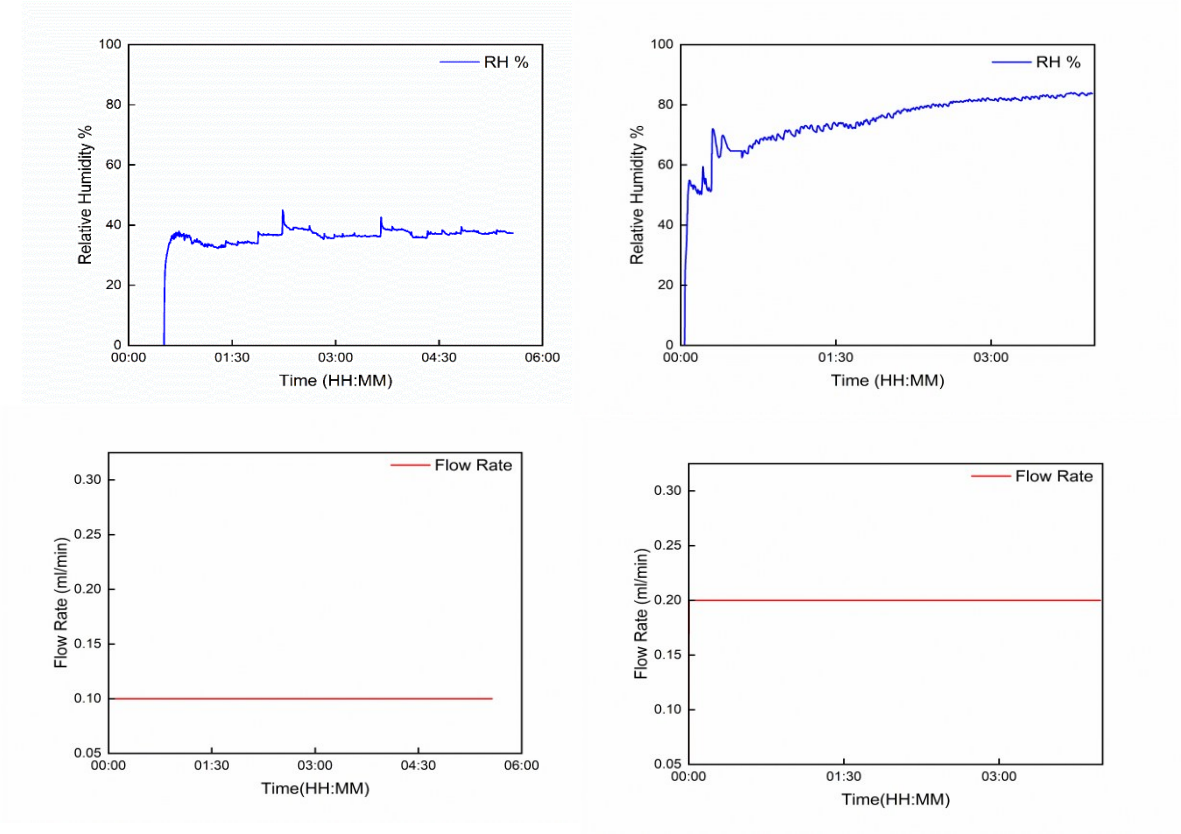


Figure 9: Variations of RH with time for 0.100 mL/min (left) and 0.200 mL/min (right), with constant flow profiles. The gas mixture (N_2: 3116 mL/min, CO_2: 543 mL/min) flow rate remains constant. The temperature of the lines are kept constant at 40 ºC.

Once stable humidity control was achieved, full adsorption-desorption cycles were carried out to simulate real operating conditions. During the adsorption phase (N_2 flow: 3116 mL/min; CO_2 flow: 543 mL/min; line temperature: 40 °C), the pump was switched on to introduce humidity into the gas stream. During the desorption phase (N_2 flow: 3116 mL/min; line temperature: 40 °C), the pump was switched off to achieve dry conditions. These tests were performed at different pump flow rates, while maintaining constant gas mixture flow rates and line temperature, to evaluate (i) the time required to reach the target RH dur-ing adsorption, (ii) the dry-down time during desorption, and (iii) the cycle-to-cycle reproducibility of humidity control.

These tests showed that the system could repeatedly reach the desired humidity levels during CO_2 capture and maintain consistent performance from cycle to cycle. At higher humidity levels (60-80 % RH), the system required more time to fully dry during the regeneration step, mainly due to moisture remaining in the gas lines (Figure 10). While completely eliminating moisture is challenging, this can be managed by extending drying times or using higher temperatures. Overall, these results confirm that the demonstrator is well suited for testing CO_2 capture materials under realistic humid conditions, providing a reliable platform for future material evaluation and technology development.

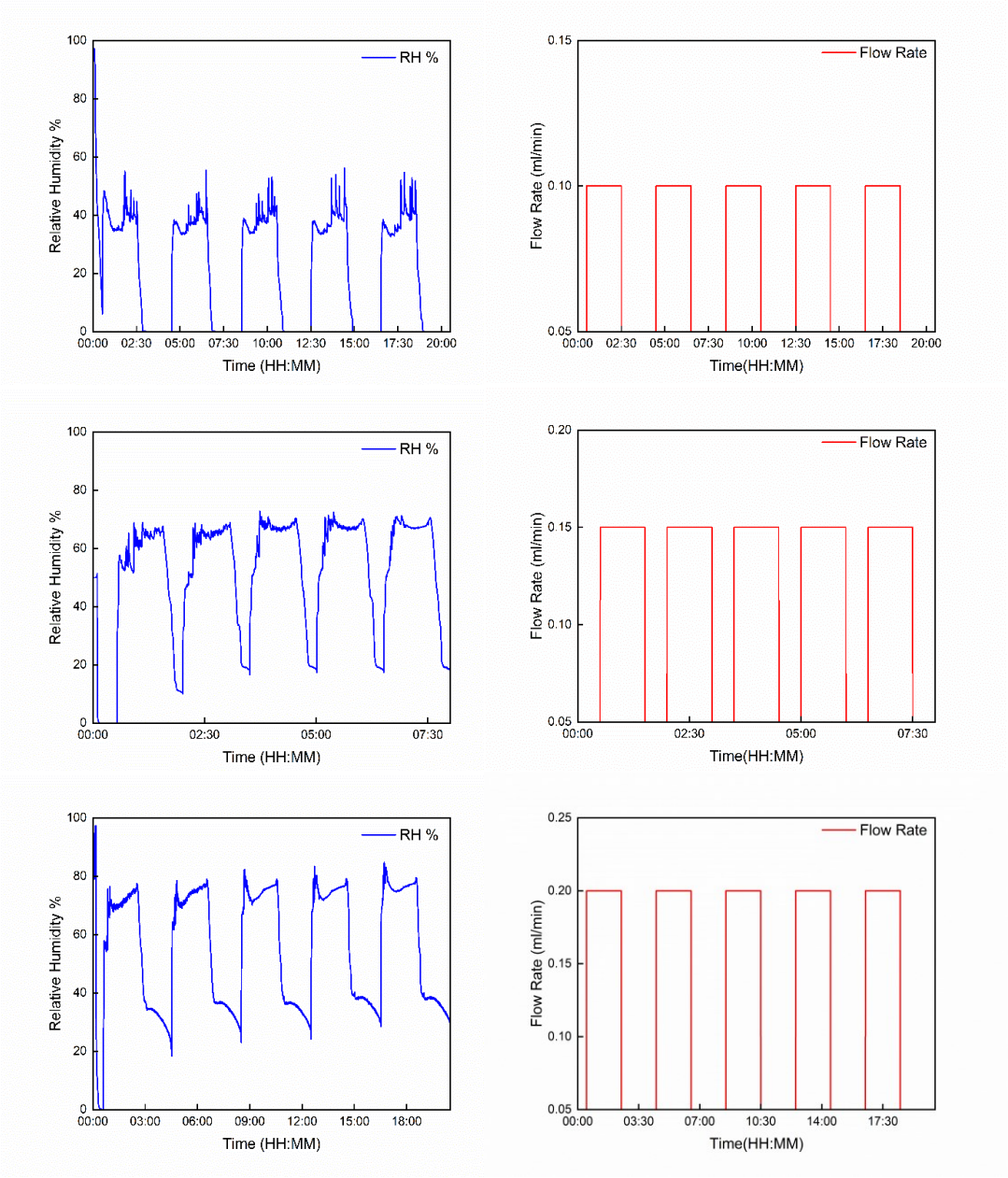


Figure 10: Relative humidity (RH, left) and corresponding pump flow rate (right) profiles recorded over multiple adsorption–desorption cycles for different flow rates: (top) 0.100 mL/min, (middle) 0.150 mL/min, and (bottom) 0.200 mL/min. The system demonstrates stable and reproducible RH control across cycles.

2.2 WP2 Design, scale-up and structuring of adsorbents for CO_2 capture

To test CO_2 capture in the demonstrator unit, we selected three types of adsorbent materials: an amine-functionalized metal–organic framework (MOF), an amine-infused mesoporous silica (KIT-6), and a commercial zeolite (zeolite 13X). Zeolite 13X was used as a benchmark material to commission and validate the pilot plant, because it is commercially available and well-characterized. As a result, most of our research effort in WP2 was directed toward developing, scaling up, and structuring MOF and silica-based adsorbents (detailed protocol in Appendix WP2). These two materials serve as a support for amine-based polymers, which are expected to provide high CO_2 capture performance, even in the presence of water.

At the start of the project, we developed a synthesis for the MOF, Cr-BDC, in a 1-liter reactor, producing about 18 g per batch. However, we found that producing the Cr-BDC MOF at laboratory scale was expensive: about 200 CHF per 100 g, due to the large amounts of organic solvents used during washing. In fact, around 90% of the synthetic cost came from washing, rather than the MOF building blocks themselves. To solve this, we focused on making the same high-quality MOF using far less solvent, while aiming to keep its porosity and performance intact (detailed protocols in Appendix WP2). To reduce cost while screening washing conditions, we cut the reaction volume by a factor of 4, to 250 mL reactors. We then carefully optimized the washing process, which is meant to remove unreacted ligands trapped inside the MOF pores (protocols 1-4, Table 1).

We used ^{1}H-NMR spectroscopy to measure how much ligand was removed in each wash (detailed protocol in Appendix WP2). This allowed us to identify the minimum number of washing steps needed to properly remove excess ligand from the MOF pores. Refer to Figure 11 for the NMR analysis.

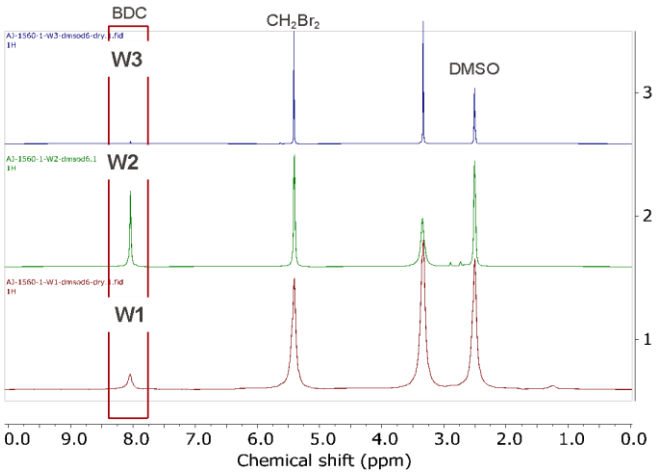


Figure 11: ^{1}H NMR of aliquot of washed solvent, dried in vacuum oven and dissolved back in DMSO-d_6 with 2.5 µL of CH_2Br_2 as internal standard. W1, W2 and W3 is wash 1, wash 2 and wash 3, respectively.

Further, PXRD analysis (Figure 12 and Table 1) was also used to assess the phase purity and crystallinity of the as-synthesized Cr-BDC MOF in the four different washing protocols. For protocol 1, 2 and 4, the material was found to be phase pure, while the diffraction pattern obtained from protocol 3 indicated unreacted BDC ligand present in the product. Hence, protocol 3 was discarded as the quantitz of solvent employed, only 1 x 50 mL DMF wash per 250 mL of MOF reaction, was deemed insufficient. Importantly, results from protocol 4 indicate that 1 x 100 mL of DMF (protocol 4) per 250 mL MOF reaction is enough to remove unreacted BDC ligand, providing a phase pure MOF.

Next, N_2 adsorption measurements at 77 K were employed to assess the porosity of the phase pure MOF obtained from protocols 1, 2 and 4. The samples were activated at 150 °C under vacuum for 12 h prior to the adsorption measurements. The measurements showed that the optimized MOFs still offer high surface areas (2800–3000

m²/g) that are only slightly lower than our extensively washed reference samples having surface areas of 3300–3400 m²/g.[13]

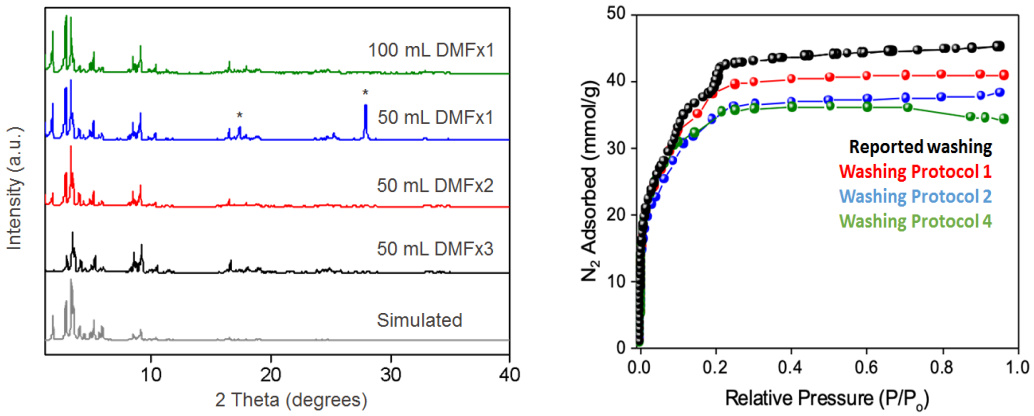


Figure 12: (left) MOF PXRD after several different washing protocols. Simulated Cr-BDC (grey), for 1 L synthesis, 150 mL DMF (50 mL three times, protocol 1) (black),100 mL DMF (50 mL two times, protocol 2) (red), 50 mL DMF (blue, protocol 3), 100 mL L DMF (olive, protocol 4). Asterisks (*) indicate unreacted ligand trapped in the MOF pores. (right) N_2 adsorption (at 77) K for Cr-MOF obtained from protocols 1 (red), 2 (blue) and 4 (olive) is compared to Cr-BDC obtained from extensive washing of 200 mL DMF x 6 times in 1 L scale synthesis (black).

Table 1: Optimizing the washing step via different washing protocols (1-4). We have multipled the reaction quantities by a factor of 4 for direct comparison to our original 1L reaction (1L reaction).

Ref	Cr salt	BDC	H_2O	HNO_3	Wash DMF	Wash EtOH	Yield (%)	BET (m^2/g)	Cost (CHF/L)
Ref. protocol[13]	192 g (0.48 mol)	81.3 g (0.48 mol)	2.4 L	0.49 mol	4.5 L x 2 times	4.5 L x 2 times	68 %	3400	66.25
1L reaction	52.8 g (0.13 mol)	18.0 g (0.11 mol)	660 mL	8.56 mL (1.13 mmol)	200 mL x 6 times	200 mL x 4 times	47 %	3300	36.5
Protocol 1	52.8 g (0.13 mol)	18.0 g (0.11 mol)	660 mL	8.56 mL (1.13 mmol)	200 mL x 3 times	200 mL x 3 times	47 %	~3000	18.5
Protocol 2	52.8 g (0.13 mol)	18.0 g (0.11 mol)	660 mL	8.56 mL (1.13 mmol)	200 mL x 2 times	200 mL x 3 times	47 %	~2800	14.5
Protocol 3	52.8 g (0.13 mol)	18.0 g (0.11 mol)	660 mL	8.56 mL (1.13 mmol)	200 mL x 1 times	200 mL x 3 times	unreacted BDC ligand present		10.5
Protocol 4	52.8 g (0.13 mol)	18.0 g (0.11 mol)	660 mL	8.56 mL (1.13 mmol)	400 mL x 1 times	200 mL x 3 times	47 %	~2800	14.5

After optimizing the washing steps, further work on the scale-up of the Cr-BDC was carried out in our laboratory. To accumulate more MOF, various batches were made from the optmized protocol carried out in a 1-liter reactor (yielding 18 g per batch). After characterization of each batch, to ensure consistency, they were combined to reduce the work-up time. Given the large volume of supernatant after combining several batches, we tried to replace the centrifugation step with a filtration step using a vacuum pump, which is a common procedure for the large-scale industrial processes. However, filtration was found to be difficult (Figure 13). For example, there were problems related to filter clogging, and the process was much slower than centrifugation. Further, handling such large quantities of solvent posed other problems that led to damaged pumps. Given this, after several trials, we reverted back to centrifugation.

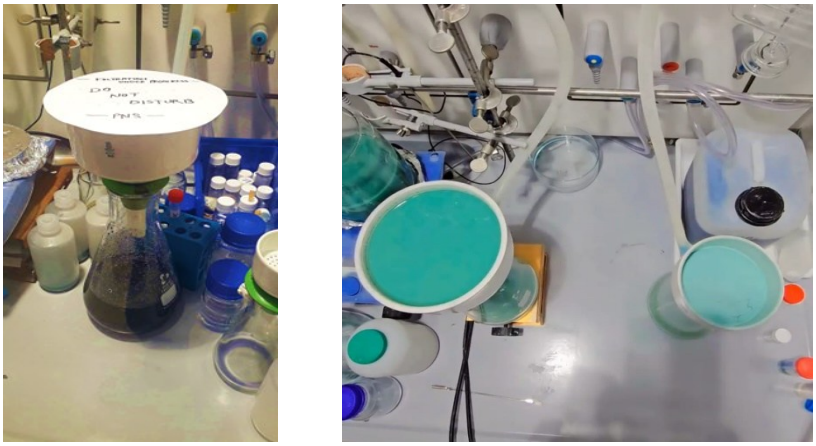


Figure 13: (left) Front view of filtration setup. (right) Top view of simultaneous filtration in 2L and 1L scale.

Next, we focused on adding amines into the MOF pores, which enable CO_2 capture. This was done using a two-step method: first amines were impregnated into the MOF, and then, they were crosslinked with epoxides to prevent amine loss during repeated adsorption–desorption cycles. For the amine-impregnation, we used a protocol previously developed in our laboratory.[12] For this process, phase pure MOF was first obtained from protocol 1 and 2 (with surface area of 3000 m^2/g and 2800 m^2/g, respectively). The purpose of this study was to understand if the new washing protocols described above impact the CO_2 adsorption performance of the materials after amine impregnation in the pores. Given this, CO_2 adsorption measurements (at 40 °C) were carried out on the resulting MOF-amine-composites and compared to the ones previously developed (Figure 14). Interestingly, the material with a surface area of 3000 m^2/g (Protocol 1) gives the same CO_2 adsorption isotherm after impregnation compared to the MOF that was extensively washed, which has a surface area of 3300 m^2/g. The MOF obtained with a surface area of 2800 m^2/g (Protocol 2) had a slightly lower CO_2 uptake capacity. Hence, we continued with protocol 1, where the MOF is washed using three steps (200ml DMF x 3), giving a surface area of 3000 m^2/g and reproducible amine impregnation with CO_2 uptake of ~2.0 mmol/g at 0.15 bar and 40 °C. To obtain the Cr-BDC composite having reproducible CO_2 uptake, the quantity of DMF used to wash a 1-liter scale MOF reaction is 600 mL. This value that is 4 times lower than the reported procedure[13] and two times lower than our previous 1-liter reaction protocol (1L reaction, Table 1). Thus, it is estimated that the overall synthesis of Cr-BDC is approximately 18.5 CHF/L reactor, representing a 3.6-fold reduction from the original literature cost estimated to be approximately 66.25 CHF/L of reaction.

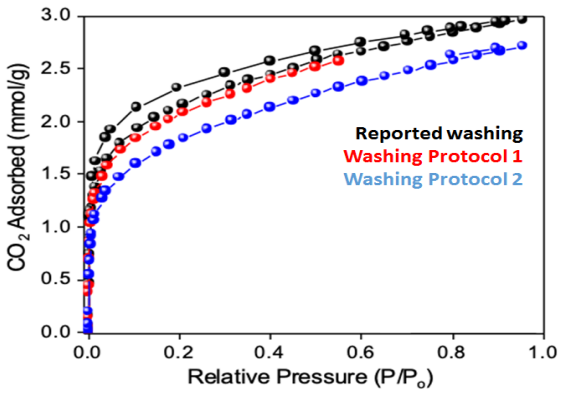


Figure 14: CO_2 adsorption at 40 °C for the amine impregnation using the original synthesis (black), protocol 1 (red) and protocol 2 (blue).

Next, the Cr-BDC reaction was scaled to a 2-liter reactor, producing 40–50 grams of MOF per batch (detailed protocol in Appendix WP2). To enable this, four 2-L reactors were purchased and employed simultaneously, allowing the successful production of over 2.4 kilograms (2400 g) of Cr-BDC (Figure 15). Importantly, the material quality was preserved as the MOF remained highly crystalline and showed a very high surface area of 2900–3000 m²/g, matching the performance of smaller-scale batches (Figure 16).



Figure 15: Accumulated batches of MIL-101-Cr synthesized through repeated 2 L reactions, resulting in a total of approximately 2400 g of bare MOF.

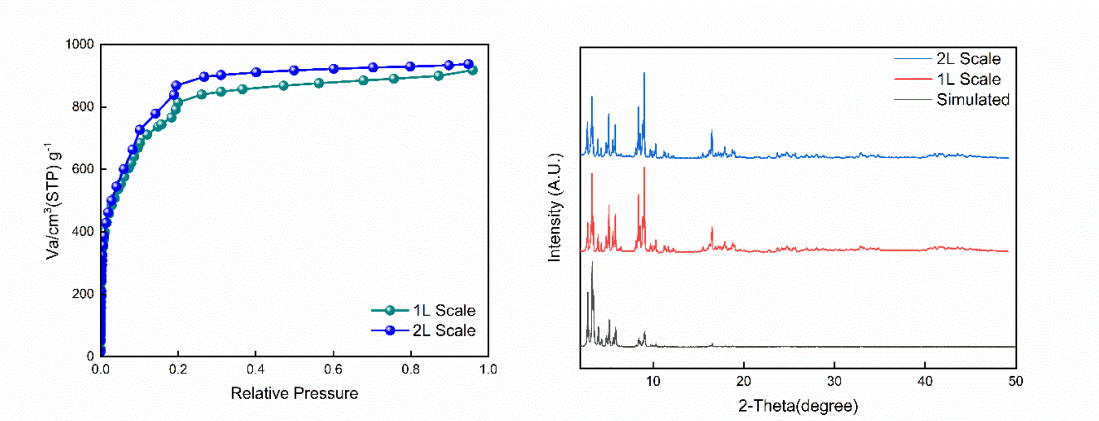


Figure 16: (left) Nitrogen isotherm at 77 K and (right) PXRD patterns of the MOF obtained from the 1 L and 2 L reaction scales.

Out of the many amine–epoxide combinations we have tested in Cr-BDC, the best-performing material contained TAEA (amine) crosslinked with BDE (epoxide), which gave an impressive CO_2 uptake (Figure 17).[12] However, when considering composite scale-up, we found this amine and epoxice combination is both expensive and toxic, relative to other starting materials, making this combination less suitable. For example, when doing lab-scale synthesis, we found BDE is ~6000 CHF per kg, while another amine, TEPA, is only 94 CHF per kg (Table 2). We therefore switched to the cheaper and less toxic pair: TEPA (amine) and TMPTE (epoxide). Although this combination initially showed lower CO_2 uptake (Figure 17), we improved it by optimizing the ratios, reaction conditions, and further optimizing the crosslinking chemistry (Table 3).

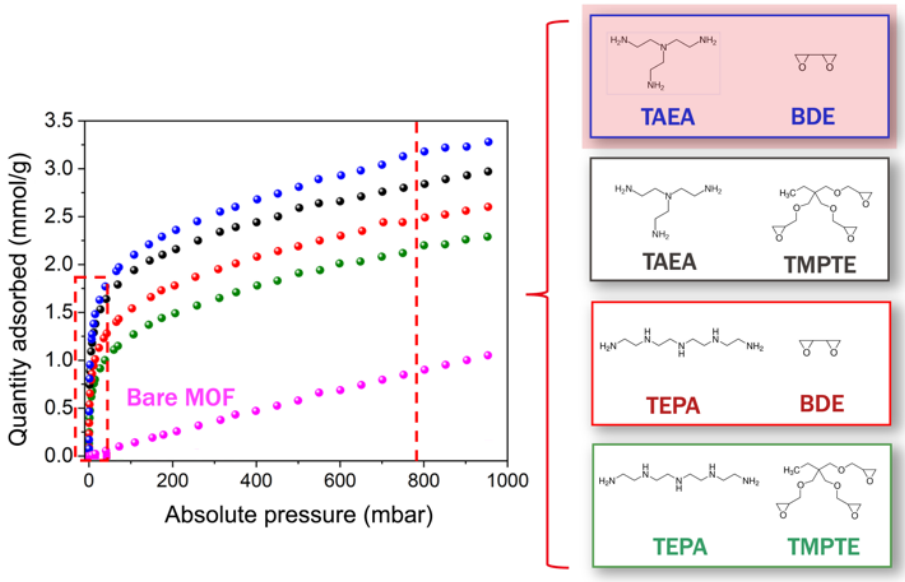


Figure 17: (left) CO_2 adsorption capacity (40 °C) collected from (right) the Cr-MOF impregnated with various amine and epoxide combinations.

Table 2: Cost analysis of lab-scale MOF and composite synthesis, excluding solvent cost.

Name	Full name	Cost (CHF/kg)
Cr-MOF	Cr-BDC or MIL-101(Cr)	925
TEPA	Tetraethylenepentamine	94
TAEA	Tris(2-aminoethyl)amine	2'440
BDE	1,3-Butadiendiepoxide	6'240
TMPTE	Trimethylolpropane triglyciyl ether	227

The CO_2 adsorption and separation performance of the amine-epoxide composites is directly related to the quantity and type of accessible amines present in the MOF pores. Thus, our intention was to boost the amine (TEPA) loading. However, to do this, we also had to increased the quantity of crosslinking epoxides, which are responsible for inhibiting amine leaching during the adsorption/desorption cycling. Overall, the amine structure and loading in the MOF can be impacted by the quantity and ratio of amines and epoxides in the reaction, reaction time, and/or reaction temperature. Hence, we proceeded to further optimize the synthetic protocol varying these parameters during amine impregnation reactions. For example, Table 3 and Figure 18, show examples of protocols screened, where the MOF:Amine:Epoxide ratios were varied. Importantly, the quantity of CO_2 adsorbed at 0.15 bar and 40 °C (the concentration of CO_2 in post-combustion flue gas) varies greatly depending on the protocol employed.

Table 3: Different synthesis procedures for MOF composites.

Protocol	Cr-BDC**:TEPA:TMPTE**	**Leaching**	**Capacity at 0.15 bar (mmol/g)**
P1	59:2:1	No	1.1
P2	59:4:1	Yes	2.6
P3	12:4:1	No	1.7
P4	29:2:1	No	1.9

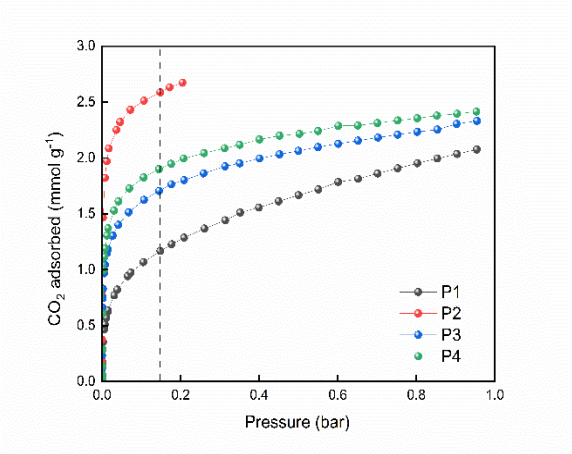


Figure 4: CO_2 isotherm at 40 °C for different ratios of Cr-BDC:TEPA:TMPTE. P represents protocols 1 to 4.

In Figure 18, four different synthetic protocols are compared. After some optimization, the capacities were improved from 1.1 mmol/g (P1) to 1.9 mmol/g (P4). It is worth noting that the protocol referred to as P2 shows the highest CO_2 capacity. However, as indicated in Table 3, amine leaching occurs in the sample tube during the activation process required to measure the CO_2 adsorption capacity. As a result, this protocol is deemed unsuitable and was therefore discarded. P4 was first carried out on a 0.55 mg scale. Later, we also scaled this up from 0.55 mg to the ~2 g scale (detailed protocol in Appendix WP2). Cr-BDC-TEPA-TMPTE is the cheapest and more environmentally friendly composite, and with the improved synthesis protocol (P4), our capacities were enhanced close to that of Cr-BDC-TAEA-BDE. Further, the adsorption isotherms of Cr-BDC-TEPA-TMPTE produced via P4 at different scales and from several batches are shown in Figure 19, indicating that the process is scalable in the lab and reproducible.

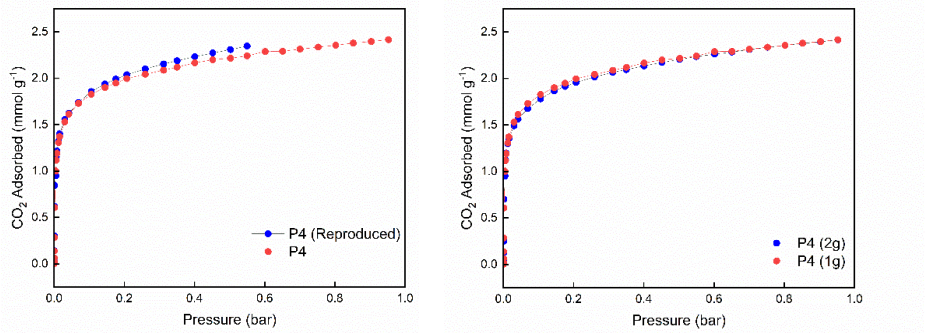


Figure 5: (left) CO_2 isotherm at 40 °C of P4 Cr-BDC-TEPA-TMPTE. (right) CO_2 isotherm at 40 °C of P4 at 1 g and 2 g scales.

The best performing composite of Cr-BDC-TEPA-TMPTE, P4, was next tested in a CO_2 gas mixtures (15 % CO_2, 85 % N_2, 70–80 % relative humidity) with adsorption at 40 °C and desorption at 120 °C (Figure 20). After more than 60 cycles, the material showed stable CO_2 uptake, no amine leaching and no chemical degradation. Small fluctuations in capacity were traced to changes in room temperature, which also impact the relative humidity level.

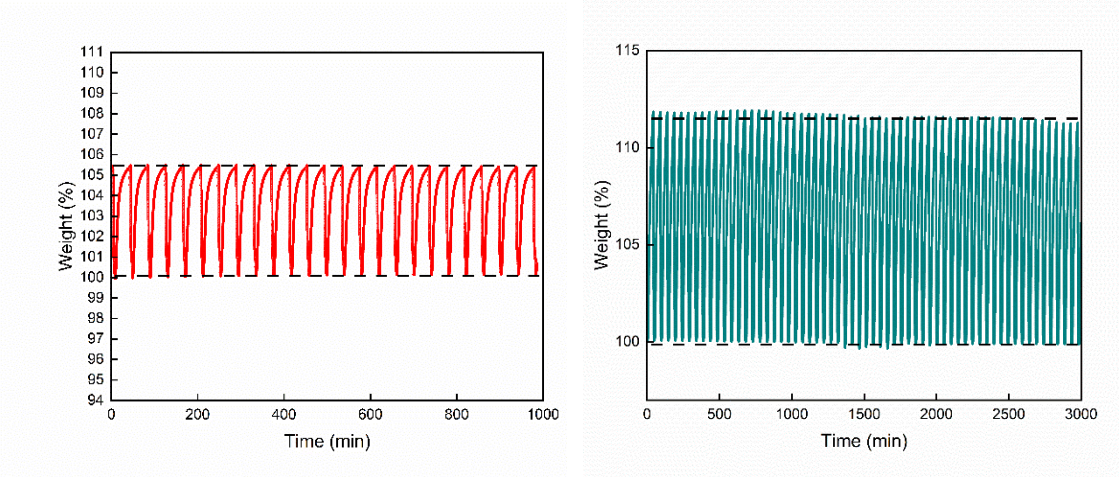


Figure 20: (left) Dry cyclic data of Cr-MOF-TEPA-TMPTE produced via P4 at 40 °C under 15% N_2 and 85% CO_2. (right) Humid cyclic data of P4 at 40 °C under 15% N_2, 85% CO_2, and 80% RH.

Initial attempts to scale up the composite from 2 g to 4 g (detailed protocol in Appendix WP2), following the same protocol at the larger scale, resulted in processing challenges (handling changes in mixture volume, irregular mixing) and a decline in performance. However, by optimizing the reaction time (e.g. leaving it for longer periods of time, 12 h for instance) the composite regained its original CO_2 adsorption performance (Figure 21).

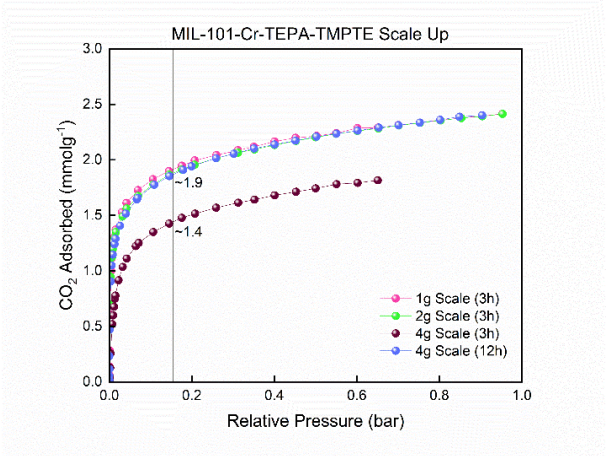


Figure 21: CO_2 adsorption isotherms of MIL-101-Cr-TEPA-TMPTE composite at different scales with different reaction times.

After re-testing older batches of the Cr-BDC–TEPA–TMPTE composite (having a several month shelf life) we noticed a gradual drop in CO_2 capacity along with a loss of MOF crystallinity (Figure 22). We attribute this to chemical attack of the chromium nodes by the amines within the MOF pores. To address this in the future, we aim to test various modification strategies that may limit amine access to the metal centers while preserving CO_2 adsorption. Assessment of such modified materials will require full aging tests to confirm long-term performance and spectroscopic measurements aimed at quantifying the primary amine content. Due to the observed degradation of Cr-BDC-amine composite while sitting on the lab shelf, we temporarily limited large-scale production of the composite until the most stable formulation can be validated for use in the demonstrator unit in the future.

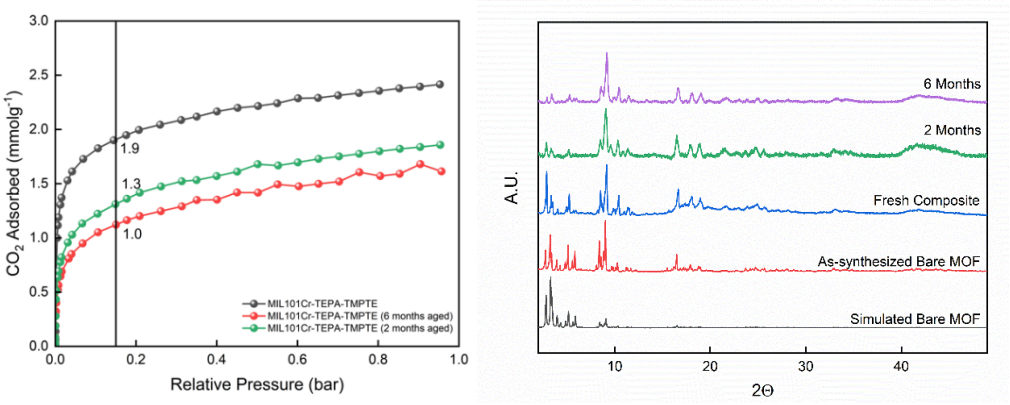


Figure 22: (left) CO_2 isotherms of MIL-101-Cr-TEPA-TMPTE composites showing decline in capacity over period of time. (right) PXRD patterns of aged MIL-101-Cr-TEPA-TMPTE.

Grafting amines inside the Cr-MOF, Cr-BDC-NH_2

As a continued effort in materials design, we also assessed a new strategy for amine impregnation inside a Cr-MOF, known as Cr-BDC-NH_2. It has the same structure as Cr-BDC but with ligands functionalized with amine groups, which provide an anchoring point for grafting alkyl amines to the MOF wall. Notably, it was hypothesized that this may better inhibit amine leaching as the amine is immobilized in the pore via covalent grafting.[14]

Like the in-situ polymerization approach described above, we found that this novel grafting strategy leads to significant enhancements in the CO_2 adsorption properties, much higher breakthrough times (Figure 23), and extensive cyclability (Figure 24) (tested >400 times for the best materials). The covalent grafting study was published in *Advanced Functional Materials* in 2023 and provides us with a second typed of material that could be assessed in the demonstration unit in the future.[15]

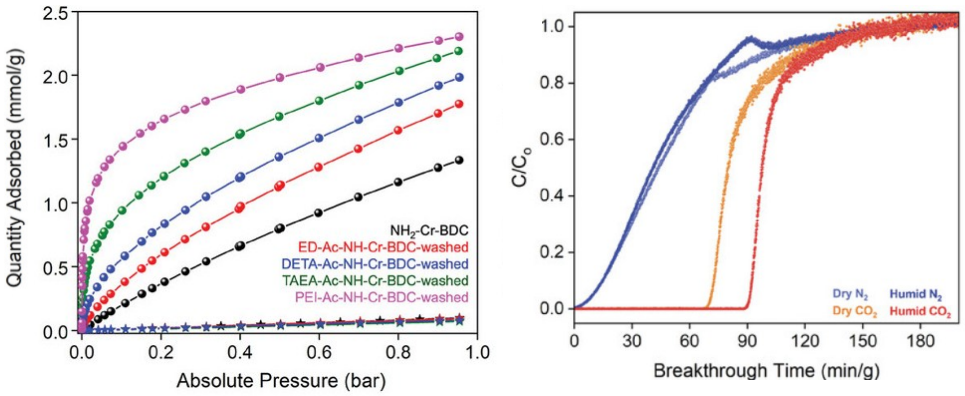


Figure 23: (left) CO_2 adsorption isotherms at 40 °C for the grafting of amines onto the ligand of a Cr-MOF. Different amines were grafted (blue, black, red and green circles) inside the Cr-MOF and then compared to the bare Cr-MOF (magenta). N_2 adsorption of the same materials in stars. (right) Breakthrough plots at 40 °C and a 15% CO_2 85 % N_2 gas composition for the best-performing material having amines grafted on the ligand of Cr-MOF. Dry tests (N_2 in light blue and CO_2 in orange) and humid including 80% RH in the gas mixture after 2 h pre-saturating with humid He (N_2 in dark blue and CO_2 in orange).

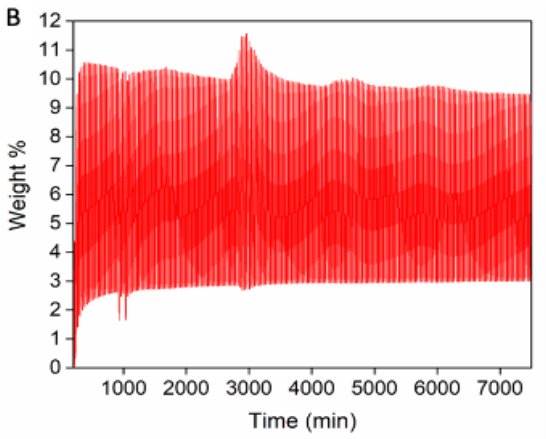


Figure 24: TGA cycling data of amine grafted on the ligand of Cr-BDC-NH_2. Adsorption at 40 °C of humid 15% CO_2 85% N_2 gas stream and desorption at 120 °C under humid 100% CO_2. The weight increase is attributed to the adsorption of CO_2 and water.

Shaping and structuring Zeolite 13X

MOFs and zeolites show excellent CO_2 capture in powder form, however powders cannot be used in pilot plants because they are difficult to handle, pose health risks if inhaled, and create high pressure drops when gases flow through packed beds. For this reason, the materials must be converted into pellets, beads, or extrudates while keeping as much of their performance as possible.

To develop reliable shaping methods, we started a collaboration with HES-SO Valais (Prof. Mathieu Soutrenon) and focused first on tableting. After shaping, the mechanical quality of the tablets was evaluated using (details of the material synthesis and shaping can be found in Appendix WP2):

- Crush-strength tests, which measure the force needed to break a tablet, and

- Friability tests, where tablets were rotated for 500 cycles and the resulting weight loss was recorded.

Zeolite 13X (NaX) powder was pressed into binder-free tablets at pressures between 25 and 400 MPa. Next, N_2 adsorption isotherms (Figure 25) revealed the surface area drops from 501 m^2/g (powder) to 311 m^2/g when the pressure is increased from 25 to 400 MPa and the pore volume decreases from 0.24 cm^3/g to 0.15 cm^3/g (Table 4). PXRD suggested that the crystal structure of the Zeolite 13X is well maintained during the structuring process albeit there is a decrease in intensity and peak broadening observed above 300 MPa (Figure 25).

Table 4: BET surface area and pore volume of Zeolite 13X (NaX) before and after pressing into tablets.

	BET surface area ($m^2\ g^{-1}$)	pore volume ($cm^3\ g^{-1}$)
No binder		
Powder	501	0.2480
Tablet (25 MPa)	502	0.2485
Tablet (50 MPa)	499	0.2414
Tablet (75 MPa)	479	0.2309
Tablet (100 MPa)	472	0.2175
Tablet (200 MPa)	436	0.2120
Tablet (300 MPa)	409	0.1885
Tablet (400 MPa)	311	0.1523

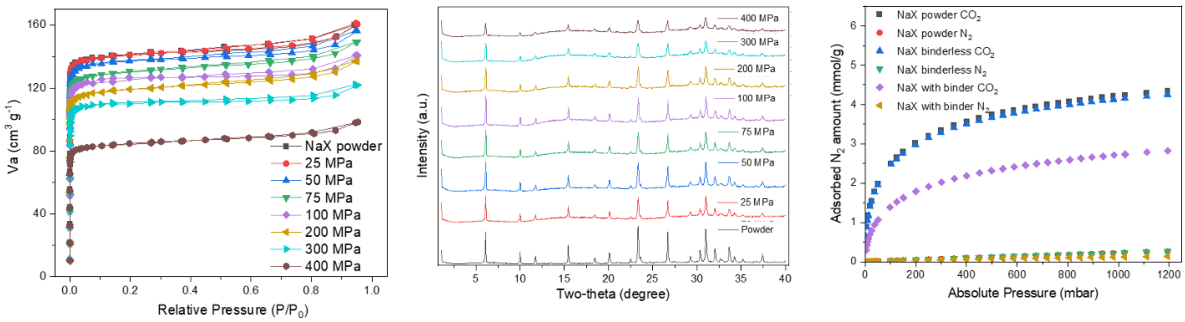


Figure 25: (left) N_2 adsorption isotherms taken at 77 K and used to calculate BET surface areas and pore volumes. (middle) PXRD patterns after tableting. (right) CO_2 and N_2 adsorption isotherms taken at 40 °C. The red dotted line corresponds to 0.15 bar, the partial pressure of CO_2 in post-combustion flue gas.

Notably, as observed from CO_2 adsorption isotherms at 40 °C (Figure 25), the capacity of binder-less tablets (2.78 mmol/g) at 0.15 bar is well-maintained. Unfortunately, when doing the friability tests, the binderless NaX tablet was found to be too fragile. Thus, the NaX powder was then mixed with various additives and then pressed into tablets to better bind the zeolite powder together. The additives also served as a plasticizing/lubricating agents, which enhances the rheological behavior in the press. After screening various possible additives, we were able to identify several binders that lead to robust NaX tablets, which was assessed via friability and crush strength tests (Table 5).

For the binder-based NaX tablet, the CO_2 adsorption capacity at 0.15 bar and 40 °C is 2.79 mmol/g and 1.50 mmol/g for the parent powder and tablet (a 46% capacity drop), respectively. Despite this, the CO_2/N_2 selectivity of the tablet (80) is well-maintained when compared to the powder (82). Unfortunately, the cellulose-based binder was not further explored because after activation the materials show

a very large decrease in surface area (Table 5). It was hypothesized that this decrease stems from the decomposition of the binder, which may lead to partial blocking of the zeolite pores. Notably, the zeolite requires a high activation temperature (e.g., 320 °C) to remove adsorbed water from the pores. Looking at the TGA results, obtained from the cellulose based binders, there is decomposition at low temperatures of 250~300 °C. Notably, at the activation temperature, there is an oily byproduct observed, which could possibly diffuse into the zeolite pores. In contrast, the second selected binder (betonite) was quite stable until heating to 400~500 °C according to the TGA curve; therefore, the N_2 and CO_2 adsorption performance of the zeolite in the tablet is not decreased as much by the binder 2 after activation.

Table 5: BET SA and pore volumes obtained from powder and tablets.

Material	BET surface area (m^2 g^{-1})	pore volume (cm^3 g^{-1})
NaX powder	501	0.2480
NaX tablet (no binder)	498	0.2458
NaX tablet with betonite	406	0.2222
NaX-Methyl cellulose	190	0.1196
NaX-Ethyl cellulose	---	-----
NaX-(Hydroxypropyl)methylcellulose	177	0.1392

Shaping and structuring Cr-BDC

Next, we set out to also structure the Cr-MOF via tableting using various pressures ranging from 50 to 300 MPa (details of the material synthesis and shaping can be found in Appendix WP2). Notably, the BET surface area drops significantly at higher pressure, particularly at 200 MPa where there is over a 20% reduction (Table 6, Figure 26), possibly indicating a loss in the MOF integrity. Despite this, the PXRD pattern still indicates that the material is crystalline at 200 MPa albeit there is a slight decrease in peak intensity (Figure 26). However, a full loss in the structural integrity is noted at 300 MPa as indicated by the disappearance of the peaks associated with crystalline Cr-MOF structure. This indicates that the material is becoming amorphous, and there is an even more significant decrease in the surface area. While the CO_2 adsorption (at 40 °C) capacity at 0.15 bar is not significantly affected by the pressure, we note that the CO_2 uptake of this MOF is already very low, likely making it more difficult to compare the loss (Figure 26)**.** Fortunately, the Cr-MOF tablets formed at 100 MPa, which still offer a high surface area, were found to be robust via friability tests and offer reasonable strength when the tablets during crush tests. Given this, it is the sample that we decided to move forward with in our studies.

Table 6: BET SA and pore volumes obtained from Cr-MOF powder and tablets.

Material (Pressure)	BET SA (m^2 g^{-1})	pore volume (cm^3 g^{-1})
Cr-BDC powder	3278	1.4409
Tablet (50 MPa)	3251	1.4310
Tablet (100 MPa)	2943	1.2849
Tablet (200 MPa)	2570	1.1242
Tablet (300 MPa)	1723	0.7608

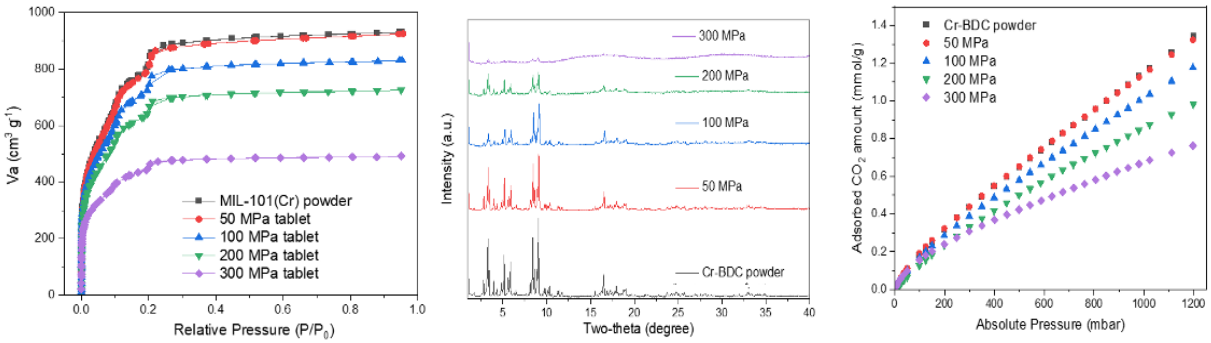


Figure 26: (left) N_2 adsorption isotherms at 77 K for the Cr-MOF powder and after pressing at different pressures. (center) PXRD patterns for the same samples. (right) CO_2 adsorption isotherms at 40 °C for the same samples.

Once the optimal tablet conditions were established, they were transferred to an automated high-throughput tablet press. Protocols for the pelletization using the industrial tabletting machine are found in Appendix WP2. The specifications for the high throughput tableting press (Figure 27) include the following:

- Makes 3 to 25 mm diameter tablet with ease;
- Produces up to 1,500 tablets per hour;
- Hopper holds up to 5 kg of sample;
- Is equipped with a transparent turret shield that provides operator safety (from fine powder inhalation) and prevents cross-contamination of powder between batches;
- Up to 100 kN pressure can be achieved for strong, properly finished pharmaceutical grade tablets;
- Tunable pressure;
- Safety shut-off button for emergencies.

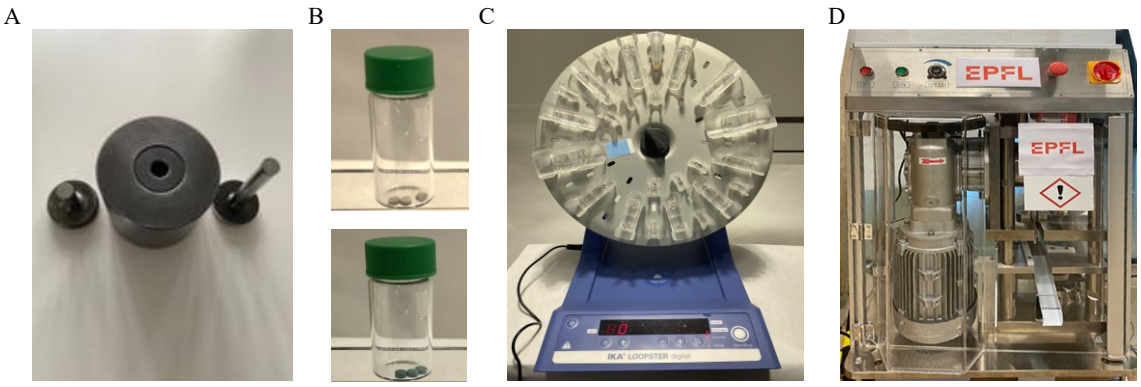


Figure 27: Image of the process flow for tableting from a (A) single punch press allowing variable pressures to be tested, (B) tablet formation, and (C) testing the friability of tablets using a rotary wheel, to (D) the automated, high throughput tableting press that can operate under continuous flow, with up to 1,500 tablets per hour produced.



Figure 6: Pellets of Cr-BDC.

Cr-BDC (also MIL-101(Cr)) pellets were produced from the industrial tableting machine at various pressures (Figure 28) and their BET surface area determined from Figure 29. The surface areas and pore volumes derived from the N_2 adsorption isotherms are shown in Table 7. For example, for pressure 1, the pores collapse fully; however, lower pressure 3 has minimal to no impact on the surface area, and the Cr-MOF pellets are found to be robust.

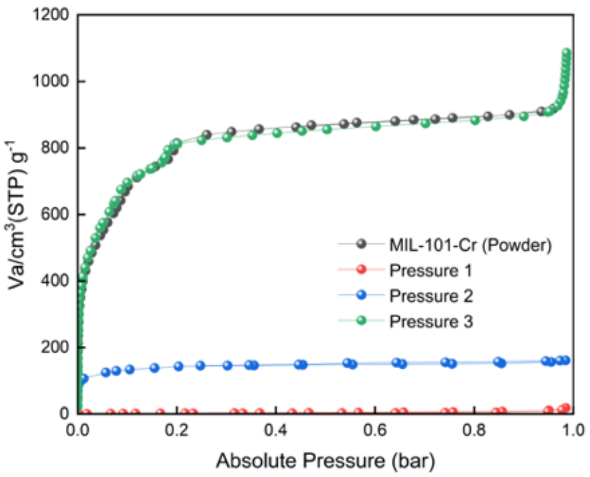


Figure 29: N_2 isotherms at 77 K of MIL-101-Cr pellets from the industrial tableting machine.

Table 7: Surface areas and pore volumes determined from pellets made from the industrial tableting machine at varying pressure.

Pressure	Surface Area (m^2/g)	Pore Volume (cm^3/g)
Powder	2800	1.6793
Pressure 1	7	0.0278
Pressure 2	516	0.2493
Pressure 3	2700	1.4194

To date, we have developed a strategy to structure both the NaX, Cr-MOF, and Cr-MOF-amine composite; however further tests in adsorption cycling experiments are needed to see how robust the tablets are, particularly in the presence of humidity and over extended periods of time with extensive cycling. Further, we note that the density of the NaX (0.54 g/cm^3) and the Cr-MOF (0.179 g/cm^3) are increased by approximately a factor of 3 during tablet formation to 1.49 g/cm^3 and 0.53 g/cm^3, respectively (Table 8). Very dense structures could inhibit accessibility of the CO_2 to the inside the tablet leading to low performance under continuous flow. On the contrary, this higher density can also improve volumetric capacity in the separation process. So, assessing such materials in flow in the future is also important.

Shaping other MOFs

To explore the general applicability of the tableting method, the structuring process was extended to a group of structurally diverse MOFs/zeolites, that are of interest for CO_2 capture applications. Their synthesis protocols can be found in Appendix WP2. So, we have included several other materials, particularly several MOF physisorbents, such as Mg-dobdc, SIFSIX-3, CALF-20, and Al-formate (details of the material synthesis and shaping can be found in Appendix WP2). Table 8 shows a comparison between the properties of NaX and Cr-MOF tablets with these CO_2 adsorbents. The table includes the selected tableting approach (with or without binder), the pressure at which the best performing tablets were formed, and also results from crush tests, friability, and density measurements for each material. Further, Table 8 shows comparisons of the gravimetric and volumetric CO_2 adsorption capacity (40 °C and 0.15 bar) of the best performing tablet for each adsorbent, and this value is compared against those of the parent powder. Notably, in all cases, for the tested MOFs and zeolites, the gravimetric capacity decreases, an observation that could stem from loss of material integrity and/or the added mass of dense binders. On the contrary, the volumetric capacity increases by factors ranging from 1.78 to 4.24, depending on the identity of the starting material. This is important as high volumetric capacities could permit smaller adsorbent bed volumes, a factor that could also help reduce the energy consumption of the separation process.

Table 8: Shows gravimetric and volumetric CO_2 adsorption capacity at 0.15 bar and 40 °C for various tableted adsorbents.

Materials	Tableting method	Powder gravimetric capacity (mmol/g)	Tablet gravimetric capacity (mmol/g)	Decrease	Powder volumetric capacity (mmol/cm^3)	Tablet volumetric capacity (mmol/cm^3)	Increase (times)
NaX	With binder	2.70	1.63	39%	1.02	2.08	2.04
Cr-MOF	Binder-free	0.23	0.22	4%	0.041	0.117	2.85
Cr-MOF-NH_2	Binder-free	0.32	0.277	13%	0.049	0.208	4.24
Al-formate	With binder	0.90	0.62	31.2%	0.448	0.925	2.06
CALF-20	With binder	2.20	1.4	36.4%	0.981	2.09	2.13
SIFSIX-3-Ni	With binder	1.75	1.15	34.3%	0.663	1.674	2.52
Mg-dobdc	Binder-free	3.87	2.14	45%	1.598	2.838	1.78

Shaping and structuring – Cr-BDC containing an amine

To prepare amine-MOF composites for use in the demonstrator column, pellets were made without external binders, since binders reduce CO_2 capacity. Instead, we explored whether the amine–epoxide chemistry inside the MOF could also act as an binder. The Cr-MOF-amine composite was pressed into 8 mm pellets at 60–90 MPa. Interestingly, we observed a drop in CO_2 adsorption capacity after applying pressures of 60 and 90 MPa from the original 2.2 mmol/g to 1.5 mmol/g at 0.15 bar and 40 °C (Figure 29). While this reduction could be attributed to a partial collapse of the MOF during tableting, we note that the parent Cr-MOF treated at 50 MPa and 100 MPa shown above (Figure 26, Table 6) reveals

almost no change to a minimal change in the surface area after compression, respectively. This implies that the MOF is mechanically robust in this pressure regime, 0-100 MPa. Given this, the drop in the CO_2 adsorption performance is more likely to stem from lower access to amines in the MOF pores, which could decrease the CO_2 adsorption capacity. Despite that the gravimetric CO_2 capacity decreased, tableting increased the bulk density of the adsorbents by ~three-fold, which is important for real reactors. The volumetric CO_2 capacity increased by 1.8–4.2 times, meaning more CO_2 can be captured per unit reactor volume (details of the shaping can be found in Appendix WP2). However, in the case of amine-functionalized MOF, we also note that the materials become quite sticky, adhering to the die and causing pellets to break during ejection. This issue could be solved with die coatings or alternative shaping methods once more composite material becomes available. Given this, we will likely need to employ die coatings to reduce surface adhesion or other structuring methods in the future. Once more of the Cr-MOF TEPA-TMPTE is produced, efforts can be better made to optimize the structuring protocol for the composite in the future.

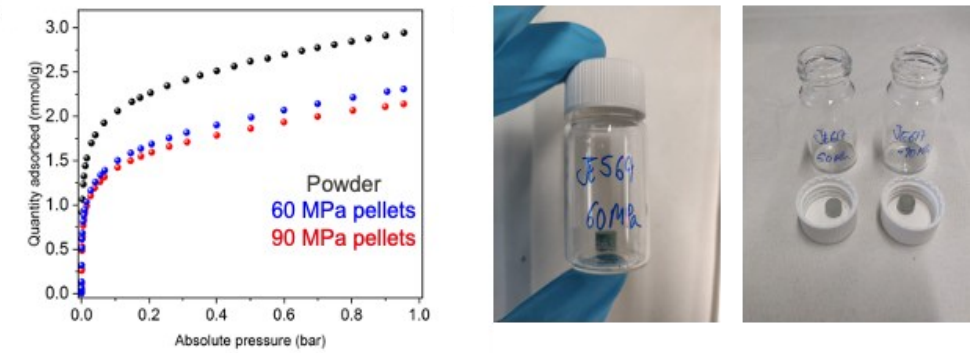


Figure 30: (left) CO_2 isotherms at 40 °C for the structured MOF composites. Different pressures were applied, 60 MPa (blue) and 90 MPa (red) compared to powder (black). (right) Pictures of the final 8 mm diameter pellets obtained.

Amine-grafted mesoporous silica, KIT-6

In this project, a mesoporous silica was also post-synthetically modified with amines. Silicas were selected because they are chemically robust and offer large pore apertures, which allow amines to readily go inside. Notably, the use of silicas with larger pore volumes, such as KIT-6, favor higher loadings and permit the use of larger amine-containing polymers like polyethyleneimine (PEI, Mw 800). So, we scaled-up the synthesis of KIT-6, judiciously selecting a method that leads to the highest pore volume.[16] It is well described that the use of different temperatures during the hydrothermal synthesis of KIT-6 promotes different nucleation around the templating agents, which directly impacts the pore volume. Given this, we have used 135 °C for the temperature synthesis, which provides a final pore volume >1 cm^3/g. We scaled-up the reported procedure to the 2 L scale and then repeating this procedure multiple times, to accumulate the desired amount of KIT-6 silica. On average, each 2 L reaction yielded ~21 g of final KIT-6, and ~1.2 kg of final material was accumulated (Figure 31, details of the silica synthesis can be found in Appendix WP2).



Figure 7: Accumulated KIT-6 from 2 L reactions, yielding to ~1 kg of total silica.

The quality of the successive batches was assessed via N_2 adsorption at 77 K. By increasing the scale of synthesis and calcination, we obtained silica with a high pore volume of ~1 cm^3/g and a BET surface area of ~560 m^2/g. We also used small-angle X-ray scattering (SAXS) to identify the main peak below 1°, which confirms the proper structure of the silica (Figure 32). This lab-made scale-up protocol leads to a cost of 921.37 CHF/kg (Table 9), which is at least 10 times lower than purchasing 1 kg of KIT-6 silica on the market (~9000 CHF/kg, Table 10).

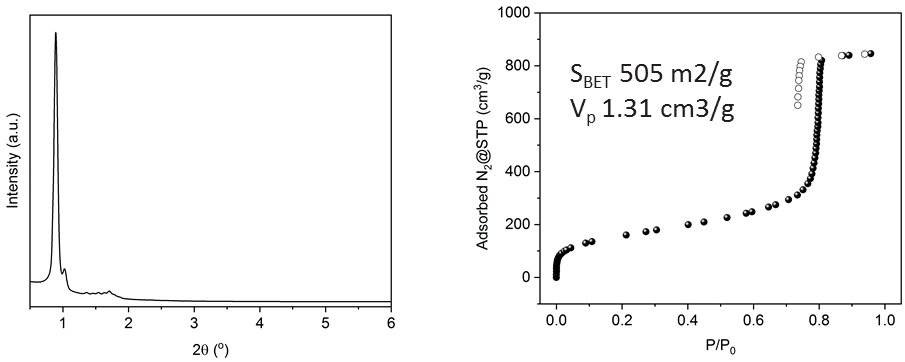


Figure 8: (left) Small-angle X-ray scattering K of the bare KIT-6 silica. (right) N_2 isotherm at 77 K of the bare KIT-6 silica.

Table 9: Price of reagents for the KIT-6 silica synthesis at the lab scale.

Reagent	**Quantity (kg)**	**Price (CHF/kg)**	**Price (CHF)**
TEOS	4.085	135.66	**554.10**
P123	1.901	118.50	**225.32**
HCl	3.676	18.08	66.46
1-butanol	1.901	39.70	75.49

Table 10: Prices of commercial KIT-6 silica sold by three different companies.

Company	**Price (CHF/kg)**
MSE	9904 CHF/kg
ACS	8996 CHF/kg
Matexcel	24120 CHF/kg

The synthesized KIT-6 silica was then grafted with an amine-containing polymer (PEI, Mw 800) in a two-steps: the silica was reacted with 3-glycidoxypropyltrimethoxy silane and then with PEI, allowing the PEI to become covalently tethered to the silica support, as shown in Figure 33 (details of the modification can be found in Appendix WP2). Figure 34 shows that the grafted silica has a CO_2 capacity of 1.48 mmol/g at 0.15 bar and 40 °C, which is also retained after reactivation and a second CO_2 adsorption cycle (1.44 mmol/g). Most reported grafting procedures required high-vacuum activation prior to grafting, and anhydrous toluene as a solvent. To enable a more practical and scalable process, we simplified these conditions: KIT-6 was used as synthesized (without activation), and toluene was employed without drying. The reaction scale was also increased from 100 mg to 5 g of silica. The resulting composite exhibited a CO_2 adsorption capacity of ~1 mmol/g at 40 °C, which was fully regenerated by heating to 100 °C under N_2 flow (Figure 34). The baseline remained stable over multiple adsorption–desorption cycles, indicating that PEI was covalently anchored to the silica support. This tethering prevents amine leaching and ensures retention of the CO_2 capacity across repeated cycles. However, the resulting CO_2 working capacity, achieved via temperature swing adsorption in the TGA was slightly lower than what was determined via adsorption isotherms (~1.4 mmol/g at 0.15 bar) indicating that the overall capacity was reduced with scaling. For example, there may be poorer heat exchange or diffusion in the porous materials during the grafting step when working with larger batches of solution.

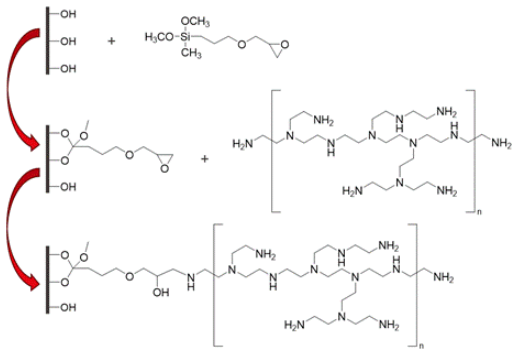


Figure 9: 2-step grafting method of polyethyleneimine onto the pores of KIT-6 silica.

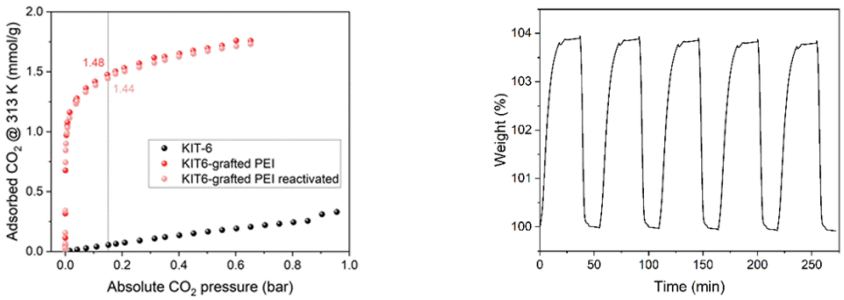


Figure 34: (left) CO_2 adsorption isotherms of PEI-grafted KIT-6 silica collected at 40 °C. (right) Adsorption-desorption cycles of PEI-grafted KIT-6 silica, at 40 °C under 15% N_2 and 85% CO_2.

To tackle the issue related to the scale up synthesis, we also tried a continuous flow method for the amine grafting. In this method, the grafting agent and the porous silica support are continuously pumped through a heated reactor, allowing for a continuous output stream of the grafted product (Figure 35). This is in contrast with the batch reactions previously tried, where both reactants were mixed in a closed vessel until completion of the reaction. Continuous flow methods are known for leading to better heat and mass transfer in chemical reactions, resulting in faster reactions, or to safer reactions, thanks to the small reaction volumes at each given time point. This method is also directly scalable, as one can produce more grafted silica by having more reactants in the input of the reactor.

Unfortunately, we find the reactor tubing gets clogged quite rapidly and stops the process, maybe steming from a very fast reaction and interparticle crosslinking of the KIT-6 via the grafting agent. We are currently trying to tune the reaction parameters, to enhance the diffusion of the grafting agent inside the pores, to increase the surface functionalization of the pores, rather than interparticle crosslinking. Such an optimization involves tuning the temperature, the flow, and the solvent of the reaction.

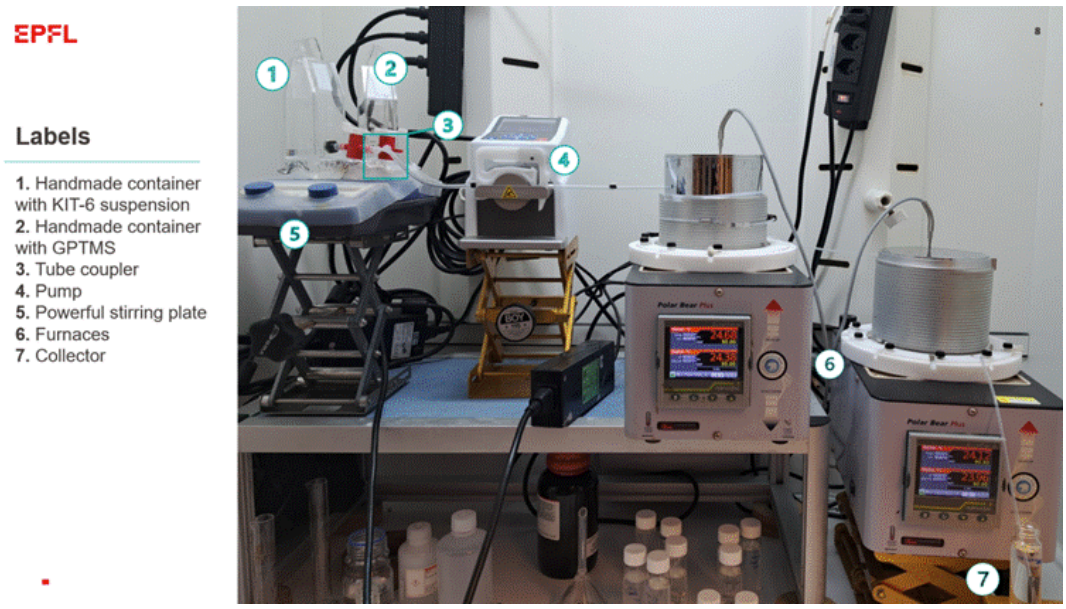


Figure 10: Continuous flow set-up for the grafting of KIT-6 with GPTMS.

Shaping the KIT-6 composite

It was hypothesized that the amines would also act as a binder and help structure the amine-grafted silica during a subsequent pelletization step. To assess the stability of the obtained pellet, the pellet was made and placed inside a rotary friability machine, which was rotated 100 times at 25 rpm. We inspected for visible signs of breakage during the rotations and weighed the largest part of the pellet before and after the rotations allowing us to qualitatively assess pellet robustness. We tested pellets obtained from the bare KIT-6 and the amine impregnated KIT-6. As expected, we found the amine indeed plays a binding role, as shown in Figure 36: in fact, the pellet produced from the pressed silica powder crumbles as soon as it is removed from the die used for pressing. On the other hand, the pellet obtained from the amine-grafted silica is robust and able to sustain 100 rotations in a friability device without breakage (details of the shaping and friability tests can be found in Appendix WP2).



Figure 11: (left) Pellet of bare KIT-6. (right) PEI-grafted KIT-6.

Nitrogen-rich microporous carbons

In parallel to the main scale-up projects, we also worked on developing new nitrogen-doped porous carbons. The carbon materials are known to be chemically and thermally stable, good thermal conductors, and have physisorptive interaction with CO_2, which are promising features for a long-term use and reduced energy needs in a temperature swing adsorption CO_2 capture processes. However, most carbons suffer from a low CO_2 capacity and are difficult to functionalize given their inert nature. Therefore, our group developed a bottom-up approach to form nitrogen-doped carbons by pyrolyzing nitrogen-rich coordination polymers, made up of cobalt and and 3,8-dibromo-1,10-phenanthroline. This results in highly porous carbon having a high N-content (12.2 %) and a CO_2 adsorption capacity at 40 °C and 0.15 bar of 1.1 mmol/g, which is twice that of existing commercial carbons, Norit (0.54 mmol/g) and Filtrasorb-400 (0.47 mmol/g). We note this high-capacity stems from a high density of micropores (>70%), which we believe is owed to the small pores of the parent coordination polymer. This, combined with the high N-content, boosts the binding energy of CO_2 inside the carbon pores. Notably, in addition to the heightened CO_2 adsorption capacity, we have shown that the material performs well in separating CO_2 from N_2, even after being pretreated under highly humid conditions for 2 hours via breakthrough experiments (Figure 37). Importantly, the cyclability of this carbon adsorbent was fully retained for 100 cycles (Figure 37). Moreover, cobalt can be recycled and reused to remake the coordination polymer post pyrolysis. This work was published in *Advanced Functional Materials* in 2023.[17] After the report, we also optimized a similar synthetic protocol with cheaper monomers, featuring a bipyridine core instead of a phenanthroline one (2,2"-bipyridine, bipyrimidine, 5,5"-dibromo-2,2"-bipyridine and 4,4"-dibromo-2,2"-bipyridine, as shown on Figure 38). This resulted in carbons with a CO_2 capacity of up to 1.2 mmol/g, slightly higher than the previous reported phenanothroline monomer, while cutting the cost by a factor of 3.5 (Figure 38).

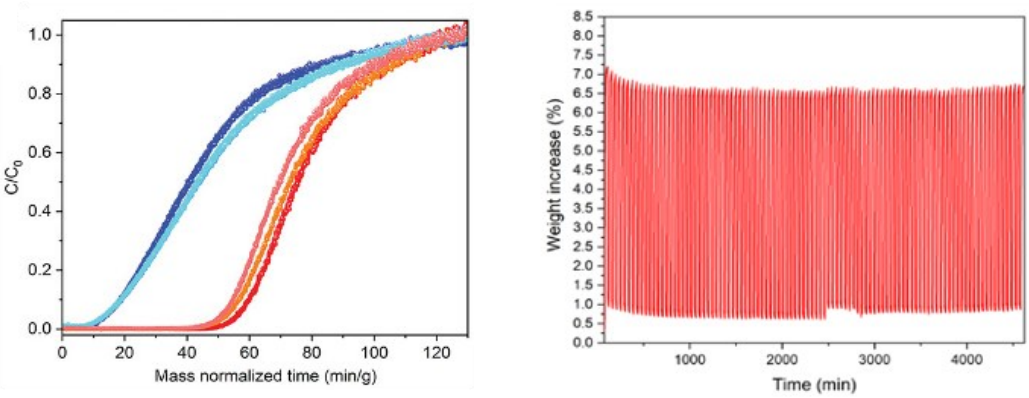


Figure 12: (left) Breakthrough plot using a 15% CO_2 and 85 % N_2 gas mixture at 40 °C under dry (N_2 in cyan and CO_2 in red), humid 80% RH gas mixture (N_2 in blue and CO_2 in orange) and pre-saturating the bed with humid He prior to the start of the experiment (N_2 in light blue and CO_2 in pink). (right) 100 cycles of CO_2 adsorption/desorption using TGA (adsorption at 40 °C for 30 min, desorption at 120 °C for 15 min using dry CO_2).

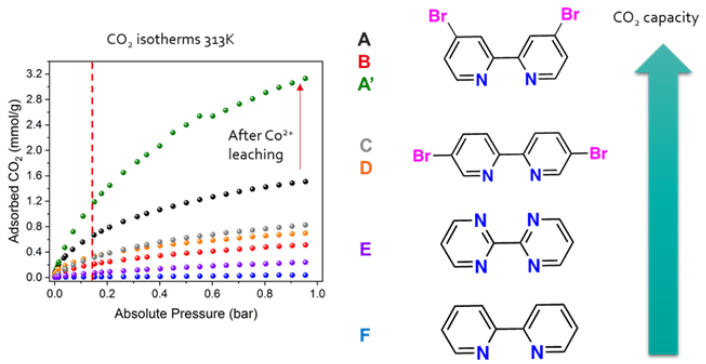


Figure 13: (left) CO_2 adsorption isotherms at 40 °C from various (right) monomers combined with $Co(NO_3)_2$.$6H_2O$ and carbonized at 600 °C.

Carbon-amine composite and structuring

Porous carbons were also studied as supports for amine impregnation, as they show remarkable thermal and chemical stabilities, as well as a high thermal conductivity, which could lead to lower energy consumption during TSA processes. Furthermore, unlike MOFs, carbon materials often do not possess metals that can catalyze the degradation of amines, the active species responsible for CO_2 adsorption.

We chose to work with a chitosan-based mesoporous carbon, because of its large mesoporosity (> 2.5 cm^3/g with a pore size around 12 nm) that allows for a high amine loading. Also, this carbon is based on a low-cost and bio-based polymer. A similar ship-in-a-bottle amine-epoxide crosslinking approach was used, aiming at a reduced amine leaching and thus performance loss during repeated usage (details of the carbon synthesis and amine impregnation can be found in Appendix WP2).

To assess the in-situ crosslinking of the amine and epoxide monomers, solid-state ^{13}C NMR was used (Figure 39). The polymer was also extracted from the carbon via methanol Soxhlet over 3 days, and the resulting amine-containing solution was characterized via ESI-MS analysis. ^{13}C NMR data presented in Figure 39 shows evidence of the crosslinking reaction. The NMR spectrum shows a peak at 71.5 ppm, that is associated with the opening of the epoxide ring during the reaction of TEPA with BDE (the carbon highlighted in red in Figure 40 below has a simulated chemical shift of 73.1 ppm). This peak does not appear either for the simulated TEPA monomer on Figure 41 (with characteristic chemical shifts δ 41.6 (2C, s), 49.6-49.6 (4C, 49.6 (s), 49.6 (s), 52.2 (2C, s))) or the BDE monomer (with chemical shifts of 44.2 (2C, s), 51.3 (2C, s)). Only after reaction of TEPA and BDE can this characteristic peak be seen: TEPA-BDE has chemical shifts δ 41.6 (1C, s), 45.6 (1C, s), 49.6-49.6 (6C, 49.6 (s), 49.6 (s), 49.6 (s), 49.6 (s), 49.6 (s), 49.6 (s)), 50 (1C, s), 52.2 (1C, s), 53.5 (1C, s), **73.1** (1C, s).

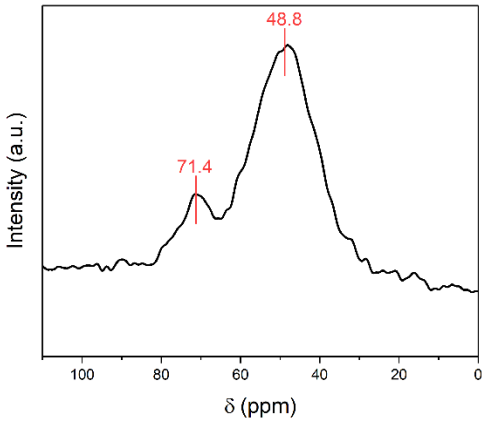


Figure 39: Solid-state ^{13}C NMR spectrum of TEPA-BDE impregnated chitosan-derived carbon.

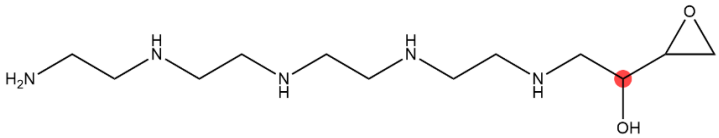


Figure 40: Structure of a TEPA-BDE dimer.

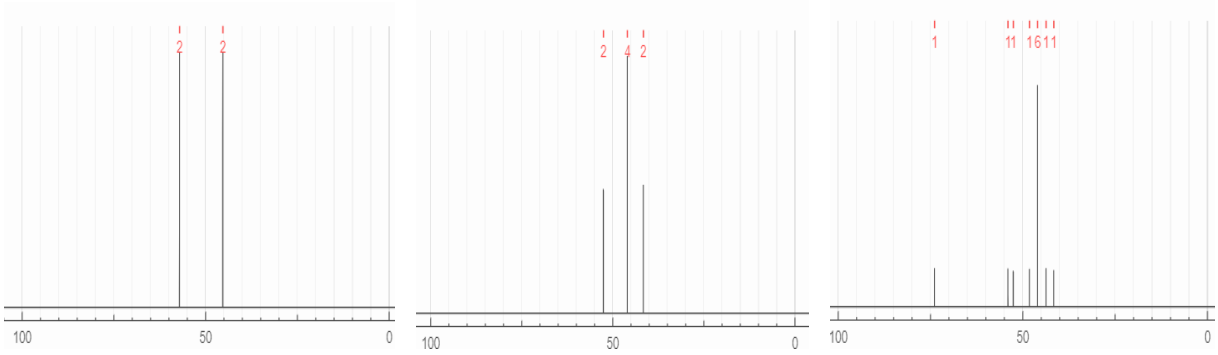


Figure 14: Predicted ^{13}C spectra of (left) BDE. (middle) TEPA. (right) TEPA-BDE.

Furthermore, ESI-MS (Figure 42 left) shows a clear shift from low m/z for TEPA (in red) to higher m/z for TEPA-BDE (in blue). The plot shows characteristic peaks of TEPA-BDE oligomers, such as a trimer consisting of 2 TEPA and 1 BDE (at 465.1) and a tetramer consisting of 2 TEPA and 2 BDE (at 549.5). This demonstrates the formation of longer polymers from the TEPA and BDE monomers. As expected, the crosslinking helped to retain the amines inside the porous carbon framework, leading to a higher cyclable CO_2 capacity. This can be seen from the repeated temperature swing cycles (Figure 42 right). Carbons containing the crosslinked TEPA-BDE polymers showed no loss of polymer during the cycles (flat baseline), while the one impregnated with TEPA monomers only showed a significant weight loss. The amine loss is apparent from the very first few cycles and stems from the small, low-molecular weight TEPA monomers flying out of the support. While CDMC better retains the crosslinked amines (TEPA-BDE polymer) than non-crosslined amines (TEPA), the CO_2 uptake during cycling is also much lower for CDMC-TEPA-BDE than that observed for the Cr-BDC-amine-based composites (see Figure 3). This likely stems from the microporosity of the MOF (pores < 2nm), which we believe better traps the amines inside the MOF relative to the mesoporous carbon (pores > 2nm).

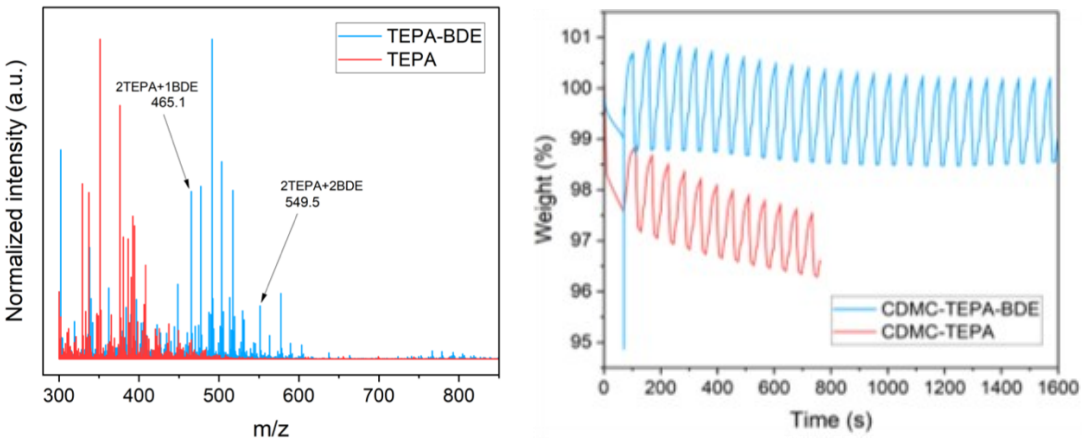


Figure 15: (left) ESI-MS spectra and (right) temperature swing adsorption cycles under 40 °C adsorption and 120 °C desorption with pure CO_2, of TEPA and TEPA-BDE impregnated carbon.

The TEPA-BDE impregnated carbons were subsequently structured using an industrial tableting machine. The stability of the obtained pellets was assessed via friability tests carried out in a device in our lab. The carbon pellets impregnated with TEPA-BDE showed good stability during friability tests, as the pellets experienced no weight loss over the course of 100 cycles indicating the pellets are robust (Figure 43). This was not the case for the pressed carbon excluding amines and epoxides, which crumbled back into powder as soon as it was removed from the die.

The pressed carbon containing TEPA-BDE had a decreased gravimetric CO_2 capacity (Figure 44) compared to the parent powder (1.8 mmol/g instead of 2.3 mmol/g, details of the shaping and friability tests can be found in Appendix WP2). This could stem from pore compression, reducing accessibility of CO_2 to the amine groups inside. It could also stem from additional crosslinking that may occur between amines and epoxides, further reducing the number of primary amines inside. However, the reduction of the gravimetric capacity is compensated by the increased density of the powder once pelletized' this leads to a similar volumetric CO_2 capacity before and after pressing (the volumetric capacities of both the powder and the pellet are ~0.4 mmol/mL).



Figure 16: (left) Pellet of carbon-TEPA-BDE before and after friability test and (right) pressed carbon powder.

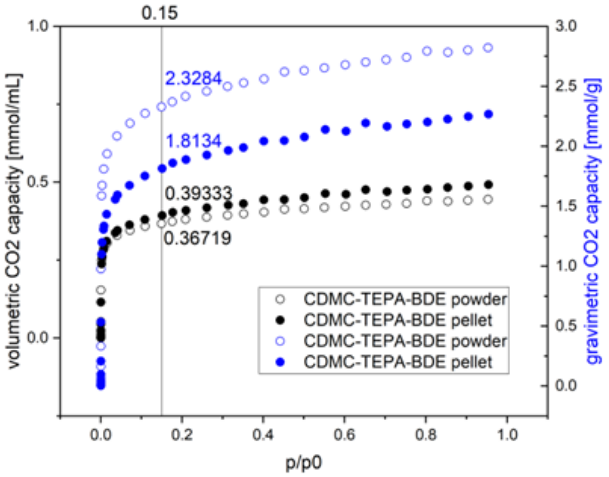


Figure 17: Gravimetric (blue) and volumetric (black) CO_2 adsorption capacity of carbons impregnated with TEPA-BDE at 40 °C.

2.3 WP3 Technoeconomic assessment to investigate for the viability of CO_2 capture process

The objective of WP3 was to develop and apply a dynamic process modelling framework to evaluate adsorption-based CO_2 capture processes, with a primary focus on zeolite 13X as the benchmark adsorbent, while also enabling comparison with the laboratory-developed MOF–amine composite adsorbent. The modelling framework was formulated to capture the transient behaviour of cyclic adsorption processes and to quantify key performance indicators relevant for process design and techno-economic assessment (TEA).

Within WP3, temperature-based adsorption processes were investigated, specifically temperature swing adsorption (TSA), temperature-concentration swing adsorption (TCSA), and temperature-vacuum swing adsorption (TVSA). TSA relies on cyclic heating and cooling of the adsorbent bed to achieve regeneration, making it particularly attractive in applications where low-grade or waste heat is readily available. Building on TSA, a concentration purge step was introduced to form the TCSA configuration, which enhances desorption by flushing the bed with a CO_2-rich stream during regeneration. TVSA further extends this concept by adding vacuum-assisted desorption to the framework, combining thermal regeneration, and vacuum to maximise CO_2 working capacity and separation performance. In addition, steam-assisted TSA (SA-TSA) was included as a reference configuration within the environmental assessment, drawing on literature-reported energy and process data, to provide a broader basis for comparison across temperature-swing process variants.

Model validation was first conducted using a TSA configuration to establish confidence in the predictive capability of the dynamic framework. Two complementary validation approaches were employed. First, the model was validated against experimental data obtained from a pilot-scale adsorption unit. Second, key model predictions were benchmarked against representative results reported in the open literature to ensure consistency with established experimental and modelling trends.

Following successful validation, the modelling framework was progressively extended, first to TCSA and then to TVSA. To identify the most suitable process configuration for industrial deployment, TSA, TVSA, and SA-TSA were comparatively evaluated through life-cycle assessment, estimating the carbon capture efficiency as a measure of net CO_2 captured after accounting for process-related emissions. This environmental screening confirmed TVSA as the preferred configuration, on the basis of its lowest carbon footprint and highest carbon capture efficiency among the three alternatives evaluated. The pilot-scale TVSA simulations further demonstrated that, under optimized operating conditions, the process achieved promising separation performance, meeting the DOE recovery target of 90% while approaching the 95% purity threshold. Having established both environmental suitability and process feasibility at pilot scale, the validated and optimized TVSA framework was subsequently applied to an industrial-scale assessment for a representative municipal solid-waste incineration facility using zeolite 13X, from which process performance indicators and energy requirements were extracted as direct inputs to the TEA. In parallel, the MOF–amine composite adsorbent was evaluated through pilot-scale TVSA process modelling, to assess whether DOE performance targets could be achieved, and through life-cycle assessment, to identify dominant environmental hotspots and improvement opportunities for this emerging material class.

Accordingly, the analysis conducted in WP3 comprised the following sequential steps:

(i) development and validation of a TSA process configuration, which served as the baseline and validation framework for the dynamic modelling approach;

(ii) progressive extension of the validated framework, first to TCSA through the introduction of a concentration purge step, and then to TVSA through the addition of vacuum-assisted desorption, followed by comparative environmental screening of TSA, TVSA, and SA-TSA through life-cycle assessment to identify the most sustainable configuration, noting that SA-TSA was assessed as a reference configuration for comparision;

(iii) selection of TVSA as the preferred configuration on the basis of the LCA screening, and optimization of its operating conditions at pilot scale to identify feasible and representative operating points;

(iv) pilot-scale simulation of the optimized TVSA process to evaluate CO_2 purity and recovery against U.S. DOE performance targets, demonstrating promising separation performance and establishing process feasibility prior to industrial-scale assessment;

(v) application of the optimized TVSA framework to a municipal solid-waste incineration case study using zeolite 13X, from which process performance indicators and energy requirements were extracted as inputs to the techno-economic assessment;

(vi) pilot-scale process modelling and life-cycle assessment of the MOF–amine composite adsorbent integrated into the TVSA framework, to evaluate separation performance against DOE targets and to identify key environmental hotspots and improvement opportunities.

TSA process development and model validation

The performance of TSA cycles was governed by strongly coupled transient phenomena, including adsorption heat effects, axial temperature gradients, pressure transients under vacuum, and mass-transfer rates. As a result, steady-state separator models are insufficient to represent cycle performance. Therefore, employing a dynamic cyclic modelling approach, enables direct computation of cyclic steady-state behavior for each operating condition considered. At cyclic steady state, the model quantified the following key performance indicators (KPIs): CO_2 product purity, CO_2 recovery, process productivity, specific energy consumption, which includes thermal and electrical contributions. Electrical energy demands included vacuum generation and auxiliary compression or blowing, while thermal energy requirements were associated with regeneration and heating steps.

TSA was investigated as the baseline process configuration and served as the primary case for model validation. TSA is a well-established adsorption-based CO_2 capture process in which adsorption and regeneration are driven by cyclic temperature variations. In typical post-combustion applications, CO_2 is adsorbed from flue gas at moderate temperatures (~40-60 °C), while regeneration is achieved by increasing the bed temperature, commonly in the range of 80-200 °C depending on the adsorbent material.

Regeneration in TSA systems is predominantly achieved through indirect heating of the packed bed. Common heating configurations include external jackets, electrical heating elements, or internal or external heat-exchange tubes circulating hot and cold fluids. This regeneration step is energetically dominant and has been reported to account for a substantial fraction of the total process energy demand. As a result, TSA performance is highly sensitive to regeneration temperature, heating strategy, and thermal management within the adsorption column.

In the present work, the TSA cycle was implemented with three distinct steps (Figure 45):

1. Adsorption, carried out at a designated adsorption temperature (T_{ads});
2. Regeneration, achieved by indirect heating of the bed to a higher desorption temperature (T_{des}) to release adsorbed CO_2;
3. Cooling, during which the bed was returned to adsorption conditions prior to the next cycle.

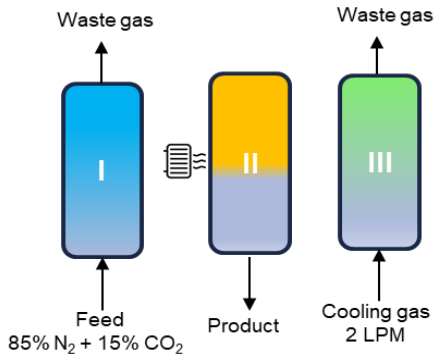


Figure 18: Schematic representation of the TSA cycle.

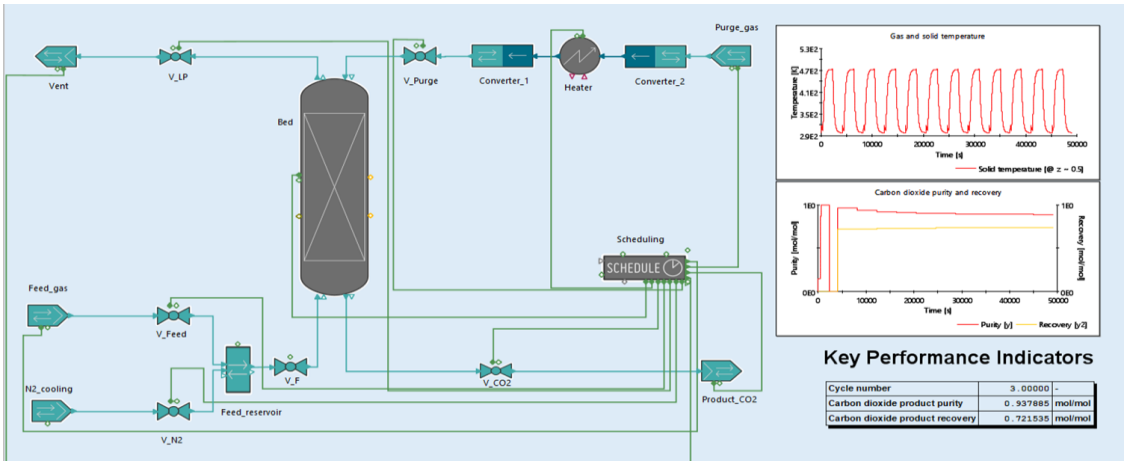


Figure 19: TSA process implementation in the gPROMS simulator.

For the purpose of initial model validation, NaUSY (sodium-exchanged ultra-stable Y zeolite) was selected as the adsorbent. This choice was motivated by the higher availability of literature data over zeolite 13X,[18] including adsorption isotherms and heats of adsorption, which enabled a transparent and reproducible validation exercise. All relevant thermodynamic and kinetic parameters were taken from the literature. The modelling was carried out using gPROMS.[19] Model predictions were compared against reported experimental data for CO_2 purity and recovery over a range of regeneration temperatures.

As shown in Table 11, the simulated results agree well with experimental values, with consistently low deviations across all operating conditions investigated. This agreement confirmed that the model accurately captured the dominant transport and thermal phenomena governing TSA performance.

Table 11: Comparison of simulated and experimental TSA performance in terms of purity and recovery.

Simulated			Reported (Experimental)		Deviation	
Temp (°C)	Purity (%)	Recovery (%)	Purity (%)	Recovery (%)	Purity (%)	Recovery (%)
150	91.72	54.10	91.21	53.24	0.05	1.21
200	92.23	72.86	91.36	76.60	0.87	3.74
250	93.61	86.18	91.68	88.27	1.93	2.09

In addition to separation performance, the specific energy consumption of the TSA process was evaluated as a function of regeneration temperature (Table 12). At a regeneration temperature of 150 °C, the simulated specific energy consumption was approximately 2.68 MJ kg^{-1} CO_2, which is lower than values typically reported for state-of-the-art liquid amine-based absorption processes, such as monoethanolamine (MEA), where energy requirements of approximately ≥ 4 MJ per kilogram of CO_2 captured.[20] This difference is primarily attributed to the lower effective heat capacity of the solid adsorbent system, as well as the absence of large solvent inventories that must be heated and circulated in liquid absorption processes. As a result, sensible heat requirements are reduced, thereby leading to lower energy consumption.

Table 12: Simulated TSA performance in terms of productivity and energy consumption.

Temp (°C)	Productivity (kg CO_2/kg adsorbent.h^{-1})	Energy consumption (MJ/kg CO_2)
150	0.40	2.68
200	0.53	2.75
250	0.61	2.92

A second validation exercise was performed using breakthrough experiments conducted with dry flue gas mixture containing 15 % CO_2 and 85 % N_2.

The experimental feed flow corresponded to 3116 mL·min^{-1} of N_2 and 543 mL·min^{-1} of CO_2 .CO_2 breakthrough (Figure 47) was observed at approximately 35 minutes, closely matching the simulated prediction of 33 minutes. A minor discrepancy was noted in the slope of the breakthrough curve: the experimental profile exhibited a more gradual transition, whereas the simulation produced a sharper front. This difference is attributed to dispersion effects within the packed bed and dead volumes in the pilot plant, which broaden the experimental response but are not fully captured by the model. Despite these differences, the model is considered reliable, as it accurately reproduces the breakthrough time and therby providing confidence in its predictive capability for evaluating purity, recovery, and cycle performance under varying operating conditions.

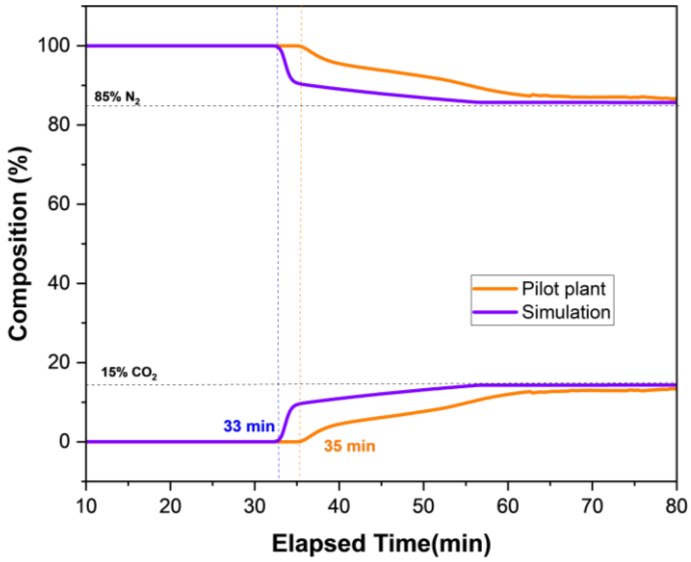


Figure 20: Comparison of experimental and simulated CO_2 breakthrough curves for a 15% CO_2 / 85% N_2 flue gas mixture. Experimental breakthrough occurred at ~35 minutes versus the model prediction of 33 minutes, demonstrating good agreement and validating the TVSA model.

Building on the previous work where the TSA model was successfully developed and validated using NaUSY, we have further developed models for both the temperature swing adsorption with purge, referred as TCSA (Temperature Concentration Swing Adsorption) and TVSA (Temperature-Vacuum Swing Adsorption) processes, incorporating a vacuum step for adsorbent bed regeneration. These models were then used to simulate data for zeolite 13X as the adsorbent material. The sustainability of these processes were also evaluated through a life cycle assessment (LCA), with the goal of reducing the environmental impact.

TVSA process development and configuration

As outlined above, the modelling framework was progressively extended from TSA to TCSA and then to TVSA. This section describes the process configurations and model formulation for both TCSA and TVSA. The TCSA process encompasses four-step cycle, which includes adsorption, desorption through heating, purge, and cooling (Figure 48). The TCSA process model has been developed using the gPROMS modeling tool that solves conservation equations including mass, energy, and heat balances. The relevant equations along with adsorbent properties including its isotherm characteristics, density, specific heat, interparticle and intraparticle voidage were derived from the literature.

The following modelling assumptions apply to both the TCSA and TVSA configurations:

- Ideal gas behavior
- Negligible radial heat and mass transport phenomena
- No axial conductivity along the wall
- Mass transfer resistance is described by the linear driving force model (LDF)
- Temperature-independent mass transfer coefficients, isosteric heats of adsorption and heat capacities of the solid phase and the wall.
- Adsorption equilibrium described by the dual site Langmuir isotherm with temperature dependence

- Non-isothermal with no conduction
- Thermal equilibrium between the fluid and the adsorbent particles

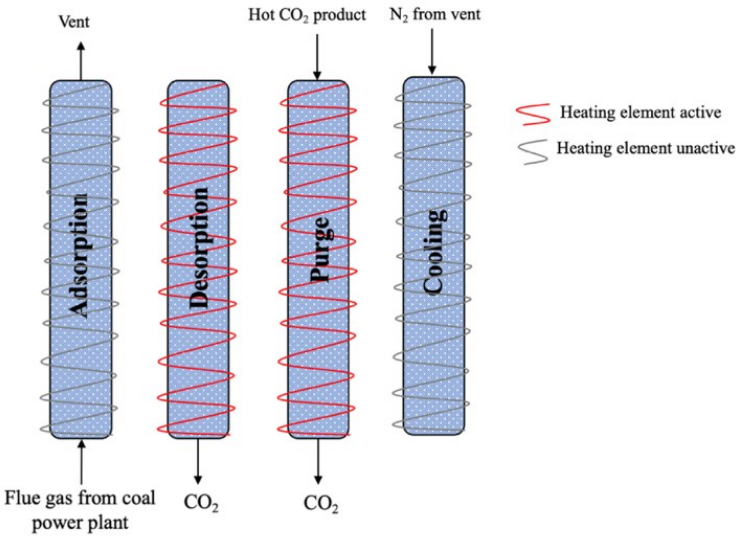


Figure 48: A schematic of four-step TCSA cycle for post-combustion carbon capture.

The model uses numerical method of lines to solve the time-dependent partial differential equations (PDEs). PDEs describe the intricate transport phenomena of mass, momentum, and energy between the gas phase and the adsorbent particles during each step of the TCSA cycle. The model ensures accuracy in depicting the dynamic behavior of the system by using a 'Smooth' upwinding approach (flow reversibility within the system is captured by considering the gradual variations in the Peclet number), aiding to minimize the numerical dispersion and ensuring a more physical representation of the transport processes.

Furthermore, the model discretization is tuned, employing a finite volume method, which is divided into a specific number of discretization points per layer allowing for a detailed spatial resolution of the bed, enabling the capture of local gradients and ensuring that the simulation accurately reflects the physical behavior of the system. In this setup, the number of discretization points per layer is set to 100. These nodes or points are where the PDEs are solved, providing a detailed profile of the temperature, concentration, and velocity within the adsorption bed at every step of the TCSA cycle. In the TVSA configuration, vacuum-assisted desorption is applied simultaneously with heating during the desorption step, replacing the purely thermally driven regeneration of TCSA. This addition enhances CO_2 desorption driving force and increases working capacity relative to TCSA. The sensitivity analysis presented in the following section was conducted using the TVSA configuration with zeolite 13X as the adsorbent, with the objective of identifying operating conditions that simultaneously achieve the U.S. DOE targets of 95% purity and 90% recovery.

Table 13: Isotherm parameters fitted to the extended Langmuir model. Isotherm data for CO_2 and N_2 at different temperatures were taken from[21]

Component	IP1	IP2	IP3	IP4	ΔH (kJ/mol)
CO_2	$2.88e^{-7}$	3574	$6.18e^{-5}$	3603	−37
N_2	$7.18e^{-7}$	1670	$6.21e^{-4}$	1359	−18.5

Sensitivity analysis of TVSA operating parameters for zeolite 13X

A sensitivity analysis was carried out by varying several process parameters, including desorption temperature, purge-to-feed ratio, adsorption time, desorption time and vacuum pressure to evaluate their impact on key performance indicators (KPIs) such as purity and recovery. The objective here is to achieve 95 % purity and 90 % recovery. For this analysis, we used a total cycle time of 3970 seconds as the starting point, with 370 seconds for adsorption, 1800 seconds for desorption, and 1800 seconds for cooling. These initial time parameters were taken from the optimized case for NaUSY-type zeolite and were used as the starting point for optimization in this zeolite 13X study.

(i) Influence of desorption temperature on purity and recovery

Figure 49 shows the effect of desorption temperature on the purity and recovery of the system. As the desorption temperature increases from **140°C to 300°C**, both purity and recovery improve significantly. At 140°C, the system achieves a purity of 82.5% and a recovery of 38.8%. With increasing desorption temperatures, these values rise steadily, reaching a purity of **89.5% and a recovery of 72.8% at 200°C**. Beyond this point, further increases in temperature provide diminishing returns, with only minor improvements observed. At 300°C, the system attains a purity of 91.4% and a recovery of 91.5%, but the energy cost required to achieve these marginal gains becomes significant.

Given these results, a desorption temperature of **200°C** was selected for further optimization. At this temperature, the process offers a good balance between system performance and energy efficiency. Although higher temperatures could yield slightly better recovery and purity, the energy demand for heating becomes a limiting factor. With this temperature chosen, the process parameters were optimized by adjusting the cycle times, including adsorption time, desorption time, and the purge-to-feed ratio.

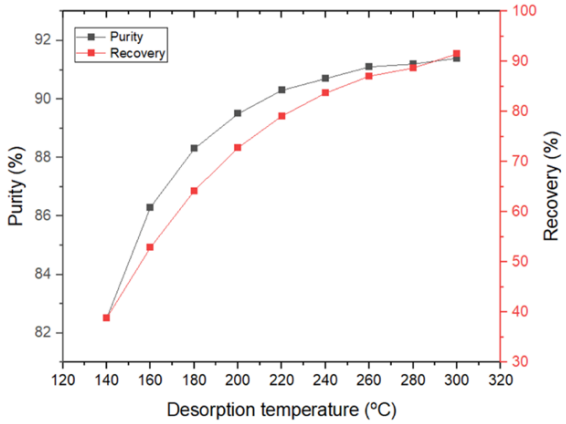


Figure 49: Effect of desorption temperature on CO_2 purity and recovery

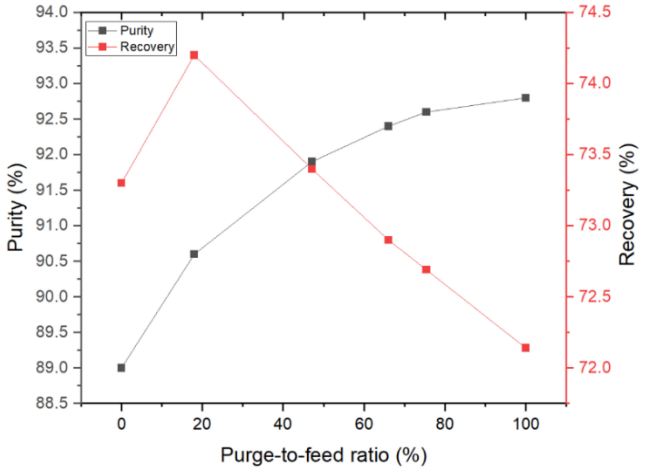


Figure 50: Influence of purge to feed ratio on purity and recovery

(ii) Influence of purge to feed ratio on purity and recovery

Figure 50 presents the effect of the purge-to-feed ratio on CO_2 purity and recovery for a fixed desorption temperature of 200°C. The purge-to-feed ratio varied between 0% to 100%. It depicts that the purity of the captured CO_2 improves with the purge-to-feed ratio, rising from 89% at 0% to 92.8% at 100%. This occurs because the hot CO_2 effectively regenerates the adsorbent, flushing out CO_2 with higher concentration in the captured stream.

On the other hand, CO_2 recovery shows a different pattern. It increases slightly from 73.3% at 0% to 74.2% at 18%, as the hot CO_2 helps regenerate the absorbent, allowing it to capture more CO_2 in the cycle. However, beyond 18%, recovery declines, reaching 72.14% at 100%. While the hot CO_2 purge initially aids desorption, excessive purging introduces too much CO_2, reducing the system's efficiency by diluting the capture process and potentially wasting energy without a corresponding benefit in CO_2 recovery.

(iii) Influence of adsorption time on purity and recovery

The influence of adsorption time on purity and recovery has been studied. From Figure 51, CO_2 purity increases with increase in adsorption time, rising from 66.5% at 150 seconds to 91.8% at 600 seconds, and reaching a maximum of 92.2% at 700 seconds. This steady increase in purity can be explained by the extended contact time between the adsorbent and the feed gas, allowing the adsorbent to selectively capture more CO_2 from the flue gas mixture. However, after 600 seconds, the rate of increase in purity becomes marginal, indicating that the adsorbent is approaching its saturation point. At this point, the system's ability to further increase CO_2 purity is limited, as the adsorbent has already captured most of the CO_2 it can handle. Thus, further increasing the adsorption time only yields slight improvements in purity.

CO_2 recovery shows a different behavior. Recovery increases steadily from 51.9% at 150 seconds to a peak of 73.8% at 390 seconds. The initial increase in recovery corresponds to the longer adsorption time allowing the absorbent to capture more CO_2 from the feed gas before reaching its saturation limit. At these lower adsorption times, the system is more effective in capturing CO_2 while limiting the capture of N_2, which is present in greater quantity in the feed gas.

However, beyond 390 seconds, the recovery begins to decline, dropping to 55.6% at 700 seconds. The decrease in recovery at longer adsorption times can be attributed to the adsorbent becoming saturated with CO_2. Once saturation is reached, the system becomes less efficient at capturing additional CO_2, and the adsorbent may begin adsorbing more of the lighter N_2 gas from the feed mixture, reducing the overall recovery of CO_2. This decline in recovery suggests that an optimal adsorption time exists beyond

which the performance of the system diminishes due to saturation and inefficiencies. Based on the results, an adsorption time of **390 seconds** is identified as the optimal point. Currently, the system achieves a CO_2 purity of **90.4%** and a recovery of **73.8%**.

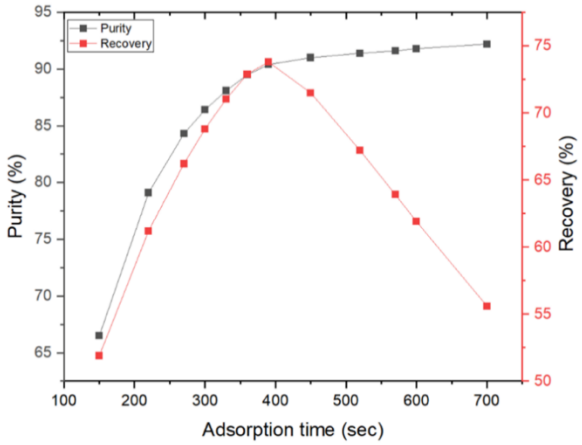


Figure 51: Influence of adsorption time on purity and recovery.

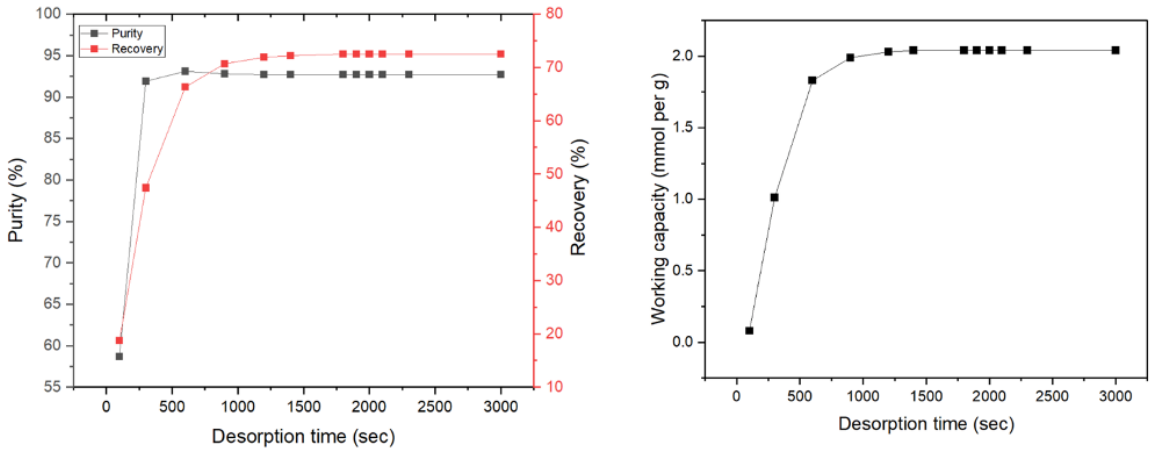


Figure 52: (left) Influence of desorption time on purity and recovery. (right) Influence of desorption time on working capacity.

(iv) Influence of desorption time on purity and recovery

Figure 52 shows the effect of desorption time on CO_2 purity and recovery. Both purity and recovery rise in the first 1000 seconds, with CO_2 purity exceeding 90% and recovery reaching 70%, after which they plateau. The working capacity increases rapidly, achieving nearly 2 mmol/g in the same time frame before stabilizing. Beyond 1000 seconds, further increase in desorption time shows minimal impact on these metrics. These results suggest that a desorption time of approximately 1000 seconds is optimal for maximizing CO_2 purity, recovery, and working capacity, making it the most efficient duration for the process. Extending the desorption time beyond this point may not be energy efficient.

(v) Influence of vacuum step on purity and recovery

To evaluate the effect of the vacuum step on the desorption process, the system was tested under varying vacuum pressures, and the corresponding CO_2 purity and recovery were measured. From Figure 53, the effect of vacuum pressure on purity and recovery has been studied. It can be observed that as the vacuum pressure decreases, both the purity and recovery increase. At a vacuum pressure of 0.2 bar, the system achieves a purity of approximately 91.5% and a recovery of around 94%. The deeper vacuum leads to facilitating an increase in the working capacity, thereby improving desorption

efficiency, which leads to a higher recovery. Thus, a deeper vacuum proves to be beneficial in enhancing both the purity and recovery of the system.

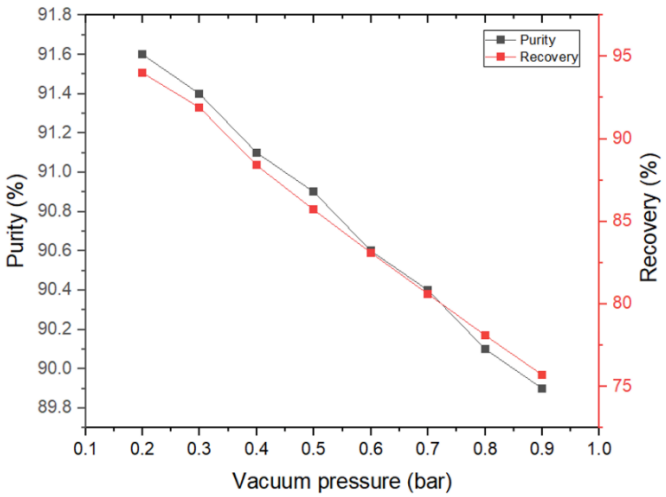


Figure 53: The influence of vacuum pressure on purity and recovery

With an adsorption time of 390 seconds, desorption time of 1000 seconds, purge time of 120 seconds, cooling time of 1800 seconds, and a vacuum pressure of 0.2 bar, the system achieves a purity of 91.5% and a recovery of 94%. While the recovery target of 90% set by the U.S. DOE was met, the purity of 91.5% approached but did not fully reach the 95% threshold. These results nonetheless demonstrated promising separation performance and provided sufficient confidence to proceed to industrial-scale assessment, where further optimization was pursued.

Life cycle assessment methodology

LCA was conducted on the TSA, TVSA and Steam Assisted Temperature Concentration Swing Adsorption (SA-TSA) based carbon capture focusing on the environmental emissions associated with capturing CO_2 with a purity greater than 90%. This analysis centered around the functional unit of 1 kg of captured CO_2 to ensure a consistent basis for comparison and evaluation. The LCA adopted a cradle-to-grave approach, encompassing the emissions associated with the technology operation, manufacturing (includes the infrastructure of adsorption columns and zeolite material production), and end-of-life stages. Data for the inventory analysis was sourced from the Ecoinvent database, ensuring a comprehensive and reliable dataset. The Impact World+ methodology was utilized to assess environmental impacts, focusing on endpoint indicators such as carbon footprint, water footprint, ecosystem quality, human health, and resource footprint. These indicators were selected to provide a broad understanding of the environmental performance of the different regeneration processes and its implications for research communities, policymakers, and environmental enthusiasts.

Life cycle assessment (LCA) of CO_2 capture process using different regeneration strategies

The goal of this LCA study is to assess and compare the environmental impact of CO_2 capture process when zeolite 13X is implemented as the adsorbent material. Temperature Swing Adsorption (TSA), Temperature Vacuum Swing Adsorption (TVSA) and Steam-Assisted TSA (SA-TSA) processes have been compared. The relevant key parameters required for conducting this LCA are taken from the work of Jiang et al.[21] and Liu et al.[22] One of the primary reasons for commissioning an LCA is to provide a rigorous and evidence-based evaluation of the environmental performance of different regeneration processes in using zeolite 13X for CO_2 capture. Another reason is to inform decision-making processes in selecting the most environmentally sustainable CO_2 capture technology among the available

regeneration techniques. The results of this LCA study perhaps would also assist policymakers and regulatory bodies in establishing guidelines and standards related to carbon capture technologies. Additionally, the impact assessment of LCA was performed, which is aimed to determine the impactful stages of the process life cycle.

Assumptions in modelling

The following assumptions have been made to make the system modeling more accessible.

Location

First and foremost, this study is assumed to take place at EPFL in Sion, Switzerland. Therefore, the electricity mix of Switzerland is used and the corresponding emissions as given in the Ecoinvent Database. Distances for transportation and landfill are considered in accordance.

Process aspects

- The lifetime of the zeolite is assumed to be 20 years, and it is considered that the zeolite landfilled at the end of its lifetime.
- The lifetime of the plant infrastructure is assumed to be 20 years, and that to be the same lifetime for the pump used in TVSA process as well. The operating days of the plant were assumed to be 330 days per year and 12 hours per day. Some parts of the infrastructure are incinerated, and some parts will be landfilled at the end of their lifetime.
- The amount of adsorbent required to provide the functional unit remains constant over the entire duration of study, as has been done in previous similar LCA studies (i.e no deterioration in zeolite quality over time).
- It is assumed that all energy required for the processes is supplied by electricity. Therefore, the total energy needed per functional unit is directly converted into electricity consumption.
- It is assumed that the cooling step does not require an energy input (as initial adsorption and cooling temperatures are the same), and instead affects the overall process productivity only due to the consequently longer overall cycle time.
- The scope of this study does not assess environmental impact beyond the CO_2 capture stage. i.e. the compression, transportation and storage of the captured CO_2 is not considered as this is equal for both processes.
- It is assumed that the columns are made of steel having a total mass calculated by the dimensions given in the data sources. The mass of the heat exchanger, steam generator and vacuum pump is assumed to be equal to what is given in the Ecoinvent Database. Additional infrastructure items needed for the process are disregarded. These items include possible expansion valves, tubes, thermostats and compressors as well as any other materials present in the columns other than steel.

Function and functional unit

The function of the model is to capture CO_2 in Switzerland in 2023. The functional unit (FU) is 1 kg of CO_2 captured with a purity above 90% in Switzerland in 2023.

Product system boundaries

This LCA includes all the life cycle stages from cradle to grave. Figures 54-56 show the process trees and the system boundaries for TSA, TVSA and SA-TSA processes, respectively. Both technologies have an infrastructure process which consists of production processes for the zeolite, the bed columns and heat exchangers. Additionally, for TVSA there is a separate process for production of the vacuum pump. In the use phase the different technologies consume energy for the process of capturing CO_2. TSA and TVSA processes utilize electricity from the electrical grid. Transportation involves firstly the column from the production site to the CO_2 capture site, and secondly, the transfer of the end-of-life infrastructure from the CO_2 capture site to the waste management facility where it is either landfilled or incinerated. The transport and the storage of the captured CO_2 are excluded as it is assumed to be the same for both the technologies.

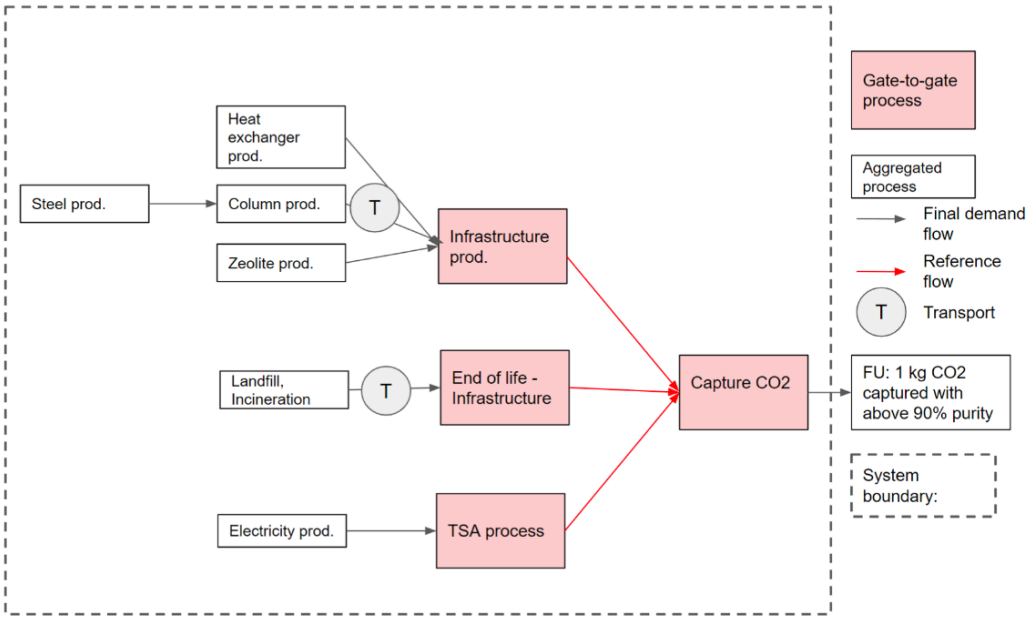


Figure 54: Process tree of TSA process.

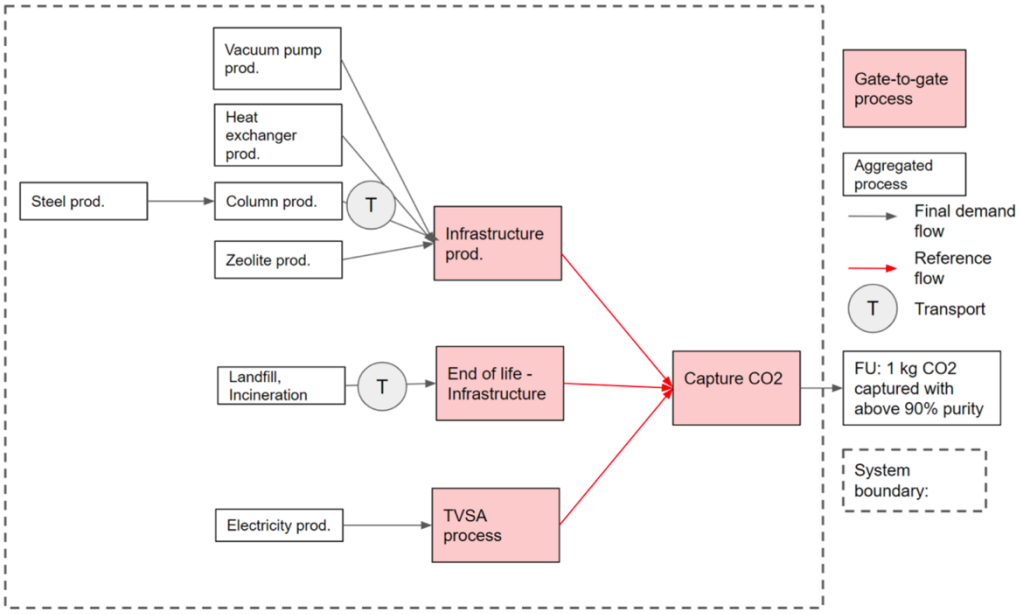


Figure 55: Process tree of TVSA process.

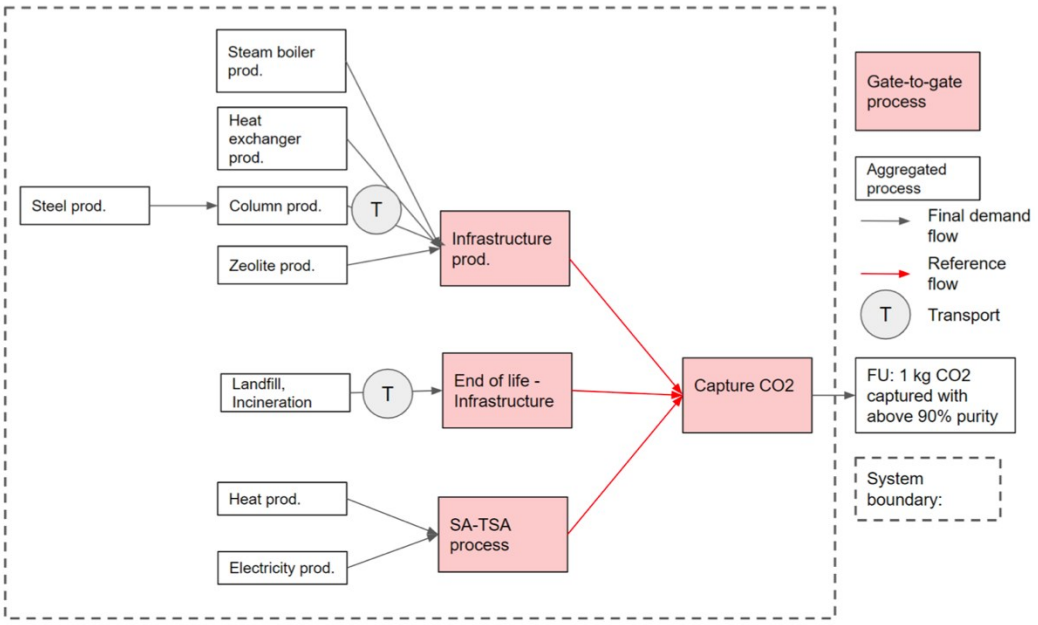


Figure 56: Process tree of SA-TSA process.

Reference Flows and Key Parameters

The process tree diagrams in Figures 54-56 illustrate three gate-to-gate unit processes: the technology (TSA, TVSA, or SA-TSA regeneration process), the infrastructure production and the end-of-life (EoL) of the infrastructure. The associated reference flows for these unit processes are the consumed energy

(RF_E [MJ/FU]), the infrastructure (RF_{inf} [p/FU]), and the end-of-life of the infrastructure (RF_{EoL} [p/FU]), respectively. The reference flows and key parameters are presented in Table 14-16. The equations used to calculate the reference flows are listed in the Appendix WP3 and are common to the TSA, TVSA, and SA-TSA.

Table 14: Reference flows and key parameters.

Reference flows	**Units**	**Key parameters**	Symbols	Units
Infrastructure	p/FU	Number of infrastructure	inf	p
		Lifetime of the infrastructure	Y	years/p
		Number of operating days in a year	D	days/year
		Number of operating hours in a day	H	h/day
		Number of hours required to fulfill the FU	X_i	h
Energy	MJ/FU	Amount of energy consumed to fulfill the FU	E	MJ
		Power consumed in X_i hours	P_i	W
		Number of hours required to fulfill the FU	X_i	h
EoL of infrastructure	p/FU	Number of infrastructure	inf	p
		End of life infrastructure rate	η_{EoL}	%

The index i in the above equations indicates that the corresponding key parameter varies according to the TSA, TVSA, or SA-TSA regeneration method. Table 16 shows the corresponding calculated reference flows.

Table 15: Key parameter values for TSA, TVSA and SA-TSA.

Key parameters		**Technologies**		
Smbols	**Units**	**TSA**	**TVSA**	**SA-TSA**
inf	[p]	1	1	1
Y	[p/years]	20	20	20
D	[days/year]	330	330	330
H	[h/day]	12	12	12
X	[h]	2.18	0.95	1.3
P	[W]	861.4	964.9	2179.5
η_{EoL}	[%]	100	100	100

Table 16: Calculated reference flows for TSA, TVSA, and SA-TSA.

Reference Flows		**Technologies**		
Symbol	**Units**	**TSA**	**TVSA**	**SA-TSA**
RF_{inf}	[p/FU]	$2.7.10^{-5}$	$1.2.10^{-5}$	$1.6.10^{-5}$
RF_E	[MJ/FU]	6.76	3.3	10.2
RF_{EoL}	[p/FU]	$2.7.10^{-5}$	$1.2.10^{-5}$	$1.6.10^{-5}$

Data sources

As shown in the below Table 17, the inventory data from Jiang et al.[21], and Liu et al.[22] were used for conducting the study.

Table 17: Data needed for calculating input parameters for OpenLCA.

	Unit	TSA	TVSA	SA-TSA
Reference		Jiang et al.[21]	Jiang et al.[21]	Liu et al.[22]
Height of Bed	m	1.00	1.00	1.20
Diameter of Bed	m	0.10	0.10	0.10
Wall Thickness of Bed	m	0.01	0.01	0.05
Mass of Steel in Column	kg	13.74	13.74	16.33
Mass of Zeolite/bed	kg	3.68	3.68	4.42
Number of beds	-	4	4	3
Feed CO_2 Composition	% CO_2	15%	15%	15%
Cycle Time	s	4000	4000	9000
Adsorption Temperature	°C	95	89	70
Desorption Temperature	°C	137	135	95
Energy Required	MJ/kg CO_2	6.76	3.22	10.20
Purity	%	95.04%	97.27%	90.24%
Recovery	%	90.27%	97.66%	96.00%
Productivity	mol/kg_{ads}/h	0.71	1.63	0.86

Impact assessment results and interpretation

Following the ISO 14040/14044 standards, the life cycle impact assessments of the TSA and TVSA technologies were conducted using the footprint version of the IMPACT World+ characterization method. This LCA method covers five environmental impact categories:

1) Carbon footprint: climate change, short term [kg CO_2-eq]
2) Water footprint: water scarcity [m^3 world-eq]
3) Remaining ecosystem quality (EQ): rest of ecosystem quality [PDF. m^2. yr]
4) Remaining human health (HH): rest of human health [DALY]
5) Resource footprint: fossil and nuclear energy use [MJ deprived]

Along with accessing the above impacts, one other important parameter of carbon capture efficiency (CCE) was accessed. CCE is the percentage of captured CO_2 that results in a net reduction of CO_2 emissions after accounting for the CO_2 generated by the capture technology itself (e.g., energy used to run the system from electricity consumption along with any other ancillary emissions). It is defined as:

$$\text{Carbon Capture Efficiency} = \left(1 - \frac{\text{CO}_2 \text{ emissions from technology}}{\text{CO}_2 \text{ captured}}\right) \times 100$$

Impact scores and profiles

Table 18 presents the impact scores of the TSA, TVSA, and SA-TSA related to the impact indicators mentioned above.

Table 18: Impact scores for each TSA, TVSA, SA-TSA technologies.

Metric	Unit	TSA	TVSA	SA-TSA
Carbon footprint	kg CO_2-eq (short)	0.221	0.105	0.886
Water footprint	m^3 world-eq	0.845	0.402	0.359
Ecosystem Quality	PDF.m^2.yr	0.037	0.017	0.081
Human Health	DAILY	$1.52e^{-7}$	$7.17e^{-8}$	$3.45e^{-7}$
Resource footprint	MJ deprived	10.1	4.80	16.9

The functional unit common to all technologies consists of capturing 1 kg of CO_2. Considering the mass of CO_2-equivalent gases emitted during each process, it can be observed that all the technologies capture more CO_2 than they emit since their carbon footprints are less than 1 kg CO_2 eq. Defining carbon capture efficiency (CCE) as the ratio of avoided CO_2 emissions to the captured CO_2, it is evident that SA-TSA demonstrates a notably low CCE at 11.4%, emitting 886 g of CO_2 equivalent to capture 1 kg of CO_2. In contrast, TSA and TVSA release 221 g and 105 g, respectively, of CO_2 equivalent to achieve the same functional unit. Consequently, TSA and TVSA exhibit significantly higher CCE values compared to SA-TVSA, standing at 77.9% and 89.5%, respectively. The results in Table 18 are graphically represented in Figure 57, illustrating the impact profiles of TSA, TVSA, and SA-TSA through an internal normalization. The normalized profile of the results allows us to directly compare technologies. SA-TSA shows the poor impact profile in the carbon footprint, ecosystem quality, human health, and resource footprint impact categories. The corresponding impact scores are two to ten times higher than those of TSA and TVSA. In contrast, TVSA has the lowest impact score in most categories and appears to be the most environmentally friendly technology.

To better understand and interpret these results, a contribution analysis (which depicts which stage contributes for the emissions associated) is required for each technology. Figure 58 and Figure 59 shows the contribution analysis per process for TSA, TVSA, and SA-TSA, via internal normalization, at the first and second level respectively. Figure 58 shows that the operations are the most contributing to the five impacts for TSA, TVSA, and SA-TSA. Conversely, the impact profiles across the other two categories are minimally influenced, or even negligible, by the unit processes of infrastructure production and EoL. Within the categories of ecosystem quality and human health the infrastructure production has a higher contribution.

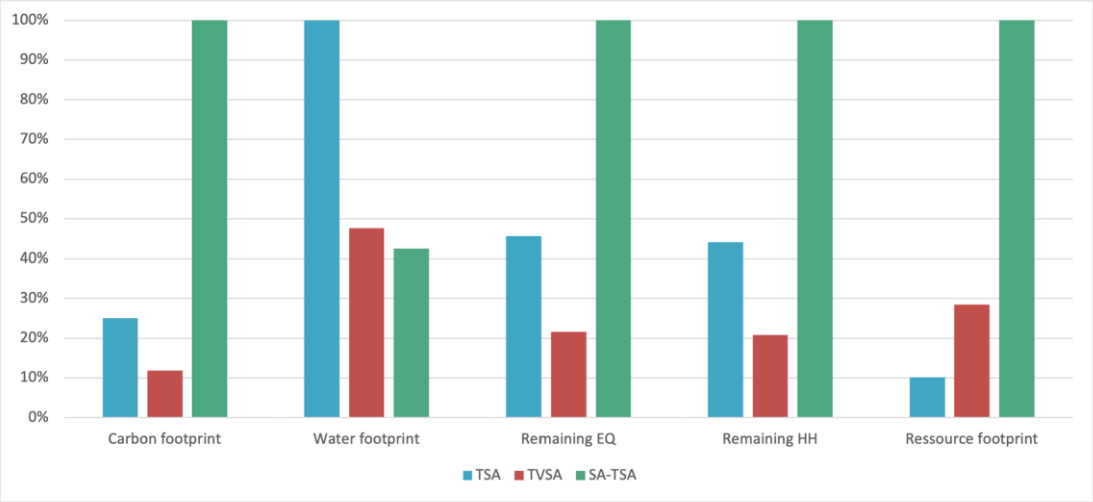


Figure 57: Impact profile of TSA, TVSA, and SA-TSA via an internal normalization.

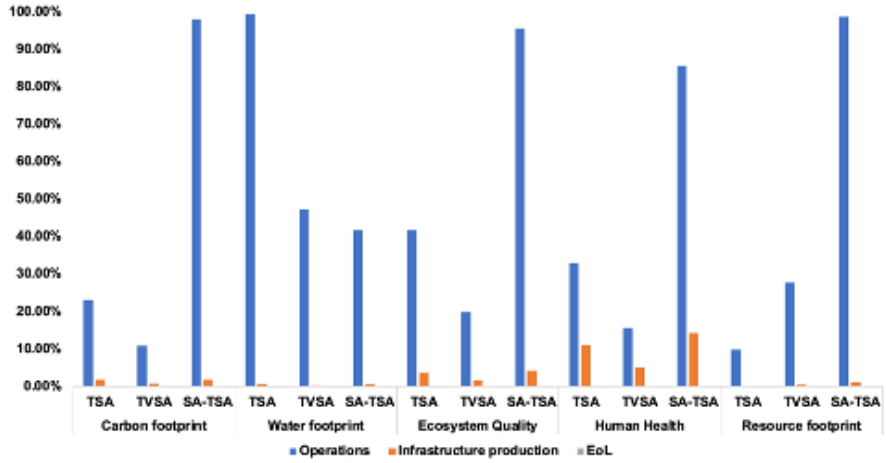


Figure 58: Contribution analysis per process at the first level for TSA, TVSA, and SA-TSA via internal normalization.

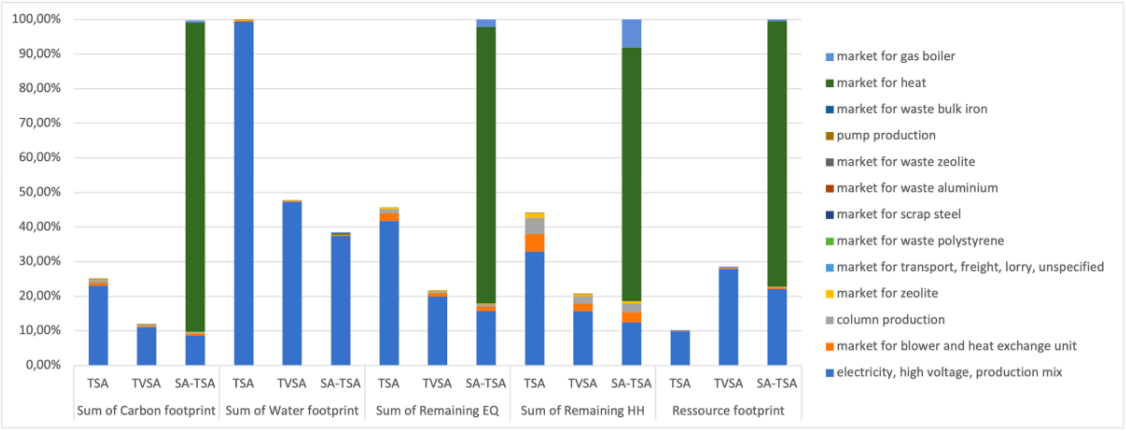


Figure 59: Contribution analysis per process at the second level for TSA, TVSA, and SA-TSA via internal normalization.

From Figure 59, it can be observed that the market for heat is the primary aggregated process contributing significantly to the higher SA-TSA impact profile in four out of the five impact categories. This can be explained by the energy mix in the SA-TSA technology. 75% of the total energy consumption in SA-TSA is derived from heat, while the remaining 25% is sourced from electricity (Appendix WP3, Table A3). This amount of electricity is about 2.55 MJ, which is less than the electricity consumption of TVSA and TSA, standing at 3.3 MJ and 6.76 MJ, respectively (please refer to Table 17). Considering the predominant use of hydropower in Switzerland's electricity mix, these numbers elucidate the TSA's more substantial impact profile in the water footprint impact category.

Overall, based on the results obtained, TVSA emerges as the most sustainable process, contributing the least emissions and achieving a net carbon capture efficiency of 89.5%. This makes TVSA the most environmentally favorable option among the evaluated processes.

TVSA process development for an incineration facility: an industrial case study

Given its superior environmental performance, as confirmed by the LCA screening, TVSA was selected as the process configuration for industrial-scale assessment. TVSA combines thermal regeneration with vacuum-assisted desorption, enabling higher CO_2 working capacities and improved separation performance compared to purely temperature-driven regeneration processes. Owing to these advantages, TVSA was selected as the basis for the subsequent sensitivity analysis, process optimization, and techno-economic evaluation.

An industrial-scale adsorption column with a height of 6 m and a diameter of 2 m was considered, corresponding to a realistic aspect ratio (L/D=3) for large-scale packed-bed operation. For the present study, a representative medium-sized MSWI facility was considered, with a modeled flue-gas flow of 41,000 Nm^3/h. Typical incineration exhaust streams contain CO_2, N_2, O_2, water vapor, and trace acid gases (SO_2, HCl, HF, NO_x). In industrial practice, such impurities are removed in upstream gas-treatment units, while moisture is condensed prior to adsorption to avoid competitive adsorption and capacity loss on zeolite 13X. Prolonged exposure to water and acidic contaminants is also known to accelerate zeolite degradation, leading to irreversible loss of adsorption performance and reduced sorbent lifetime, which further motivates stringent feed-gas conditioning. After this pre-conditioning, the flue gas can be approximated as a binary mixture of CO_2 and N_2. Since oxygen exhibits negligible adsorption capacity on zeolite 13X, it was grouped with nitrogen. Accordingly, the dry feed composition supplied to the TVSA process was a mixture of CO_2 and N_2 with 12.5 vol% and 87.5 vol% respectively.

The flue gas, to be delivered by the incineration facility, was compressed to and subsequently cooled to near-ambient temperature prior to entering the capture unit. Then, the TVSA process was operatesd through a four-step cycle (Figure 60) designed to maximize CO_2 capture efficiency while minimizing energy consumption:

Step 1 - Adsorption (ADS): The pre-treated flue gas enters the bottom of the adsorption column packed with zeolite 13X at ambient temperature. During this step, CO_2 is selectively adsorbed onto the zeolite surface while CO_2 passes through as the light product, exiting from the top of the column.

Step 3 - Blowdown (BLD): The column pressure is reduced from feed conditions to an intermediate level, releasing the N_2 -rich void gas along with a small fraction of CO_2. This step maximizes N_2 recovery, minimizes contamination of the subsequent CO_2 product stream.

Step 3 - Evacuation (EVAC): This is the key regeneration step where the column is subjected to both heating and strong vacuum conditions. The combination of elevated temperature and reduced pressure drives the desorption of CO_2 from the zeolite, producing a high-purity CO_2 stream suitable for capture and utilization.

Step 4 - Cooling (COOL): The column is cooled back to adsorption temperature in which N_2 is circulated through the bed to bring it back to the target adsorption temperature. This ensures that the adsorbent regains its high CO_2 uptake capacity and that the column is fully prepared for the next cycle.

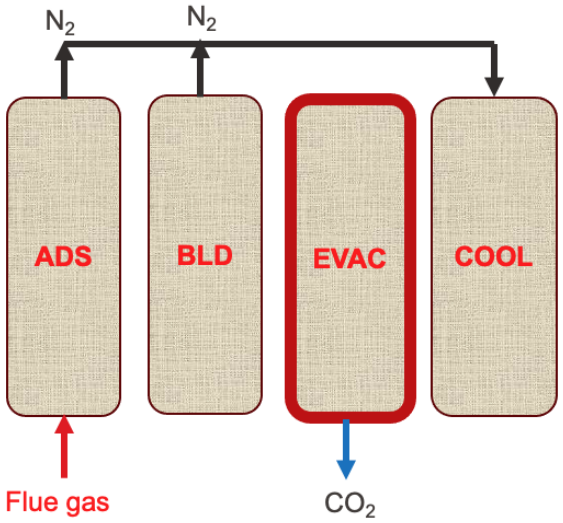


Figure 60: 4 steps CO_2 capture process.

Furthermore, the TVSA process was configured as a multi-module system to accommodate the large flue-gas flow from the incineration facility. The capture plant consists of M identical modules operating in parallel, with each module containing N adsorption columns cycled out of phase to ensure continuous operation. The configuration integrates dedicated feed gas compressors, vacuum pumps for the blowdown and evacuation steps, and cooling systems to manage the thermal requirements of the process. The overall process configuration is illustrated schematically in Figure 61. It was assumed that the plant operates continuously for 365 days per year, totaling 8760 hours annually. Seasonal variations in flue gas composition are neglected for simplification. Continuous operation is assumed with only scheduled maintenance interruptions.

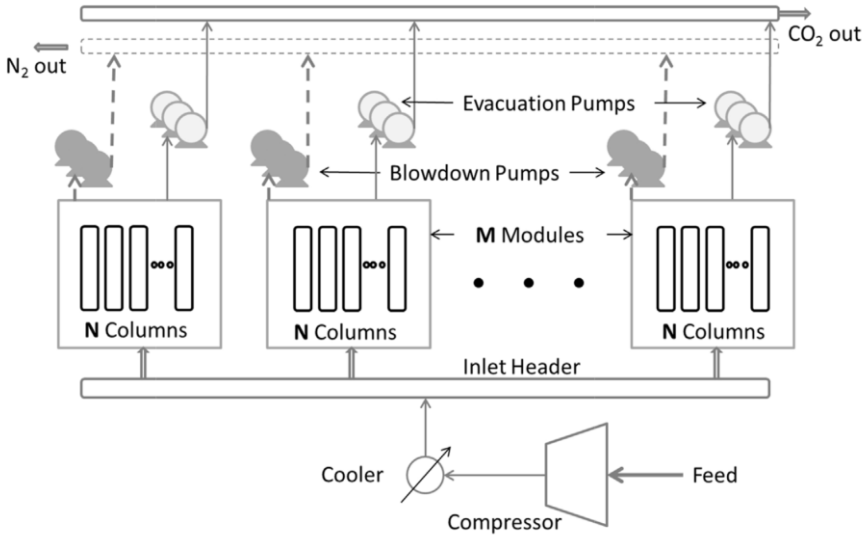


Figure 61: Schematic of the CO_2 capture facility. Adapted from Farooq et al.[23]

For the baseline industrial cycle modelling, the operating times were set as follows: 650 s adsorption, 400 s blowdown, 2200 s vacuum plus heating, and 2500 s cooling. The cycle times were selected based on transient cyclic simulation results, particularly the evolution of concentration and loading profiles along the adsorption column with time. Analysis of the breakthrough behaviour and spatial loading

distribution allowed identification of operating durations that provided sufficient utilisation of the adsorbent bed while limiting excessive CO_2 breakthrough. Similarly, the regeneration and cooling times were chosen to ensure adequate desorption and restoration of the bed to the target adsorption temperature before the subsequent cycle. Under these conditions, the process achieved a CO_2 purity of 98% and a recovery of 48% at the end of the twelfth cycle. To systematically evaluate and improve performance, a sensitivity analysis was carried out in gPROMS using the Global System Analysis (GSA) framework. In the first step, wide parameter ranges were defined for adsorption time (250-1200 s), desorption temperature (373-473 K), desorption time (1200-5000s), vacuum pressure (0.01-0.09 bar), cooling flow rate (50-300 kmol·h^{-1}), and cooling time (1200-4000 s). This broad scan identified the best trade-off at 98.5% purity and 81.3% recovery when operating at a vacuum pressure of 0.03 bar. By lowering the vacuum to 0.01 bar, recovery was increased to 87.5% while maintaining the same high purity, though the DOE recovery target of 90% was not achieved.

In the second step, another GSA was performed, in which vacuum pressure was fixed at 0.01 bar and desorption temperature at 473 K, while adsorption time, desorption time, cooling flow rate, and cooling time were varied across the same ranges.

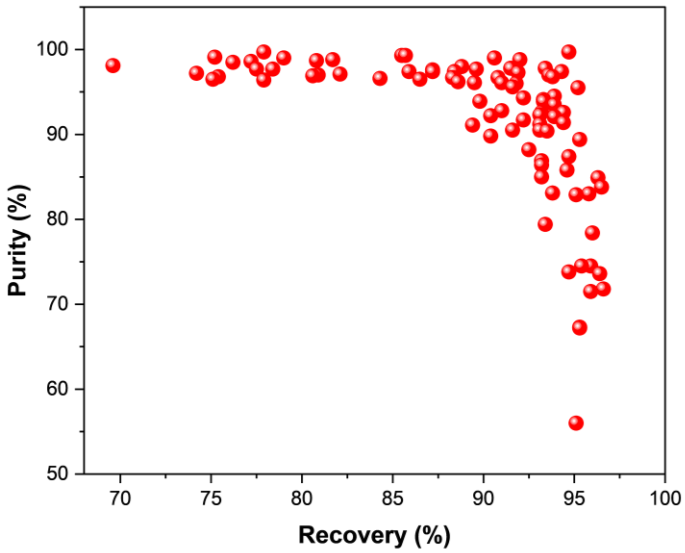


Figure 62: Design space of industrial-scale TVSA operation showing CO_2 purity versus recovery. Each red point represents one simulated operating condition within the defined parameter ranges (adsorption, desorption, cooling, and vacuum pressure).

Design space and pareto front analysis

After completing the second Global System Analysis, where operating conditions were varied at fixed desorption temperature (473 K) and desorption pressure (0.01 bar), the results were mapped as a design space of CO_2 purity versus recovery (Figure 62). Each red point represents a simulation outcome for a given set of operating conditions within the predefined parameter ranges. As expected, the results reveal a clear trade-off: conditions that maximize purity tend to reduce recovery, while operating points with high recovery often sacrifice purity. From this design space, a Pareto front was constructed by identifying the six optimal operating points (Figure 63 and Table 19). The Pareto front represents the set of solutions where neither purity nor recovery can be further improved without compromising the other. In other words, any movement along the Pareto front involves a trade-off: to gain in one performance metric, the other must decrease. This concept is crucial for process design, as it allows decision-makers to choose the most appropriate operating point depending on whether purity, recovery, or a balanced compromise is prioritized. These six Pareto-optimal points form the basis for further analysis of process efficiency and energy trade-offs. In the next step, these points were used to assess productivity in

relation to energy consumption, thereby connecting separation performance with practical operating costs.

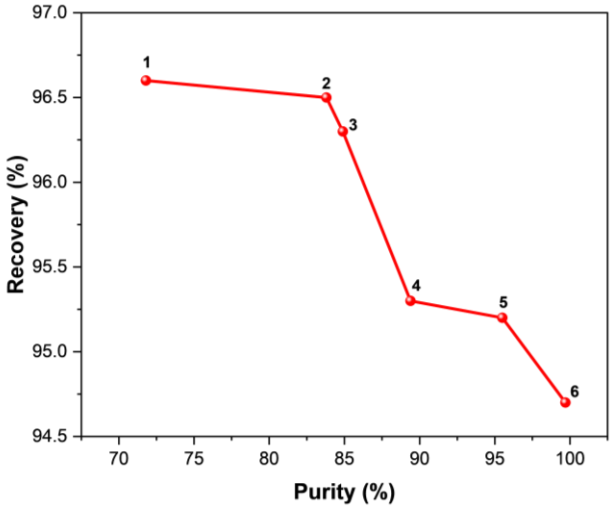


Figure 63: Optimal trade-off curve (Pareto front) between CO_2 purity and recovery, forming the upper boundary of the design space solutions.

Table 19: Operating conditions of six Pareto-optimal points from the purity–recovery trade-off analysis, showing blowdown pressure, cycle times, and resulting CO_2 purity and recovery.

Sample ID	Blowdown pressure (bar)	Time (sec)			Purity (%)	Recovery (%)
		Adsorption	Cooling	Heating		
1	0.33	261	3306	3953	71.8	96.6
2	0.26	260	2138	3974	83.8	96.5
3	0.38	379	2120	3955	84.9	96.3
4	0.21	535	3548	3605	89.4	95.3
5	0.11	613	3517	3822	95.5	95.2
6	0.10	1577	2720	3916	99.7	94.7

Productivity–energy pareto plot for a fixed recovery

From the Pareto analysis in the purity-recovery domain (Figure 63), the focus was shifted to evaluating the trade-off between productivity (kg CO_2·kg ads^{-1}·h^{-1}) and energy consumption (MJ/kgCO_2). To ensure practical relevance, only operating points with CO_2 recovery above ~90% were retained. For these points, productivity and energy consumption were calculated, and a Pareto analysis was conducted in the productivity-energy space (Figure 64 and Table 20).

From the pareto front, three solutions were identified and among them, the configuration at a blowdown pressure of 0.33 bar delivered the most favorable balance, with 97.7% purity, 89.6% recovery, 0.046 kg CO_2 kg ads^{-1} h^{-1} productivity, and 2.58 MJ·kg^{-1} CO_2 energy consumption. This point was selected as the basis for subsequent cost and scheduling analyses, since it combines low energy demand with strong separation performance.

The adsorption time, desorption time, cooling duration, and other cycle parameters corresponding to this operating point were directly carried forward into the scheduling analysis to determine the number of columns, vacuum pumps, and trains required for continuous operation. These same parameters also underpinned the CAPEX and OPEX estimations, ensuring that the techno-economic assessment was grounded in a practically optimized operating regime.

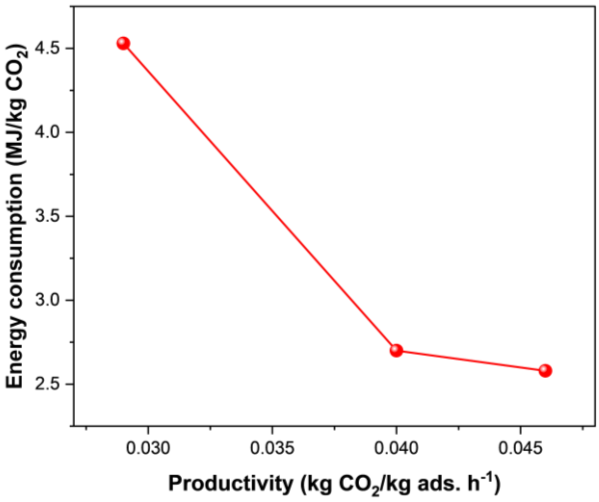


Figure 64: Optimal trade-off curve (Pareto front) between productivity and energy consumption, for points having ≥90% recovery.

Table 20: Operating conditions of three Pareto-optimal solutions from the productivity–energy trade-off analysis (≥90% recovery), including blowdown pressure, cycle times, purity, recovery, productivity, and energy consumption.

Blowdown pressure (bar)	Time (sec)			Purity (%)	Rec (%)	Productivity (kg CO_2/kg ads.h^{-1})	Energy consumption (MJ/kg CO_2)
	Adsorption	Cooling	Heating				
0.15	1365	3433	3762	99	90.6	0.040	2.70
0.33	1458	2476	3989	97.7	89.6	0.046	2.58
0.11	783	3235	2725	96.7	90.8	0.029	4.53

Sensitivity analysis and design-space exploration

To systematically assess the influence of operating variables and identify feasible operating regions, a sensitivity analysis was performed using the GSA framework implemented in gPROMS. In the first stage, wide parameter ranges were explored: adsorption time (250–1200 s), desorption temperature (373–473 K), desorption time (1200–5000 s), vacuum pressure (0.01-0.09 bar), cooling flow rate (50–300 kmol per h), and cooling time (1200–4000 s). This initial design-space exploration identified a favorable trade-off at a vacuum pressure of 0.03 bar, yielding a CO_2 purity of 98.5% and a recovery of 81.3%. Further reduction of the vacuum pressure to 0.01 bar increased recovery to 87.5% while maintaining high purity.

In a second optimization stage, the vacuum pressure and desorption temperature were fixed at 0.01 bar and 473 K, respectively, while adsorption time, desorption time, cooling flow rate, and cooling time were varied over the same parameter ranges and the attained results were mapped as a design space of CO_2 purity versus recovery (Figure 65). Each point in the design space represents a distinct operating condition within the predefined parameter ranges.

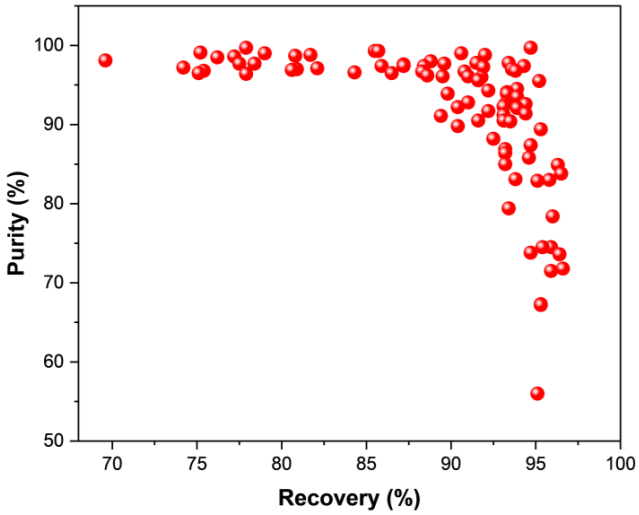


Figure 65: Design space of industrial-scale TVSA operation showing CO_2 purity versus recovery. Each point represents a simulated operating condition within the defined parameter ranges.

The resulting distribution revealed a clear and expected trade-off between purity and recovery: operating conditions yielding very high purity generally resulted in lower recovery, while higher recovery levels were associated with a reduction in purity. From this design space, a Pareto front was constructed by identifying six non-dominated operating points (Figure 66 and Table 21). These Pareto-optimal solutions represent the upper boundary of achievable performance, where neither purity nor recovery can be improved without compromising the other. As such, the Pareto front provides a structured basis for selecting operating points depending on whether the process objective prioritizes maximum purity, maximum recovery, or a balanced compromise.

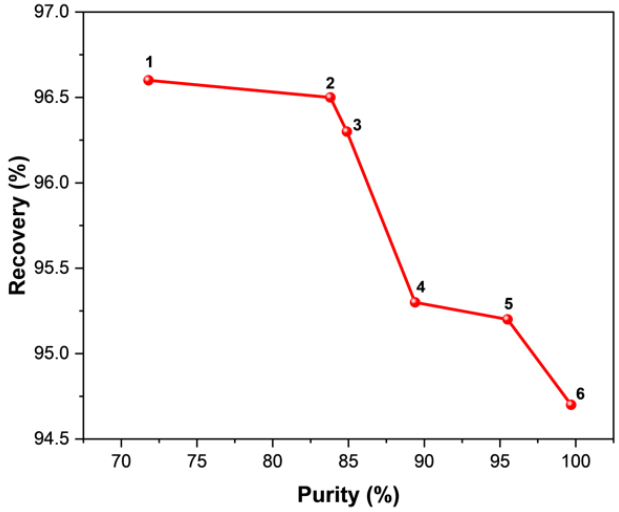


Figure 66: Pareto front of CO_2 purity versus recovery.

Table 21: Operating conditions and performance of Pareto-optimal purity–recovery points.

Sample ID	Blowdown pressure (bar)	Time (sec)			Purity (%)	Recovery (%)
		Adsorption	Cooling	Heating		
1	0.33	261	3306	3953	71.8	96.6
2	0.26	260	2138	3974	83.8	96.5
3	0.38	379	2120	3955	84.9	96.3
4	0.21	535	3548	3605	89.4	95.3
5	0.11	613	3517	3822	95.5	95.2
6	0.10	1577	2720	3916	99.7	94.7

These six Pareto-optimal operating points were subsequently carried forward for further evaluation of productivity and energy demand, enabling direct linkage between separation performance and operating cost.

Productivity–energy Pareto analysis at fixed recovery

To assess the trade-off between process productivity and specific energy consumption, the Pareto-optimal solutions identified in the purity–recovery domain were re-evaluated in the productivity–energy space. To ensure practical relevance, only operating points with CO_2 recovery ≥ 90% were retained for this analysis. For each of these points, productivity (kg CO_2 kg $ads^{-1} \cdot h^{-1}$) and specific energy consumption ($MJ \cdot kg^{-1}$ CO_2) were calculated, and a second Pareto analysis was performed (Figure 67 and Table 22).

The resulting Pareto front highlighted the inherent trade-off between productivity and energy demand: higher productivity was generally associated with increased energy consumption, while lower energy operation often required longer cycle times and reduced throughput. Among the Pareto-optimal solutions, three representative operating points were identified. Of these, the configuration operating at a blowdown pressure of 0.33 bar provided the most favorable balance between separation performance and energy efficiency, achieving 97.7% purity, 89.6% recovery, a productivity of 0.046 kg kg CO_2 kg $ads^{-1} \cdot h^{-1}$ and a specific energy consumption of 2.58 $MJ \cdot kg^{-1}$ CO_2. This operating point was selected as the reference case for subsequent column scheduling and techno-economic analysis, as it combined low energy demand with high separation performance while remaining close to the recovery target of 90%.

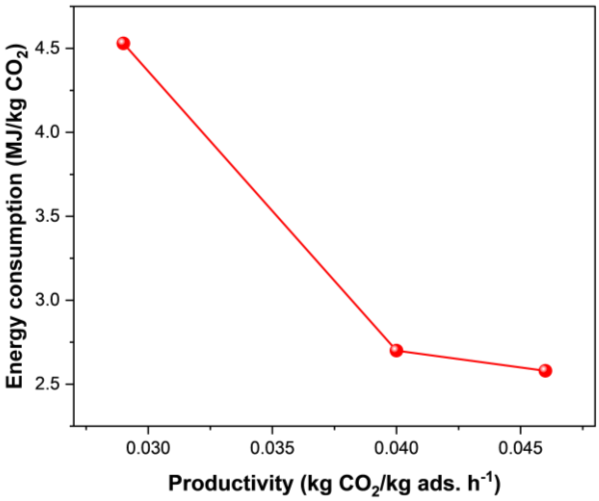


Figure 67: Optimal trade-off curve (Pareto front) between CO_2 purity and recovery, forming the upper boundary of the design space solutions.

Table 22: Operating conditions of six Pareto-optimal points from the purity–recovery trade-off analysis, showing blowdown pressure, cycle times, and resulting CO_2 purity and recovery.

Blowdown pressure (bar)	Time (sec)			Purity (%)	Rec (%)	Productivity (kg CO_2/kg ads.h^{-1})	Energy consumption (MJ/kg CO_2)
	Adsorption	Cooling	Heating				
0.15	1365	3433	3762	99	90.6	0.040	2.70
0.33	1458	2476	3989	97.7	89.6	0.046	2.58
0.11	783	3235	2725	96.7	90.8	0.029	4.53

Column scheduling

Scheduling correlations from the literature were applied to determine the equipment requirements associated with continuous TVSA operation. The corresponding equations are provided in the Appendix WP3, Table A4. Based on this scheduling analysis, each process module required seven adsorption columns, allowing the adsorption step to proceed continuously while regeneration, evacuation, and cooling occurred in parallel in the remaining columns. For the evacuation step, three vacuum pumps per module are necessary, as the evacuation time is longer than the adsorption time. An idle period of 119 seconds was also identified, representing the interval required between successive adsorption steps to maintain proper cycle alignment. For the incineration facility flow rate considered, the full system design corresponds to 28 columns, 12 evacuation pumps, 4 blowdown pumps, 1 compressor, and 1 cooler. This equipment configuration formed the basis for subsequent techno-economic evaluation.

The proposed configuration corresponds to a continuous TVSA process in which multiple adsorption columns operate simultaneously at different stages of the cycle, including adsorption, blowdown, regeneration, evacuation, and cooling. The relatively large number of columns mainly arises from the long regeneration and cooling durations associated with the selected operating conditions. Nevertheless, such a configuration is considered technically feasible and would most likely be implemented in a modular manner, with several adsorption units operating in parallel to ensure continuous processing of the flue gas stream.

Similar modular multi-column configurations are reported in industrial VPSA/PSA systems and cyclic adsorption processes for continuous gas separation applications. Previous large-scale VPSA studies[24] have also reported extensive column scheduling strategies involving parallel adsorption trains and dedicated vacuum systems to maintain continuous industrial CO_2 capture operation, with some large-scale systems requiring hundreds of adsorption columns due to substantially higher flue gas flow rates than those considered in the present work. Therefore it is that multiple adsorption trains are inherently required because of the cyclic nature of the process and the need to accommodate continuous feed operation.

The land footprint of the capture unit was estimated following the methodology of Farooq[23]. In their approach, each adsorption column is allocated a square plot of side 2D (where D is the column diameter) to account for piping, maintenance access, and safety clearance between columns. Blowdown and evacuation pumps are assigned 12 m^2 and 20 m^2 respectively, and all equipment is assumed to be installed in a two-tier building to halve the effective ground footprint. This yields the following expression:

$$\text{Footprint } (m^2) = 40 + 0.5 \times M \times (4 \times N \times D^2 + 12 \times \lceil r_bd \rceil + 20 \times \lceil r_ev \rceil)$$

where M is the number of trains, N is the number of columns per train, D is the column diameter (m), and $\lceil r_bd \rceil$ and $\lceil r_ev \rceil$ are the number of blowdown and evacuation pumps per train respectively. Applying this to the present system with : 4 trains, 7 columns per train, D = 2 m, 1 blowdown pump per train, and 3 evacuation pumps per train, yields a total land footprint of 408 m^2. For context, Farooq et al. report a footprint of 6,800 m^2 for a 500 MW coal-fired power plant capturing approximately 15 million tonnes of CO_2 per year (0.00045 m^2/t CO_2/yr), noting this represents only 9% of the host plant's total site area. The present system, capturing approximately 66,000 tonnes of CO_2 per year, requires 408 m^2 (0.006 m^2/t CO_2/yr). Linear scaling from the Farooq et al. benchmark would predict approximately 30 m^2 at the present capture rate; the higher specific footprint of the present system reflects the fixed equipment overhead inherent to any modular adsorption plant, minimum pump sets per train, compressor, cooler, and base layout allowance, which does not scale proportionally with throughput at smaller capacities. This is a well-known consequence of economies of scale: larger plants benefit from spreading fixed infrastructure costs and footprint over a much greater capture volume, while smaller installations necessarily carry a higher footprint per tonne captured. As the technology scales toward larger incineration facilities or industrial clusters, the specific land requirement is expected to decrease significantly toward the benchmark values reported in the literature.

Techno-economic analysis

The economic analysis of the TVSA capture unit was performed following standard chemical engineering cost-estimation practices. Equipment purchase costs were estimated using established correlations reported by Turton et al.[25] updated to the study year using the Chemical Engineering Plant Cost Index (CEPCI). Carbon steel construction was assumed for all major equipment, as the flue gas was considered to be fully pre-treated and dried prior to CO_2 capture. In addition, the costing methodology proposed by Farooq was adopted to ensure consistency with adsorption-based process evaluations reported in the literature. The detailed cost correlations used in the analysis are provided in the Appendix WP3.

Based on this methodology, the estimated cost of CO_2 capture for the zeolite-based TVSA process treating a dry gas stream was estimated at 49.9 CHF t^{-1} CO_2. The total annualized cost (TAC) was composed of 43.3% capital-related costs (CAPEX) and 56.7% operating costs (OPEX), as summarized in Table 23. Thermal energy required for regeneration was assumed to be fully supplied by available waste heat, while mechanical electricity consumption accounted for vacuum generation, gas handling, and auxiliary equipment. This cost split reflects the combined influence of capital-intensive separation hardware and the ongoing operating requirements associated with cyclic multi-column operation.

On the CAPEX side, costs were derived from bare-module estimates for the major process equipment, including the compressor, blowdown and evacuation pumps, adsorption columns, and cooler.

Installation factors were applied to account for balance-of-plant components such as piping, utilities, instrumentation, and controls. The largest contributions to capital cost arose from the adsorption columns and evacuation vacuum pumps, which together accounted for approximately 23% of the total annualized cost, underscoring the dominant role of core separation hardware in determining the capital intensity of a TVSA system.

On the OPEX side, operating costs were distributed across energy consumption, labor and supervision, adsorbent replacement, maintenance and operating supplies, and general overheads. The dominant contribution originated from maintenance and operating supplies (29.2% of TAC), reflecting the level of upkeep required to sustain continuous operation of multiple adsorption columns and rotating equipment. Despite full integration of waste heat, energy-related costs still accounted for 11.8% of TAC, driven by electrical power consumption for vacuum pumps and auxiliaries. Labor and supervision (8.5%) and administrative overheads (5.3%) remained non-negligible contributors, while adsorbent replacement represented a comparatively minor share (2.0%), indicating that material lifetime assumptions did not dominate the capture cost under the conditions considered. The limited impact of adsorbent replacement is primarily attributable to the low cost of commercially available zeolites, which is on the order of 0.5 € kg.[23]

Table 23: Breakdown of total annualized cost (TAC) for the zeolite-based TVSA process.

Component	% of TAC	CHF/t CO_2
Annualized CAPEX	43.3%	21.60
– Compressor	1.8%	0.92
– Blowdown pump	4.0%	1.98
– Evacuation pump	11.9%	5.94
– Column	11.1%	5.55
– Cooler	1.4%	0.72
– Balance of plant (installation, piping, utilities, controls, etc.)	13.0%	6.50
Annualized OPEX	56.7%	28.31
– Energy (waste heat + mech. electricity)	11.8%	5.87
– Labor & supervision	8.5%	4.25
– Adsorbent	2.0%	0.98
– Maintenance & operating supplies	29.2%	14.58
– Administration & overheads	5.3%	2.63
Capture cost		49.91

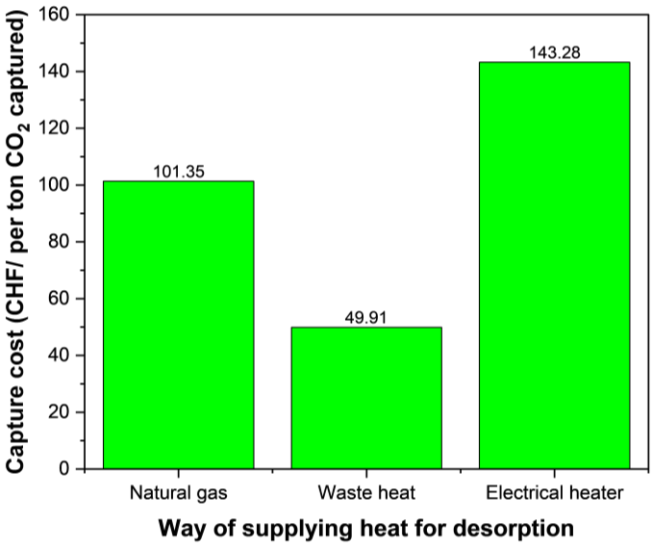


Figure 68: Effect of carbon capture cost through different means of desorption strategies.

Figure 68 illustrates the effect of different heat sources on the overall CO_2 capture cost. Supplying heat with natural gas leads to a cost of ~101 CHF per tonne CO_2, while the use of electric heaters increases the cost further to ~143 CHF per tonne CO_2, reflecting the higher price of electricity (0.14 CHF/kWh compared to 0.04 CHF/kWh for natural gas).

The sensitivity analysis (Figure 69) further shows that capture costs scale directly with the degree of waste-heat availability: at 100% availability, the cost is minimized at 49.9 CHF per tonne CO_2; at 30% availability, it rises to 72 CHF per tonne CO_2. In practice, literature indicates that 30-40% of input energy can typically be recovered as waste heat, with higher values reported for modern waste-to-energy incineration plants integrated with district heating.[26]

Comparable magnitudes of recoverable energy are also reported in other industrial contexts: in steel production, for instance, sinter and blast furnace operations can recover up to ~30% of their input heat.[27] These findings highlight waste-heat integration as the effective lever for maintaining the economic competitiveness of adsorption-based CO_2 capture systems.

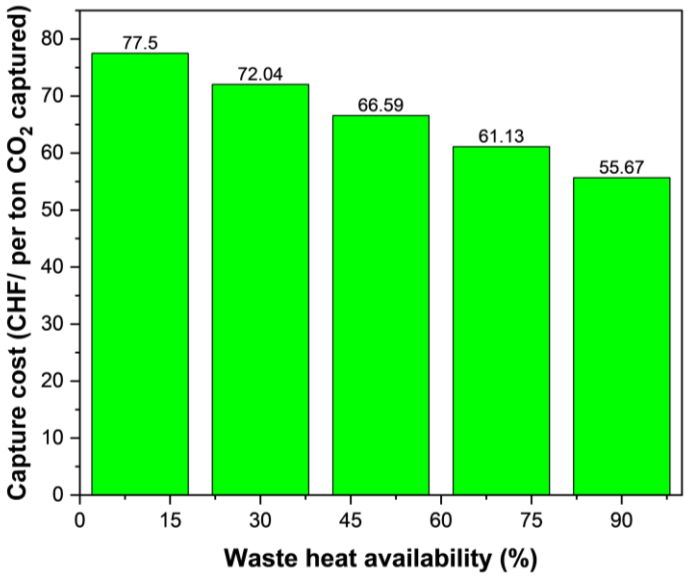


Figure 69: Sensitivity of capture cost to waste-heat availability. Full waste-heat integration yields 50 CHF/t CO_2, at 30% waste heat availability (usually available in industry) yields 72 CHF/tCO_2.

Further, the cost of drying the humid flue gas stream was evaluated.Using the moisture-removal costing methodology established by Hasan et al.[28] and adopted by Farooq et al.[23], the total annualized cost of a tri-ethylene-glycol (TEG) dehydration unit was estimated from the reference case (0.1 kmol s^{-1} wet flue gas with 15 mol % H_2O, C_1 = 213000 USD yr^{-1}) using the six-tenth rule:

$$C_2 = C_1 * \left(\frac{F_{wet}}{0.1}\right)^{0.6}$$

Table 24: Parameters used for cost calculation in drying of the flue gas

Parameter	Value	Unit	Note
Wet flue-gas flow (F_{wet})	0.516	kmol s^{-1}	from a total flow of 41, 629 m^3 h^{-1}
H_2O in gas	19.6 %	-	
CO_2 captured	78980	t yr^{-1}	from the process simulation
Base cost[28] C_1	213000	USD yr^{-1}	total annualized cost for 0.1 kmol s^{-1}

This corresponds to 9.8 USD t^{-1} CO_2 captured, or 7.7 CHF t^{-1} CO_2, assuming an exchange rate of 1 USD = 0.80 CHF. The scaled cost includes both capital-charge and operating components; when decomposed following Hasan,[28] the annualized capital portion accounts for roughly 68 % (≈ 0.53 M USD yr^{-1}) and the operating portion 32 % (≈ 0.25 M USD yr^{-1}), corresponding to an installed CAPEX of ≈ 2.6 M USD for the TEG dehydration train. The operating cost mainly arises from the reboiler steam demand and pumping electricity required to regenerate the glycol. It is expected, in the case of the zeolite, where water competes and can saturate CO_2 adsorption sites, that an additional drying step, as described above, would be required.

It should also be noted that the overall economic performance remains sensitive to the availability of low-cost thermal energy for regeneration. In practical implementation, particularly for municipal solid waste incineration facilities, thermal energy may compete with district-heating demand and other internal

energy requirements. As shown previously in the sensitivity analysis, reduced thermal-energy availability increased the capture cost from approximately 50 CHF per tonne of CO_2 captured to approximately 73 CHF per tonne of CO_2 captured when only 30% thermal-energy availability was assumed.

Since large-scale commercial adsorption-based TVSA systems for post-combustion CO_2 capture are still limited, direct benchmarking of capture costs remains challenging. Nevertheless, the obtained values remain within the broader cost ranges commonly reported by the IEA for post-combustion CO_2 capture systems (50–100 USD per tonne of CO_2 captured), indicating that the estimated costs are within a realistic order of magnitude for industrial implementation.[29]

Overall, incorporating moisture removal into the humid-flue-gas case increases the total CO_2 capture cost by approximately 8 CHF t^{-1} CO_2 relative to the dry-gas baseline. Nevertheless, this additional cost remains moderate when weighed against the operational advantages of maintaining stable adsorption performance and preventing sorbent deactivation under humid conditions. Future work can involve a comparative assessment of two strategies (i) integrating an upstream drying unit prior to the adsorption column and (ii) processing humid gas directly through the adsorbent followed by regeneration, to determine the more energy- and cost-efficient configuration for large-scale operation.

It should furthermore be recognised that the economic estimates presented in this work are based on analytical cost correlations and scaling methodologies commonly used for techno-economic assessments. Consequently, the reported equipment and operating costs should be interpreted as order-of-magnitude estimates rather than exact market prices. In practical industrial implementation, actual costs may differ significantly depending on supplier quotations, material availability, manufacturing complexity, and the degree of equipment customisation required for large-scale TVSA operation. This is particularly relevant for adsorption systems, vacuum equipment, heat integration units, and large adsorption columns, which may require application-specific design modifications that are not fully captured by generic costing correlations. In addition, fluctuations in raw material prices, steel costs, energy prices, and supply-chain constraints may further influence the final investment cost. Nevertheless, the present analysis remains valuable for comparative process evaluation and for identifying the dominant economic drivers affecting adsorption-based CO_2 capture systems.

Process modelling of MOF-amine-epoxide composite system in pilot scale system

The pilot-scale modelling focused on a Cr-BDC (alternatively known as MIL-101(Cr)) composite functionalized with tetraethylenepentamine (TEPA) and cross-linked with trimethylolpropane triglycidyl ether (TMPTE). The objective was to identify TVSA operating conditions capable of achieving >95% CO_2 purity and >90% recovery, in line with the performance benchmarks defined by the U.S. DOE for post-combustion capture. Simulations were carried out at pilot-scale dimensions corresponding to the experimental installation, with an adsorption column of 1.2 m height and 2.54 cm diameter.

To systematically explore the operating window, four key decision variables were varied and their influence on process performance mapped through contour plots: (1) adsorption time (1000–3000 s), (2) heating time (1000–4000 s), (3) cooling time (1000–3000 s), and (4) vacuum pressure (0.1–0.9 bar). GSA was then applied to identify the most influential parameters and to determine operating regimes capable of simultaneously meeting the targeted purity and recovery thresholds.

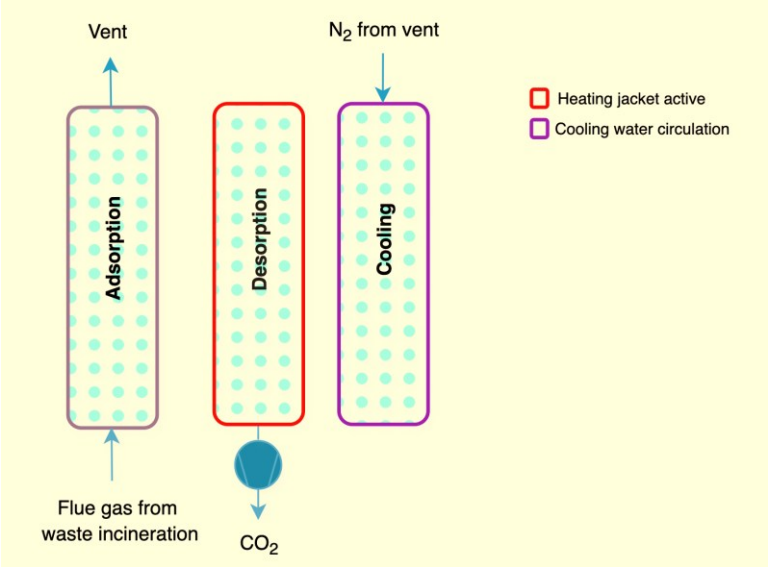


Figure 70: Schematic of the three-step TVSA cycle (adsorption, desorption, cooling) used for pilot-scale modeling in MIL-101(Cr)–TEPA–TMPTE composite.

The contour plots (Appendix WP3, Figures A2–A5) revealed key sensitivities in process performance. Recovery above 90% is achieved with adsorption times of ~1500–1700 s; extending beyond this leads to breakthrough and oversaturation. Complete regeneration requires heating times longer than 3200 s, while strong vacuum levels (<0.25 bar, ideally 0.1 bar) are critical to achieve >94% recovery. Adequate cooling (>2400 s) is also necessary to restore bed performance, as insufficient cooling directly reduces capacity in subsequent cycles.

From these results, a feasible operating region capable of delivering >95% purity and >90% recovery was identified. A representative operating point was selected at 1500 s adsorption, 3300 s desorption, 2500 s cooling, and 0.1 bar vacuum pressure. Under these conditions, the process achieved 96.5% purity, 96.5% recovery, and a productivity of 0.034 kg CO_2 per kg adsorbent per hour, with an energy consumption of 2.45 MJ per kg CO_2 captured.

LCA of the MIL-101(Cr)–TEPA–TMPTE composite integrated with TVSA

Goal, Scope, and System Boundary

The objective of this study is to quantify the cradle-to-grave environmental impacts of a CO_2 capture process based on TVSA packed with Cr-BDC–TEPA–TMPTE, and to identify key improvement levers at both the material and process levels. To reflect these two scales of analysis, two functional units are applied:

a) Emissions occurred per 1 g of adsorbent produced, this is used to attribute burdens to MOF synthesis and functionalization, independent of process performance.

b) Emissions occurred per 1 kg of CO_2 captured in a complete TVSA cycle at steady-state operation, this is used to attribute burdens to operating energy, equipment, and materials. The operating energy inventory for this functional unit is derived directly from the dynamic TVSA simulations performed in gPROMS.

The LCA follows a cradle-to-grave perspective and encompasses:
1) raw-material production for Cr-BDC, TEPA, TMPTE, and solvents;
2) MOF synthesis and post-synthetic functionalization;
3) TVSA operation (thermal energy, vacuum pumping, and blower electricity) using operating profiles generated in gPROMS;
4) infrastructure requirements (columns, heaters, vacuum pumps/blowers) amortized over a 20-year plant lifetime;
5) transportation of equipment and materials; and
6) end-of-life treatment for both equipment and adsorbent.

Key Assumptions for the LCA

1) Adsorbent lifetime and replacement : MOF-amine-epoxide composite lifetime fixed at 3 years, after which replacement is assumed. Adsorbent disposal route is treated as inert solid waste (e.g., landfill) unless otherwise specified.

2) Plant lifetime of 20 years for infrastructure amortization (columns, pumps, blowers, heaters) has been assumed.

3) Electricity price and footprint: Swiss grid mix as baseline; sensitivity to higher-carbon grids explored.

4) Material inventories: Precursors for MOF and amines (TEPA, TMPTE, Cr nitrate) modeled from ecoinvent or proxy datasets built from stoichiometry. The stoichometric equations are provided in the appendix section.

5) Transport: Standardized transport distances assumed (e.g., 100–500 km by truck within Europe for precursors and equipment).

6) System exclusions: Civil works and site-specific buildings excluded. Balance-of-plant services (cooling water, instrument air, etc.) are excluded as it is believed to have very minimal impact.

The system boundary of this LCA study is shown in Figure 71.

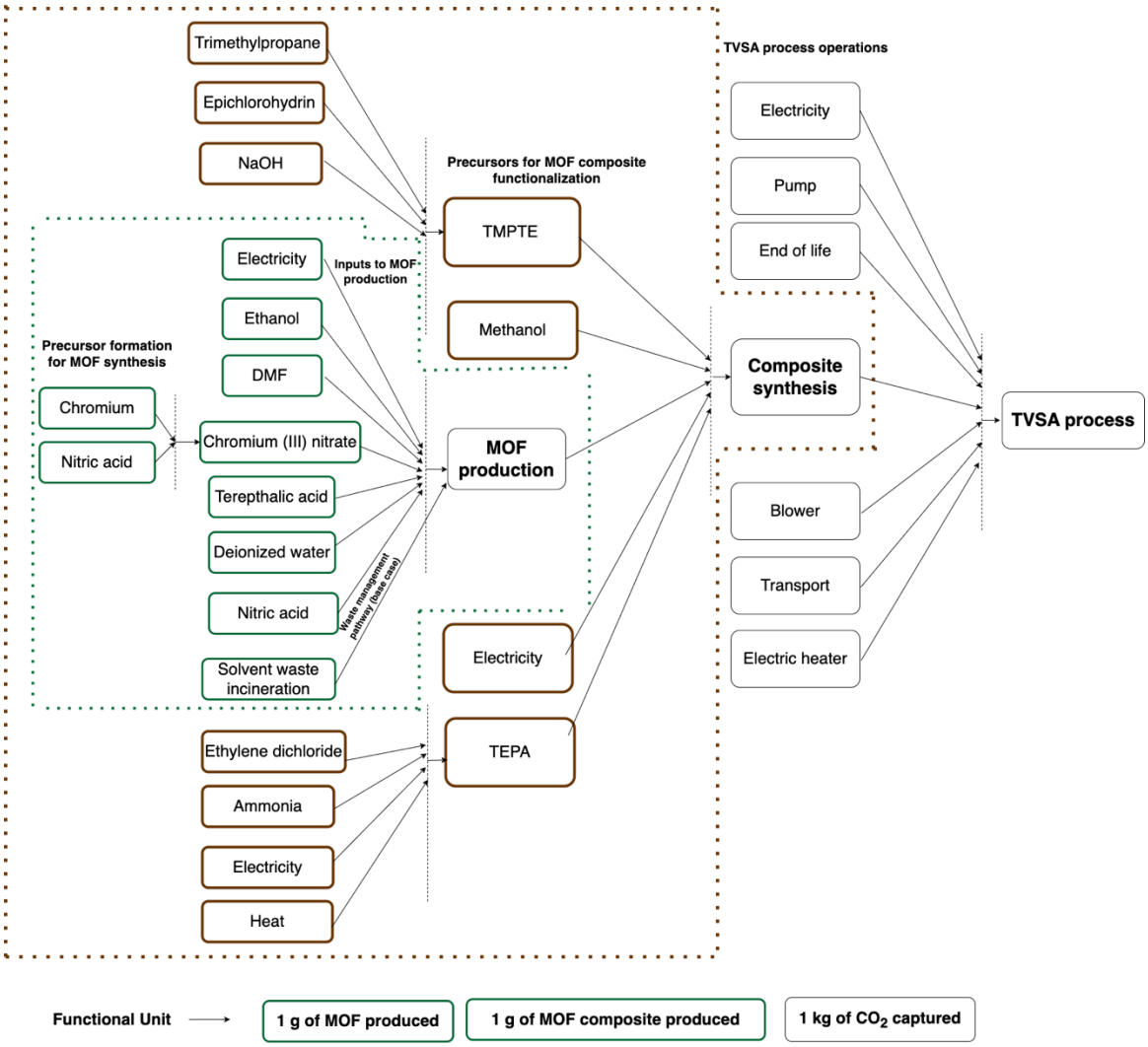


Figure 71: System boundary for this LCA study. The system encompasses three sequential functional units: (1) production of 1 g of Cr-BDC, (2) synthesis of 1 g of amine-epoxide functionalized MOF composite, and (3) capture of 1 kg of CO_2 via a temperature vacuum swing adsorption process. Material inputs, energy requirements, and streams for each stage are detailed, with system boundaries indicated for precursor synthesis, MOF formation, functionalization, TVSA operation, and end-of-life management.

Life cycle impact assessment of MOF-amine composite in a TVSA process

Life cycle impact assessment was performed using the IMPACT World+, footprint version, a midpoint-oriented LCIA methodology that offers broad geographical coverage and characterization of multiple environmental indicators. This method is particularly suited for evaluating global supply chains and adsorbent production systems with diverse upstream and downstream inputs.

The following five impact categories were used to assess the environmental emissions associated with the capture system.

- Climate change (CC), characterized by carbon footprint (kg CO_2-eq)
- Ecosystem quality (EQ), measured in PDF·m²·yr (Potentially Disappeared Fraction of species over area and time)
- Non-renewable energy use (NR), quantified as MJ eq of fossil and nuclear energy
- Human health (HH), reported in DALYs (Disability-Adjusted Life Years) indicating potential harm to human well-being
- Water footprint (WF), assessed via the water scarcity footprint (m³ world eq)

Energy requirements for MOF synthesis

Cr-BDC was synthesized following a protocol from literature and the details are given in the Appendix WP3. The energy analysis for Cr-BDC synthesis quantifies the power requirements across all process steps to establish the energy inventory for adsorbent production. The energy distribution is shown in Figure 72 (left). The synthesis process requires 19.02 kWh total energy, equivalent to 1.06 kWh per gram of final product (Appendix WP3, Table A5). This energy demand stems from the multi-step synthesis pathway involving reaction, washing procedures, and drying. Vacuum drying represents the largest single energy consumer, accounting for 63.1% of total consumption at 12 kWh.This substantial requirement results from the 24-hour drying period at room temperature using a vacuum oven to achieve solvent removal.

The synthesis step constitutes the second largest energy demand at 21.2% of total consumption, requiring 4.03 kWh to maintain reaction conditions at 200°C for 16 hours. The remaining energy requirements distribute across post-synthesis purification operations. Centrifugation procedures consume 3.2% of total energy across multiple washing cycles necessary for solvent exchange. Solvent washing operations, including both DMF and ethanol exchange steps, account for 3.8% of consumption through extended magnetic stirring requirements totaling 42 hours across multiple cycles.

Energy requirements for MOF-composite functionalization

Cr-BDC amine-functionalized composite was synthesized following the protocol developed in the laboratory and it is provided in the Appendix WP3. The functionalization process introduces a substantial additional energy burden beyond that of MOF synthesis, requiring a total of 20.30 kWh, equivalent to 2.54 kWh per gram of the final composite material (Appendix WP3, Table A6).

Vacuum drying is the dominant energy consuming step, accounting for 63.6% of the total energy input (12 kWh), as shown in the energy distribution analysis, Figure 72 (right). This is due to the 24 hour drying period at room temperature under vacuum, required to remove residual methanol and prepare the material for thermal curing. The curing step at 393 K represents the second largest contributor, demanding 6 kWh (31.9% of total energy) over a 12 hour treatment period, which is critical for completing the crosslinking reaction between amine and epoxide groups. The curing stage, which includes both the temperature ramp up to 393 K and maintaining it, collectively contributes 35.6% of the total functionalization energy. Specifically, the heating phase consumes 0.70 kWh over one hour, assuming a power input of 700 W, while the curing phase at 393 K operates at a lower power input (500 W) for 12 hours. The remaining energy demand arises from auxiliary preparatory operations, including initial dispersion, stirring, and centrifugation, which together account for less than 1% of the total energy consumed.

Overall, in both MOF synthesis and its functionalization, energy distribution highlights vacuum drying as the dominant process step, consuming nearly two-thirds of the total energy. Its disproportionate

contribution underscores the importance of optimizing this operation for industrial scale-up, where minimizing drying energy could significantly reduce overall environmental impact.

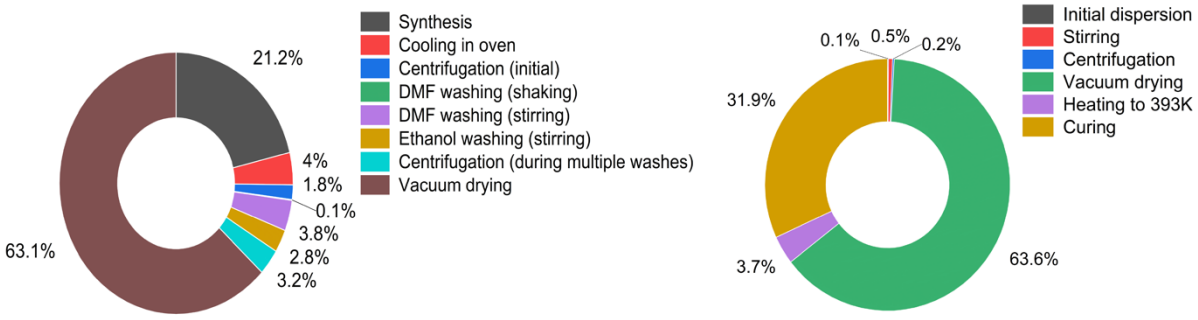


Figure 71: Energy distribution in MIL-101(Cr) synthesis (left) and functionalization with TEPA–TMPTE (right). Vacuum drying accounts for >60% of energy use in both cases.

Material-level impacts: pristine MOF and functionalized composite

Figure 73 shows the contribution of individual inputs to five midpoint impact categories for pristine Cr-BDC synthesis (per 1 g MOF). The dominant drivers are DMF, electricity, ethanol, and solvent waste disposal, with their importance varying by impact type (absolute values in Table 25). DMF, used heavily in washing/exchange, accounts for ~53% of climate change and non-renewable energy impacts, while ethanol burdens stem from agricultural supply chains. Electricity use, mainly from the ~24 h vacuum-drying step, drives water-scarcity impacts in Switzerland due to hydropower-dominated electricity grid. Solvent incineration contributes to human-health and ecosystem damages through residual NO_x, SO_2, and VOCs, making waste management as critical as energy efficiency. By contrast, inorganic precursors (chromium nitrate, nitric acid, terephthalic acid) remain minor contributors (<4%).

For the functionalized composite (per 1 g; absolute values in Table 25), the embedded MOF production dominates, contributing 66.6% of the carbon footprint, 36.8% of non-renewable energy use, and 52.5% of health impacts. Electricity from drying and curing is the next hotspot. Among organics, TMP (precursor to TMPTE) stands out with >35% of ecosystem-quality impacts, while other reagents (epichlorohydrin, ethylene dichloride, ammonia, NaOH, methanol) add smaller contributions. Overall, solvent-intensive MOF synthesis and energy-intensive drying steps are the primary levers for footprint reduction in both pristine and functionalized materials.

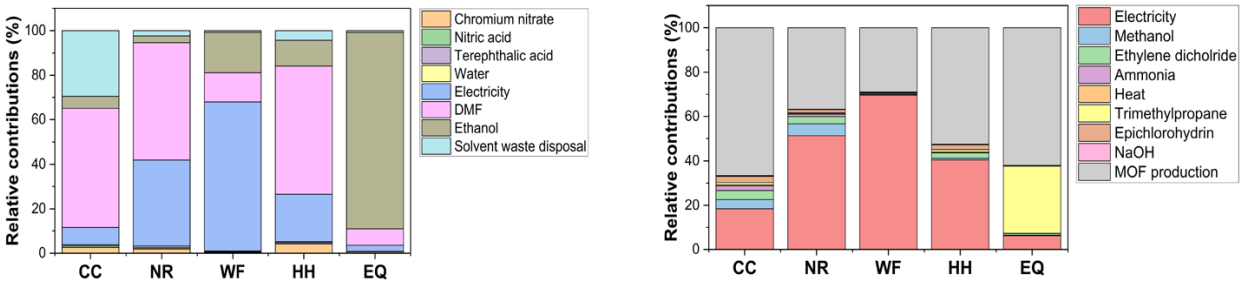


Figure 73: Environmental impact assessment of pristine Cr-BDC and functionalied MOF synthesis. The functional unit is for 1 gram of the adsorbent produced

Table 25: Life-cycle impact results per kg CO_2 captured in TVSA using Cr-BDC–TEPA–TMPTE, reported across five midpoint categories.

Indicator (impact category)	MOF	MOF composite	Unit
Carbon footprint (CC)	0.457	0.471	kg CO_2-eq
Fossil and nuclear energy use (NR)	8.320	15.54	PDF·m²·yr
Water scarcity footprint (WF)	0.673	1.60	MJ eq
Remaining human health damage (HH)	4.13×10^{-7}	5.40×10^{-7}	DALYs
Remaining ecosystem quality damage (EQ)	0.530	0.589	m³ world eq

Process level impacts: TVSA process

Under Swiss electricity conditions, Table 26 reports the carbon footprint of 0.450 kg CO_2-eq per kg CO_2 captured in TVSA process for the MOF composite. As shown by the stacked contributions in Figure 74, the functionalized MOF production dominates every midpoint category (~70–95% share across CC, NR, WF, HH, EQ). This dominance traces to solvent-intensive synthesis and the electricity required for vacuum drying and curing, which together embed substantial upstream burdens in the material.

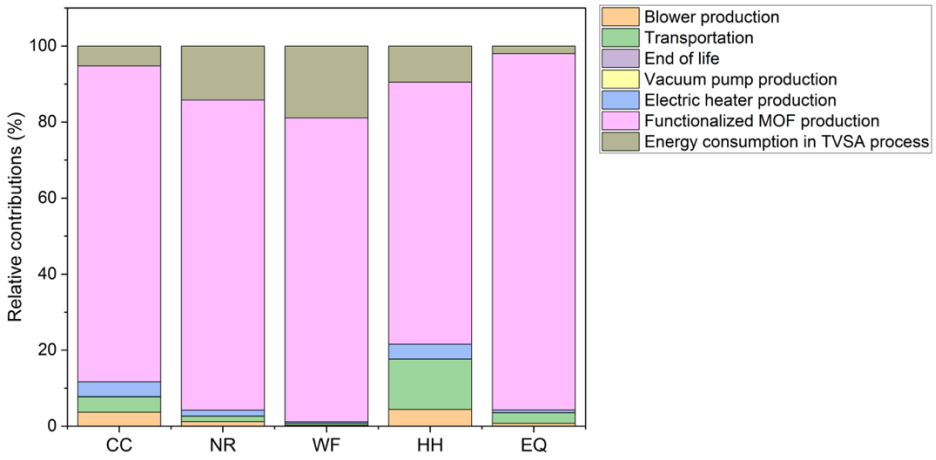


Figure 74: Life-cycle impacts per kg CO_2 captured in TVSA using MIL-101(Cr)–TEPA–TMPTE. Material production dominates (70–95% share), followed by operational energy, with infrastructure minor.

Table 26. Life-cycle impact results per kg CO_2 captured in TVSA using MIL-101(Cr)–TEPA–TMPTE, reported across five midpoint categories.

Indicator (impact category)	Total Impact	Unit
Carbon footprint (CC)	0.450	kg CO_2-eq
Fossil and nuclear energy use (NR)	15.14	MJ eq
Water scarcity footprint (WF)	1.59	m^3 world eq
Remaining human health damage (HH)	6.22×10^{-7}	DALYs
Remaining ecosystem quality damage (EQ)	0.499	PDF·m^2·yr

Operational energy for the TVSA cycle is the second most important block, especially in climate and non-renewable energy use. Even with Switzerland's low-carbon grid, the thermal duty for regeneration and the power required for evacuation and gas handling remain substantial. This points directly to heat-integration, reducing energy consumption as high-leverage levers on the process side.

Infrastructure and logistics (heaters, vacuum pump, blower manufacture; transport; end-of-life) are minor contributors at this scale, with comparatively larger visibility in human health and ecosystem quality due to materials processing and disposal. Their share may grow at deployment scale, but the immediate priorities are clear: reduce material-stage burdens (solvent recovery/air-drying) and lower operating energy, as these two actions will yield the largest, most reliable reductions in the TVSA life-cycle footprint.

Process improvements at the material stage

The environmental assessment highlights two main hotspots in MOF synthesis: energy use from vacuum drying and solvent usage in washing. To address these, two process modifications were evaluated on a per-gram basis of adsorbent production: replacing vacuum drying with air drying and performing solvent recovery.

Air drying showed that a simple change in the drying method can yield tangible reductions in material impacts (Table 27). The effect is strongest for the pristine MOF, where water and energy use drop substantially, but smaller for the functionalized MOF, where curing and additional reagents dominate

the burden. This indicates that while air drying is a useful improvement, its influence diminishes once functionalization steps are added. In practice, air drying is most effective at reducing the baseline footprint of large-scale MOF production, but less decisive when the composite synthesis is included.

Solvent recovery, in contrast, has a transformative effect (Table 28). Recovering DMF and ethanol eliminates the single largest contributor to environmental burden. For pristine MOF, the carbon footprint falls by nearly 80%, shifting the impact profile from being solvent-driven to being dominated by electricity and reagents. In the functionalized MOF, where solvents still represent a major share, the reduction is smaller in relative terms but still significant. These results show that solvent management, rather than energy use, is the key lever for improving the sustainability of MOF synthesis.

Taken together, the results demonstrate that drying and solvent recovery tackle different aspects of the synthesis burden. Air drying reduces background electricity demand and water scarcity impacts, while solvent recovery directly targets the dominant contributor in the baseline process. For future scale-up, solvent recovery stands out as the most effective single improvement, but combining it with optimized drying protocols provides a more balanced strategy for reducing the environmental footprint of both pristine and functionalized MOFs.

In addition, the choice of solvent exerts a strong influence on the overall environmental profile. Substituting high-impact aprotic solvents such as DMF with greener alternatives like Cyrene can markedly reduce both the carbon and water-related footprints, as Cyrene is bio-based, biodegradable, and its synthesis generates significantly lower CO_2 emissions per kilogram of solvent. Future work will explore the use of Cyrene in MOF synthesis to assess its impact on material performance and environmental outcomes.

Table 27: Comparison of environmental impacts of pristine MOF and functionalized MOF under baseline and air-drying scenarios (per gram of material produced).

Indicator (impact category)	MOF		MOF composite	
	Baseline	Air drying	Baseline	Air drying
Carbon footprint (CC)	0.457	0.435	0.471	0.456
Fossil and nuclear energy use (NR)	8.320	6.29	15.54	14.14
Water scarcity footprint (WF)	0.673	0.389	1.603	1.408
Remaining human health damage (HH)	4.13×10^{-7}	3.57×10^{-7}	5.40×10^{-7}	5.01×10^{-7}
Remaining ecosystem quality damage (EQ)	0.530	0.521	0.589	0.582

Table 28: Comparison of environmental impacts of pristine MOF and functionalized MOF under baseline and solvent-recovery scenarios (per gram of material produced).

Indicator (impact category)	MOF		MOF composite	
	Baseline	Solvent Rec.	Baseline	Solvent Rec.
Carbon footprint (CC)	0.457	0.0932	0.471	0.221
Fossil and nuclear energy use (NR)	8.320	3.970	15.54	12.55
Water scarcity footprint (WF)	0.673	0.479	1.60	1.47
Remaining human health damage (HH)	4.13×10^{-7}	1.40×10^{-7}	5.40×10^{-7}	3.52×10^{-7}
Remaining ecosystem quality damage (EQ)	0.530	0.0702	0.589	0.273

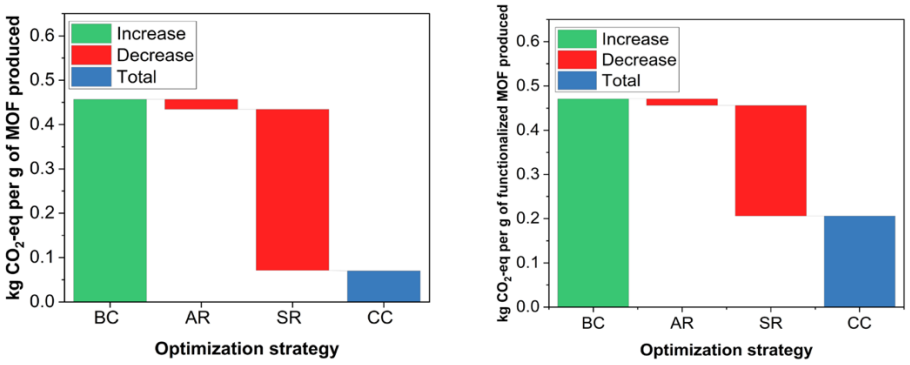


Figure 75: Effect of optimization strategies on the carbon footprint of pristine MOF (left) and functionalized MOF (right), reported per gram of material produced. BC = baseline case, AR = air drying, SR = solvent recovery, CC = combined case which includes the impacts from both air drying and solvent recovery.

Figure 75 shows the waterfall plot show how each optimization step contributes to lowering the carbon footprint of MOF synthesis, starting from the baseline case (BC).

- Baseline (BC): About 0.45–0.50 kg CO_2-eq per g MOF.
- Air drying (AR): Very small effect, reducing the footprint by only ~5%.
- Solvent recovery (SR): Major improvement, emissions drop by nearly 80% for pristine MOF (down to ~0.1 kg CO_2-eq/g) and about 55–60% for functionalized MOF (to ~0.2 kg CO_2-eq/g).
- Combined case (CC): Adding air drying on top of solvent recovery gives the lowest footprint, showing ~85% reduction for pristine and ~60% for functionalized MOF compared to baseline.

In short, solvent recovery is the dominant driver of reductions, while air drying adds a modest but complementary benefit.

Effect of MOF lifetime, electricity grid and heating strategy on CO_2 emissions

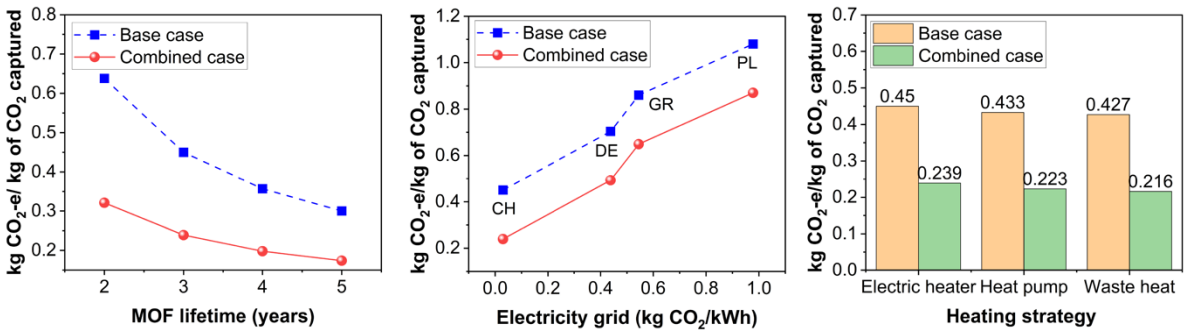


Figure 76: Sensitivity of life-cycle CO_2 emissions on (a) MOF lifetime (2–5 years), (b) varying regional electricity grid, and (c) heating strategy (waste heat, heat pump, electric). MOF synthesis improvements dominate overall footprint reduction.

Extending the analysis to MOF lifetime (Figure 76, left) highlights the strong influence of adsorbent durability on the process footprint. In the base case, increasing MOF lifetime from 2 to 5 years lowers the carbon footprint from ~0.63 to ~0.30 kg CO_2-eq per kg CO_2 captured, as impacts are amortized over

more capture cycles. The combined optimization case (air drying + solvent recovery) consistently outperforms the baseline, starting at ~0.32 kg CO_2-eq at year 2 and dropping further to ~0.17 kg CO_2-eq at year 5. This implies that the longer adsorbent lifetimes and improved synthesis strategies therefore substantially increase the net climate benefit of capture.

The sensitivity to regional electricity mix (Figure 76, middle) shows how deployment context shapes performance. Under coal-heavy conditions (Poland), the footprint exceeds 1.0 kg CO_2-eq/kg CO_2 in the base case, but drops below 0.4 kg in the combined case, showing optimization gains are magnified in carbon-intensive grids. For Germany and Greece, intermediate baselines also shrink substantially under the combined strategy, while Switzerland (low-carbon grid) already shows the lowest values. Finally, heating strategies (Figure 76, right) reveal smaller variations: waste heat, heat pump, and electric heating differ only marginally in the combined case (0.216–0.239 kg CO_2-eq), compared to ~0.43–0.45 kg in the baseline. This underlines that MOF synthesis improvements dominate the footprint, while heating choices offer only incremental benefits.

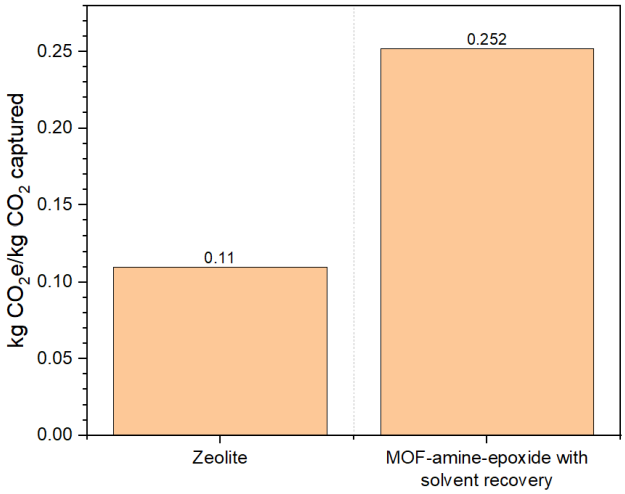


Figure 77: Life-cycle CO_2 emissions per kg CO_2 captured for zeolite and MOF–amine–epoxide with solvent recovery

Figure 77 compares the life-cycle CO_2 emissions associated with the investigated capture systems. Among the evaluated adsorbents, zeolite exhibited the lowest carbon footprint at approximately 0.11 kg CO_2-eq per kg CO_2 captured, whereas the MOF--amine--epoxide system with solvent recovery showed a higher footprint of approximately 0.25 kg CO_2 eq per kg CO_2 captured. The higher emissions associated with the MOF-based system mainly originate from the energy- and material-intensive synthesis steps required for MOF and amine functionalisation. Future improvements in solvent formulation and recovery may further reduce the environmental footprint of the process, particularly through the use of more sustainable, low-toxicity, and environmentally friendly solvents.

3 Conclusion and Outlook

This project results indicate that adsorption-based post-combustion CO_2 capture has matured into a technically credible, energetically efficient, and economically competitive alternative to conventional liquid amine scrubbing. Through the parallel development of dynamic process models, pilot-scale validation, life-cycle assessment, and adsorbent scale-up, a consistent and quantitative understanding of both material-level and system-level performance has been achieved. A key outcome is the establishment of a validated TVSA modelling framework, benchmarked against experimental breakthrough data, which enabled confident extrapolation from laboratory and pilot studies to industrial-scale scenarios. This framework showed that optimized TVSA operation can consistently deliver CO_2 purities above 95% and recoveries around or above 90%, meeting industrial requirements and DOE-relevant targets.

In the TVSA process implemented with zeolite 13X, industrial-scale simulations with full waste-heat integration resulted in capture costs of approximately 50 CHF t^{-1} CO_2 , positioning adsorption-based capture as cost-competitive with state-of-the-art solvent processes. Life-cycle assessment further demonstrated that TVSA achieved a carbon capture efficiency of 89.5%, confirming its environmental credibility alongside its economic performance. It should be noted, however, that the baseline cost estimate corresponds to an idealized dry-flue-gas scenario. In practice, flue gas from municipal solid waste incineration facilities contains significant moisture, which competes with CO_2 for adsorption sites on zeolite 13X and can lead to irreversible capacity loss if not addressed. Accounting for upstream flue-gas drying via a triethylene glycol dehydration unit adds approximately 8 CHF t^{-1} CO_2, bringing the total capture cost to approximately 58 CHF t^{-1} CO_2. This additional cost remains moderate and manageable, and does not undermine the overall competitiveness of the technology. Furthermore, sensitivity analysis showed that even at reduced waste-heat availability of 30%, capture costs remain within approximately 72 CHF t^{-1} CO_2, still within the cost ranges reported by the IEA for post-combustion CO_2 capture systems.[29]

In parallel to process development, the project delivered substantial advances in adsorbent design and scale-up. Beyond benchmarking zeolite 13X, amine-functionalized composite adsorbents based on both KIT-6 silica and Cr-BDC were successfully developed, scaled, and assessed. The KIT-6–amine composites demonstrated stable CO_2 capacities around 1 mmol g^{-1} at post-combustion-relevant conditions with good cyclic stability, while Cr-BDC –amine composites were scaled to the kilogram level without loss of crystallinity or porosity.

These MOF–amine composites were subsequently evaluated within a TVSA framework using pilot-scale process simulations. The objective of this assessment was not to establish industrial readiness, but to examine how such composites would perform when integrated into a realistic cyclic adsorption process. The simulations indicate that, under optimized cycle conditions, MOF–amine-based systems can achieve CO_2 purities and recoveries exceeding 95%, with specific energy consumptions on the order of 2.5 MJ kg^{-1} CO_2. While these results are derived from process modelling rather than extended pilot operation, they demonstrate that MOF–amine composites can be meaningfully assessed at the process level and provide a useful basis for comparison with conventional adsorbents within the same TVSA framework.

From an environmental standpoint, the work shows that signficant impacts may arise from the synthesis of the selected MOF-based material rather than its operation in post-combustion capture. Solvent-intensive washing and vacuum drying were identified as key contributors, yet the project demonstrated that solvent recovery and alternative drying strategies can reduce the carbon footprint by up to 80%. This finding highlights clear and actionable pathways to align advanced adsorbents with sustainability requirements. For zeolite-based systems, impacts were primarily driven by operational energy use, reinforcing the importance of heat integration and efficient regeneration strategies.

Overall, the project establishes that adsorption-based CO_2 capture, and TVSA in particular, has reached a level of technical, energetic, and economic maturity that justifies progression toward integrated demonstration and pre-commercial deployment. The combined development of scalable amine-

functionalized adsorbents, ranging from KIT-6 silica to Cr-BDC-based MOF composites, and validated process models provides a strong foundation for the next phase, which should focus on achieving long-term composite stability, integrated pilot operation, and further reduction of material production impacts. In parallel, alternative regeneration strategies, including pressure swing adsorption (PSA) and vacuum pressure swing adsorption (VPSA), should be explored, particularly for applications where waste heat is unavailable. If these aspects are addressed, adsorption-based CO_2 capture represents a credible, scalable, and flexible pathway for industrial CO_2 mitigation.

For the technology to reach market-scale deployment, several conditions must be met in a coordinated and sequential manner. On the material side, tonne-scale production of advanced adsorbents, including MOF–amine and silica–amine composites, must be demonstrated in collaboration with industrial manufacturers such as Zeochem, BASF, or Clariant, with reproducible quality and acceptable cost. At the process level, the technology must advance from its current TRL 4–6 to TRL 7 through fully integrated demonstration at an industrial host site, most immediately at municipal solid waste incineration facilities such as Satom SA or Enevi, where favorable flue gas composition and available waste heat provide the most competitive conditions, generating the operational data needed to validate techno-economic and life-cycle assessments under real conditions. Finally, most importantly, long-term sorbent durability beyond 1,000 adsorption–desorption cycles under realistic flue gas conditions, including exposure to humidity, SO_x, and NO_x, must be confirmed.

4 Publications and other communications

- Now that the pilot plant is up and running we aim to put project results on a tab on the LFIM website for all stakeholders to see project results now that the pilot plant is up and running.

  Here is the link to the project tab on LFIM website.

- We have already engaged twice in Scientistic events (open-door events to the public) held at EPFL-Valais, allowing us to communicate the results of the project to the public on our carbon capture project.
- We have shown the demonstrator and highlighted the results of our projects at multiple informal meetings held at EPFL, that has engaged industry, the public, and other academics.
- Several research papers were already submitted to peer-reviewed journals communicating results to the scientific community. There is already an additional report under peer review at the moment, and we expect to have several more before and/or after the project end.
- Presentations/seminars were given at academic institutions, conferences, company visits, and at EPFL events to politicians, industry, high school students and teachers, and/or the general public. For example, in the past two years, Prof. Queen and the rest of the team have presented the title project in a host of invited or keynote seminars given at:

  a. *The Out of the Blue Conference* in Crete, Greece (2024),
  b. *The 9th EuChemS Meeting* in Dublin Ireland (2024),
  c. *The UK PorMat Meeting* at Liverpool, England (2024),
  d. Frühjahrssymposium 2024, titled “Rethinking Chemistry: Towards A Greener Future” in Ulm, Germany,
  e. *The Swiss Snow Symposium 2024* in Saal-Allmagell, Switzerland,
  f. *EuroMOF 2023* in Grenada, Spain,
  g. A *GRC* titled “Nanoporous Materials and their Applications” in New Hamshire, USA,
  h. A *GRC* titled “Atomically Precise Nanochemistry” (2024) in Galveston Texas (USA)
  i. A Telluride Conference on Porous Materials in Telluride Colorado, USA,
  j. Japanese Decarbonization Delegation Meeting Sion, Swtizerland
  k. The 1st Mediteranean Conference on porous materials (MEDPore 23) in Crete, Greece,
  l. A CCUS workshop in 2024, which had many players from the cement industry, Lausanne, Switzerland
  m. An event for high school teachers (2024) held at EPFL in Sion Switzerland
  n. *Sustainability Week* for High School Students (2023 & 2024) held at EPFL Lausanne, Switzerland
  o. The University of Zurich, Switzerland
  p. The University of Basel, Switzerland
  q. The University of California Berkeley, USA
  r. Clemson University, South Carolina, USA
  s. *The Modification of Metal-Organic Frameworks for Improving Performance in Globally Relevant Separations*, SCIRES 2025 International Meeting, University of Zagreb,

Croatia (Plenary Lecture), https://www.meetinzagreb.hr/news/scires-2025-international-meeting-in-zagreb-brings-together-scientists-from-16-countries

t. *Optimizing MOFs in the Removal of Heavy Elements from Water and Waste*, 4th International School on Porous Materials – MOF School 2025, Lake Como, Italy, https://mofs.lakecomoschool.org/

u. *The Design of Highly Porous Materials for Metal Recovery from Waste*, Fireside Chat on Critical Raw Materials and Energy, EPFL Energy Center and Master in Energy Students and Alumni Association of EPFL, Lausanne Switzerland, May 1, 2025. https://www.epfl.ch/campus/associations/messaa/page-130923-en-html/

v. *Realizing the global benefits of the world's most porous materials*, presentation given to Spiez Lab, Sion Switzerland, June 4, 2025.

w. Modification of porous materials for globally relevant liquid and gas separations, Swiss MatChem Symposium 2025, Adolphe-Merkle Institute, University of Fribourg, Fribourg, Switzerland; https://mat25.scg.ch/

x. Sanjay presented a poster at the prestigious Gordon Research Conference (GRC) on Carbon Capture, Utilization, and Storage (CCUS) held in California in April 2025. His poster, focused on the techno-economic and life-cycle assessment of Zeolite 13X for CO_2 capture, was awarded one of the Best Poster Prizes at the conference.

y. Sanjay was selected to participate in the IEA CCUS Summer School 2025, held in July 2025 in Ventura, Canada, where he presented a research poster on his ongoing work in carbon capture and utilization systems. https://ieaghg.org/events/2025-ieaghg-international-ccs-summer-school/

- We have also discussed the results with various industries throughout Switzerland, including incineration and cement plants. Normally, we interact with multiple industries per year during their visits to EPFL (like Total, ExxonMobil, Rolex, Forbes Marshall, Poste, Spiez Lab, Sulzer, Oiken, OCP, and the Global Cement and Concrete Association). Last, we also have yearly project meetings with Gaznat, which will also be very interested to see the results.

List of published material

- Post-synthetic Covalent Grafting of Amines to NH_2-MOF for Post-Combustion Carbon Capture" A. Justin, J. Espín, M. J. Pougin, D. Stoian, T.Schertenleib, M. Mensi, I. Kochetygov, A. Ortega-Guerrero, W. L. Queen*, Adv. Funct. Mater. **2023**, published online.
- N-containing carbons derived from microporous coordination polymers for use in post-combustion flue gas capture" V. V. Karve, J. Espín, M. Asgari, S. Van Gele, E. Oveisi, W. L. Queen*, Adv. Funct. Mater., **2023**, 33, 2212283.
- Densification and shaping of pure Cu-BTC powders using a solid-state chemical transformation" V. V Karve, A. Mabillard, J. Espin, M. Asgari, W. L. Queen, M. Soutrenon, Mater. Res. Express **2024**.
- A Ship-in-a-Bottle Strategy: Crosslinking Amines and Epoxides Inside MOF Pores for Enhanced CO2 Capture Performance" J. Espin, A. Justin, A. Hueber, A. Belin, S. Venkatachalam, H. D. Singh, E. Oveisi, W. L. Queen, *Adv. Mater.,* **2025**, e10138.
- *Method of Preparing Porous CO2 Adsorbent Material & Uses Thereof, W. L. Queen; J. M. Espin* Application Ser. No: EP 23 219539.6.

- Post-synthetic Covalent Grafting of Amines to NH2-MOF for Post-Combustion Carbon Capture" A. Justin, J. Espín, M. J. Pougin, D. Stoian, T. Schertenleib, M. Mensi, I. Kochetygov, A. Ortega-Guerrero, W. L. Queen*, *Adv. Funct. Mater.* **2023**, published online.
- N-containing carbons derived from microporous coordination polymers for use in post-combustion flue gas capture" V. V. Karve, J. Espín, M. Asgari, S. Van Gele, E. Oveisi, W. L. Queen*, *Adv. Funct. Mater.*, **2023**, 33, 2212283.
- Densification and shaping of pure Cu-BTC powders using a solid-state chemical transformation" V. V Karve, A. Mabillard, J. Espin, M. Asgari, W. L. Queen, M. Soutrenon, *Mater. Res. Express*, **2024**.
- A Ship-in-a-Bottle Strategy: Crosslinking Amines and Epoxides Inside MOF Pores for Enhanced CO2 Capture Performance" J. Espin, A. Justin, A. Hueber, A. Belin, S. Venkatachalam, H. D. Singh, E. Oveisi, W. L. Queen, *Adv. Mater.*, **2025**, e10138.
- *Method of Preparing Porous CO2 Adsorbent Material & Uses Thereof, W. L. Queen; J. M. Espin* Application Ser. No: EP 23 219539.6.

5 References

1. Yuan, B. *et al.* Intrinsic insight of energy-efficiency optimization for CO2 capture by amine-based solvent: effect of mass transfer and solvent regeneration. *Int. J. Greenh. Gas Control* **118**, 103673 (2022).
2. Peeters, W., Neerup, R. & Fosbøl, P. L. Solvent degradation & influences on amine-based carbon capture operations. *Int. J. Greenh. Gas Control* **147**, 104500 (2025).
3. Adil, A. & Chohan, U. W. Climate Change as Socioeconomic Threat: International Perspectives. SSRN Scholarly Paper at https://doi.org/10.2139/ssrn.3544582 (2020).
4. Winski, D. *et al.* A 400-Year Ice Core Melt Layer Record of Summertime Warming in the Alaska Range. *J. Geophys. Res. Atmospheres* **123**, 3594–3611 (2018).
5. Melet, A., Meyssignac, B., Almar, R. & Le Cozannet, G. Under-estimated wave contribution to coastal sea-level rise. *Nat. Clim. Change* **8**, 234–239 (2018).
6. Sun, D. T. & Queen, W. L. Mystical Material Might Help Solve Global Energy Problems. *ACS Cent. Sci.* **5**, 1307–1309 (2019).
7. Quadrelli, R. & Peterson, S. The energy–climate challenge: Recent trends in CO2 emissions from fuel combustion. *Energy Policy* **35**, 5938–5952 (2007).
8. *Gas Purification*. (1997).
9. Reitze, A. W. Federal Control of Carbon Capture and Storage. SSRN Scholarly Paper at https://papers.ssrn.com/abstract=2143623 (2011).
10. Ünveren, E. E., Monkul, B. Ö., Sarıoğlan, Ş., Karademir, N. & Alper, E. Solid amine sorbents for CO2 capture by chemical adsorption: A review. *Petroleum* **3**, 37–50 (2017).
11. Wang, J. *et al.* Recent advances in amine-functionalized silica adsorbents for CO2 capture. *Renew. Sustain. Energy Rev.* **203**, 114724 (2024).
12. Espín, J. *et al.* A Ship-in-a-Bottle Strategy: Crosslinking Amines and Epoxides inside MOF Pores for Enhanced CO2 Capture Performance. *Adv. Mater.* **37**, e10138 (2025).

13. Zhao, T. *et al.* High-yield, fluoride-free and large-scale synthesis of MIL-101(Cr). *Dalton Trans.* **44**, 16791–16801 (2015).
14. Milner, P. J. *et al.* Overcoming double-step CO2 adsorption and minimizing water co-adsorption in bulky diamine-appended variants of Mg2(dobpdc). *Chem. Sci.* **9**, 160–174 (2017).
15. Justin, A. *et al.* Post-Synthetic Covalent Grafting of Amines to NH2-MOF for Post-Combustion Carbon Capture. *Adv. Funct. Mater.* **34**, 2307430 (2023).
16. Deng, X., Chen, K. & Tüysüz, H. Protocol for the Nanocasting Method: Preparation of Ordered Mesoporous Metal Oxides. *Chem. Mater.* **29**, 40–52 (2017).
17. Karve, V. V. *et al.* N-Containing Carbons Derived from Microporous Coordination Polymers for Use in Post-Combustion Flue Gas Capture. *Adv. Funct. Mater.* **33**, 2212283 (2023).
18. CO2 Capture by Temperature Swing Adsorption: Use of Hot CO2-Rich Gas for Regeneration | Industrial & Engineering Chemistry Research. https://pubs.acs.org/doi/10.1021/acs.iecr.5b01384.
19. gPROMS Digital Process Design and Operation. *Siemens* https://www.siemens.com/global/en/products/automation/industry-software/gproms-digital-process-design-and-operations.html.
20. Sharma, S. & Maréchal, F. Carbon Dioxide Capture From Internal Combustion Engine Exhaust Using Temperature Swing Adsorption. *Front. Energy Res.* **7**, (2019).
21. Jiang, N. *et al.* CO2 capture from dry flue gas by means of VPSA, TSA and TVSA. *J. CO2 Util.* **35**, 153–168 (2020).
22. Liu, W. *et al.* Steam-assisted temperature swing adsorption for carbon capture integrated with heat pump. *Case Stud. Therm. Eng.* **49**, 103233 (2023).
23. Susarla, N. *et al.* Energy and cost estimates for capturing CO2 from a dry flue gas using pressure/vacuum swing adsorption. *Chem. Eng. Res. Des.* **102**, 354–367 (2015).
24. Subraveti, S. G., Roussanaly, S., Anantharaman, R., Riboldi, L. & Rajendran, A. Techno-economic assessment of optimised vacuum swing adsorption for post-combustion CO2 capture from steam-methane reformer flue gas. *Sep. Purif. Technol.* **256**, 117832 (2021).

25. Turton, R., Bailie, R. C., Whiting, W. B. & Shaeiwitz, J. A. *Analysis, Synthesis and Design of Chemical Processes*. (Pearson Education, 2008).
26. Reimann, D. O. *CEWEP Energy Report III*. (2012).
27. Garcia, M., Berghout, N. & Herraiz, L. *Cost of CO2 Capture in the Industrial Sector: Cement and Iron and Steel Industries*. (2018).
28. Hasan, M. M. F., Baliban, R. C., Elia, J. A. & Floudas, C. A. Modeling, Simulation, and Optimization of Postcombustion CO2 Capture for Variable Feed Concentration and Flow Rate. 1. Chemical Absorption and Membrane Processes. *Ind. Eng. Chem. Res.* **51**, 15642–15664 (2012).
29. Is carbon capture too expensive? – Analysis. *IEA* https://www.iea.org/commentaries/is-carbon-capture-too-expensive (2021).

6 Appendix

6.1 WP2 Adsorbent Design, Scale Up and Synthesis

Cr-MOF synthesis (referred to as Cr-BDC or MIL-101(Cr))

Cr-MOF was synthesized using a protocol that is similar to one previously reported. For this, a 1 L autoclave is charged with 52.8 g $Cr(NO_3)_3.9H_2O$, 18 g terephthalic acid (BDC), 660 mL DI water and 8.56 mL HNO_3 (65 %), and the mixture is stirred for 30 mins to homogeneous the solution. The autoclave is then kept in a preheated oven at 200 °C for 16 h and cooled to RT in 4 h. The reaction yields ~18 grams of green MOF powder.

Optimization of Cr-MOF washing protocol

After vacuum filtration, to remove the as-prepared MOF, the material must be extensively washed before subsequent modification with the amines. The need for washing stems from residual starting materials that are trapped inside the MOF pores, namely ligands. In the reported protocol,[13] for producing the MOF in 1 L scale with high crystallinity and surface area of 3400 m^2/g, about 3 L of DMF and 3L of ethanol is used. Hence, the total cost in producing MOF is 66.25 CHF per L of reaction. Remarkably, about 60 CHF/L reaction comes solely from the use of DMF solvent. Here, to reduce the cost, we optimized the amount of DMF used in the washing protocol. Such optimization is achieved by careful characterization of each washing step and analyzing aliquots of the washed solvent in ^{1}H-NMR to detect the concentration of MOF ligand removed in each washing step. We used four different washing protocols with DMF, to achieve the optimum material with the lowest amount required of DMF solvent.

Protocol 1: The 1 L reaction product is separated in four flasks with a volume of 250 mL each. The as-synthesized MOF is centrifuged to remove the mother liquor and dispersed in 50 mL of DMF and stirred at RT for 4 h, 12 h and 6 h with fresh solvent (50 mL each). Then the material is washed with ethanol at RT for 6 h, 12 h and 6 h with fresh solvent (50 mL each) and subsequently air dried for 2-3 days.

Protocol 2: The 1 L reaction product is separated in four flasks with a volume of 250 mL each. The as-synthesized MOF is centrifuged to remove the mother liquor and dispersed in 50 mL of DMF and stirred at RT for 24 h and 24 h with fresh solvent (50 mL each). Then the material is washed with ethanol at RT for 6 h, 12 h and 6 h with fresh solvent (50 mL each) and subsequently air dried for 2-3 days.

Protocol 3: The 1 L reaction product is separated in four flasks with a volume of 250 mL each. The as-synthesized MOF is centrifuged to remove the mother liquor and dispersed in 50 mL of DMF and stirred at RT for 72 h with fresh solvent. Then the material is washed with ethanol at RT for 6 h, 12 h and 6 h with fresh solvent (50 mL each) and subsequently air dried for 2-3 days.

Protocol 4: The 1 L reaction product is separated in four flasks with a volume of 250 mL each. The as-synthesized MOF is centrifuged to remove the mother liquor and dispersed in 100 mL of DMF and stirred at RT for 72 h with fresh solvent. Then the material is washed with ethanol at RT for 6 h, 12 h and 6 h with fresh solvent (50 mL each) and subsequently air dried for 2-3 days.

NMR analysis for Cr-MOF washing optimization

In all cases, the supernatant after centrifugation was vacuum dried at 80 °C and analyzed via ^{1}H NMR in dmso-d6, with 2.5 µL CH_2Br_2 as internal standard. For instance, the MOF washed with 50 mL DMF for three times is presented in Figure 11. Here, we ignore the wash 1 (W1) since the supernatant was greenish in color, which formed complexes with some unreacted Cr to form some complex under the drying conditions. Hence the ^{1}H NMR could not be quantified. Whereas, in W2 and W3, clearly the proton signals are sharp and there is a huge drop in BDC ligand conc at 8.2 ppm from W2 to W3. This

implies, with only two washing steps we could efficiently remove all the unreacted ligands from the MOF pores.

Scale-up protocol of Cr-MOF (2 L)

To synthesize MIL-101-Cr on a 2L scale, 105.6 g of $Cr(NO_3)_2 \cdot 9H_2O$ salt and 36 g of BDC ligand are combined with 1320 mL of H_2O as the solvent. Next, 17.12 mL of HNO_3 is added as a modulator. The mixture is placed in a 2L reactor and stirred at room temperature for 30 minutes. Afterward, the reactor is sealed and heated in an oven at 200°C for 16 hours.

After the synthesis is complete, the solution mixture is divided into three 1L bottles and centrifuged at 5000 RPM for 5 minutes. The supernatant is decanted, and 400 mL of DMF is added, evenly distributed among the three bottles. The mixture is stirred in three cycles of 6 hours, 12 hours, and 6 hours, replacing the solvent with fresh DMF after each cycle. The same washing process is repeated using EtOH. After washing, the solid is air-dried for 12 hours, yielding the final product. Each 2L reaction typically yields approximately 40–50 g of the product.

Scale-up protocol of Cr-MOF-TEPA-TMPTE (2 g)

To functionalize MIL-101-Cr, 2200 mg of bare MOF is placed in a 500 mL round-bottom flask, followed by the addition of 80 mL of methanol. Next, 42 mL of TEPA is added, and the mixture is stirred for 5 minutes. In a separate flask, 20.5 mL of TMPTE is dissolved in 80 mL of methanol, and the solution is added to the initial mixture. The combined mixture is stirred at 25°C for 3 hours, then centrifuged at 7800 RPM for 7 minutes. The supernatant is decanted, and the solid is vacuum-dried at 60°C for 24 hours.

Scale-up protocol of Cr-MOF-TEPA-TMPTE (4 g)

4400 mg of MIL-101(Cr) was dispersed in 160 mL of methanol in a 1000 mL round-bottom flask. To this suspension, 84 mL of tetraethylenepentamine (TEPA) was added, and the mixture was stirred for 5 minutes. In a separate flask, 41 mL of trimethylolpropane triglycidyl ether (TMPTE) was dissolved in 160 mL of methanol, and this solution was subsequently added to the MOF suspension. The combined mixture was stirred at 25 °C for 12 hours, followed by centrifugation at 7800 rpm for 7 minutes. The supernatant was decanted, and the recovered solid was dried under vacuum at 60 °C for 24 hours.

Protocol of CALF-20

6.60 g of zinc oxalate, 5.00 g of 1,2,4-triazole and 66.0 mL of methanol were added into a 125 mL Teflon autoclave. The autoclave was heated in a convection oven at 180 °C for 48 hours. The product was washed with 40.0 mL of methanol by soaking for 1 hour. 7.30 g of air-dried white powder was collected. The MOF was activated under dynamic vacuum at 100 °C for 12 hours.

Synthetic protocol of Al-formate

Formic acid (100 ml) and aluminum hydroxide (1.2 g, 0.015 mol) were refluxed in a 250-ml three-neck round-bottom flask at 100°C (373 K) for 48 hours. After completing the reaction, excess formic acid was extracted by centrifugation, and the white solid was rinsed with a copious amount of ethanol for 1 hour and separated using vacuum filtration. The MOF was activated under dynamic vacuum at 150 °C for 12 hours.

Protocol of SIFSIX-3-Ni ($Ni(pyr)_2(SiF_6)$)

SIFISIX-3-Ni was synthesized by slurrying 870 mg (3 mmol) of $Ni(NO_3)_2$, 534 mg (3 mmol) of $(NH_4)_2SiF_6$ and 480 mg (6 mmol) of pyrazine in 4 mL of water for 2 days. The resulting suspension was filtered under vacuum and dried in air. This precursor was soaked in 20 mL methanol for 1 day and then washed twice with two portions (ca. 10 mL) of methanol on a Buchner filter with vacuum filtration. The MOF was activated under dynamic vacuum at 140 ^oC for 24 hours.

Protocol of Mg-dobdc

Typically, in a solution of 30 mL dimethylformamide, 2 mL ethanol, and 2 mL water were dissolved 0.299 g 2,5-dihydroxyterephthalic acid and 1.244 g $Mg(NO_3)_2{\cdot}6H_2O$ with sonication. The resulting stock solution was decanted into five 10 mL PTFE microwave reaction tubes. The reaction solution was then rapidly heated to 125 ^oC in 25 min (1200 W power) and was held at this temperature for 4 h. After cooling to room temperature, the solid products were collected by centrifugation and washed three times with methanol (shaking with 50 mL methanol for 1 hour) and dry for further use. The MOF was activated under dynamic vacuum at 150 ^oC for 12 hours.

Shaping the bentonite-based NaX in tablets

The zeolite NaX powder was purchased from abcr GmbH and then shaped using a tableting approach. For this, 0.1 g of NaX powder was mixed with binder via grinding for around 5 minutes. Then 0.15 g of powder was added to a die having a diameter of 8 mm and then pressed using a commercial device D-6100, purchased from ORIEL GMBH, and held there for around 2 minutes. The resulting tablet had the following dimensions, 1.9 mm height by 8 mm diameter.

Shaping the binderless Cr-MOF and Cr-MOF-NH_2 in tablets

0.1 g of Cr-MOF powder was added to a die having a diameter of 8 mm and then pressed at 100 MPa using a commercial device D-6100, purchased from ORIEL GMBH, and held there for around 2 minutes. The resulting tablet had the following dimensions 3.7 mm height by 8 mm diameter.

Shaping the Cr-MOF-amine composite in tablets

After shaping the Cr-MOF, we set out to shape the Cr-MOF amine composite into pellets, employing a binder-free pressing technique. The pellets, which were 8 mm in diameter, were produced under two different pressing pressures including 60 MPa and 90 MPa.

Shaping the Cr-MOF in the automatic pellet machine

We experimented with a 3mm die in the automatic pellet-making machine in our laboratory. The actual column in the demonstrator pilot plant device requires a pellet diameter within the 2mm–4mm range. To produce pellets, we adjusted the die depth and corresponding pressure to optimized levels on the automatic pellet machine. The die was manually filled to the top with bare MOF powder, and the machine was activated to complete one cycle, during which it automatically ejected the pellet.

Protocol of CALF-20 tablet

0.1 g of CALF-20 powder was mixed with the selected binder via grinding for around 5 minutes. Then 0.15 g of powder was added to a die having a diameter of 8 mm and then pressed using a commercial device D-6100, purchased from ORIEL GMBH, and held there for around 2 minutes. The resulting tablet had the following dimensions 2 mm height by 8 mm diameter.**Protocol of Al-formate tablet**

Al-formate powder (0.1 g) was mixed with the selected binder via grinding for around 5 minutes. Then 0.15 g of powder was added to a die having a diameter of 8 mm and then pressed using a commercial device D-6100, purchased from ORIEL GMBH, and held there for around 2 minutes. The resulting tablet had the following dimensions 2 mm height by 8 mm diameter.

Protocol of SIFSIX-3-Ni tablet

SIFSIX-3-Ni powder (0.1 g) was mixed with the selected binders via grinding for around 5 minutes. Then 0.15 g of powder was added to a die having a diameter of 8 mm and then pressed using a commercial device D-6100, purchased from ORIEL GMBH, and held there for around 2 minutes. The resulting tablet had the following dimensions 2.1 mm height by 8 mm diameter.

Protocol of Mg-dobdc tablet

Mg-dobdc powder (0.1 g) was added to a die having a diameter of 8 mm and then pressed using a commercial device D-6100, purchased from ORIEL GMBH, and held there for around 2 minutes. The resulting tablet had the following dimensions 2 mm height by 8 mm diameter.

Automated tableting of NaX

Last, NaX-bentonite tablets were tested in process flow for their scale up production. For this, 8 mm and 3 mm NaX tablets were successfully produced using procedures that are similar to the ones outlined above, which were prepared individually and by hand.

Scale-up protocol of KIT-6 mesoporous silica

Pluronic acid polymer (P123, 40.5 g) was melted at 70 °C and weighed in the balance. The melted P123 was added to deionized water (1.46 L), stirred and then placed in a 2 L Teflon reactor. Hydrochloric acid (37 %, 78.3 g) was added dropwise and stirred until complete dissolution. The reactor was heated to 35 °C in an oven. Upon stable temperature, 1-butanol (50 mL) was added, and allowed to stir for 1 h. Tetraethyl orthosilicate (TEOS, 92.6 mL) was quickly added under vigorous stirring (450 rpm) and kept at 35 °C for 24 h. Note: a white precipitate formed in the first few hours of the reaction.

After the 24-hour period, the reactor was cooled and the stirring magnet was removed from the reactor. The reactor was then transferred into a stainless-steel autoclave and placed in a preheated oven at 135 °C for 24 h. After cooling to RT, the obtained product was vacuum-filtered using a Buchner funnel, and the solid left was dried in the oven at 100 °C overnight. The solid was then ground to break down large chunks of material, and the synthesized KIT-6 was calcinated under air using the following procedure: heated in 30 min to 180 °C, held 2 h at 180 °C, heated in 4 h to 550 °C and held 6 h at 550 °C. The material was then cooled down naturally.



Figure A1: Pictures of the KIT-6 synthesis protocol steps.

Protocol of KIT-6 mesoporous silica impregnation with amines

Prior to the grafting step, KIT-6 (1.0 g) was activated at 150 °C overnight under vacuum on a Schlenkline. The material was then transferred to a round bottom flask equipped with a stopcock and condenser. Dry toluene (50 mL) and (3-glycidoxypropyl)methyldimethoxysilane (2.5 mL) were added under nitrogen atmosphere. The reaction mixture was refluxed under magnetic stirring for 24 h. After cooling, the solid product was recovered by centrifugation. Washing with toluene (40 mL) and acetone (40 mL) yielded a white solid that was dried under vacuum overnight and stored under argon.

Protocol for shaping KIT-6 mesoporous silica containing amines

Amine-grafted KIT-6 silica powder (0.1 g) was added to a die having a diameter of 3 mm and then pressed using a commercial industrial tableting machine and held there for around 1 min.

Protocol for making N-doped carbons: 2,2"-bipyridine

2,2"-bipyridine (559 mg) and cobalt nitrate hexahydrate (200 mg) were mixed in ethanol (10 mL) and sonicated for 15 min to homogenize the reagents. Next, the solvent was removed using a vacuum oven at room temperature overnight. Finally, the solid sample was placed in a ceramic boat and introduced in a furnace, purged for 15 min under Ar, and heated up to 600 °C using a temperature ramp (5 °C/min), held at that temperature for 2 h, and let cool down naturally. In order to leach the cobalt from the synthesized carbon, 150 mg of the obtained solids were immersed in 40 mL of HCl 37% and heated at 90 °C for 24 h. The solids were centrifuged for 15 min at 7800 rpm and washed using a sodium bicarbonate solution (1 M) to obtain a neutralized suspension. Finally, the samples were washed three times with deionized water and dried at 80 °C for 12 h.

Protocol for making N-doped carbons: 2,2"-bipyrimidine

2,2"-bipyrimidine (552 mg) and cobalt nitrate hexahydrate (200 mg) were mixed in ethanol (10 mL) and sonicated for 15 min to homogenize the reagents. Next, the solvent was removed using a vacuum oven at room temperature overnight. Finally, the solid sample was placed in a ceramic boat and introduced in a furnace, purged for 15 min under Ar, and heated up to 600 °C using a temperature ramp (5 °C/min), held at that temperature for 2 h, and let cool down naturally. In order to leach the cobalt from the synthesized carbon, 150 mg of the obtained solids were immersed in 40 mL of HCl 37% and heated at 90 °C for 24 h. The solids were centrifuged for 15 min at 7800 rpm and washed using a sodium bicarbonate solution (1 M) to obtain a neutralized suspension. Finally, the samples were washed three times with deionized water and dried at 80 °C for 12 h.

Protocol for making N-doped carbons: 5-5"-dibromo-2,2"-bipyridine

5-5"-dibromo-2,2"-bipyridine (278 mg) and cobalt nitrate hexahydrate (200 mg) were mixed in ethanol (10 mL) and sonicated for 15 min to homogenize the reagents. Next, the solvent was removed using a vacuum oven at room temperature overnight. Finally, the solid sample was placed in a ceramic boat and introduced in a furnace, purged for 15 min under Ar, and heated up to 600 °C using a temperature ramp (5 °C/min), held at that temperature for 2 h, and let cool down naturally. In order to leach the cobalt from the synthesized carbon, 150 mg of the obtained solids were immersed in 40 mL of HCl 37% and heated at 90 °C for 24 h. The solids were centrifuged for 15 min at 7800 rpm and washed using a sodium

bicarbonate solution (1 M) to obtain a neutralized suspension. Finally, the samples were washed three times with deionized water and dried at 80 °C for 12 h.

Protocol for making N-doped carbons: 4-4"-dibromo-2,2"-bipyridine

4-4"-dibromo-2,2"-bipyridine (278 mg) and cobalt nitrate hexahydrate (200 mg) were mixed in ethanol (10 mL) and sonicated for 15 min to homogenize the reagents. Next, the solvent was removed using a vacuum oven at room temperature overnight. Finally, the solid sample was placed in a ceramic boat and introduced in a furnace, purged for 15 min under Ar, and heated up to 600 °C using a temperature ramp (5 °C/min), held at that temperature for 2 h, and let cool down naturally. In order to leach the cobalt from the synthesized carbon, 150 mg of the obtained solids were immersed in 40 mL of HCl 37% and heated at 90 °C for 24 h. The solids were centrifuged for 15 min at 7800 rpm and washed using a sodium bicarbonate solution (1 M) to obtain a neutralized suspension. Finally, the samples were washed three times with deionized water and dried at 80 °C for 12 h.

Protocol for synthesis of chitosan-derived mesoporous carbon

Chitosan-derived mesoporous carbon was synthesized by a hard-template route: 2.00 g of chitosan were dissolved in 200.00 g water/acetic acid (100/1 v/v); 8.75 g of LUDOX AS-40 silica colloids were then added dropwise to the solution with vigorous stirring; the mixture was stirred at ambient temperature to let the solvent almost totally evaporate (48 h); the obtained gel was further dried at ambient temperature for 24 h to result in a semi-transparent film; the film was pyrolyzed at 900 °C for 4 h with the protection of N_2; the carbonized product was washed by aqueous HF with the concentration of 10 wt% for 3 times and distilled water for 3 times; the crude product was finally dried at 120 °C for 24 h.

Protocol for amine-epoxide impregnation into chitosan-derived mesoporous carbon

Chitosan-derived mesoporous carbon (60 mg) was dispersed in methanol (6 mL) under magnetic stirring (200 rpm). Tetraethylenepentamine (512 µL) was then added, and the mixture was stirred for 5 min at 200 rpm. Butadienediepoxide (107 µL) previously diluted in methanol (2 mL) was subsequently added. The mixture was then stirred for 3 h at room temperature, and centrifuged at 7800 rpm for 5 min. The supernatant was discarded and the remaining solid was dried in a vacuum oven at room temperature overnight.

Protocol for shaping amine-impregnated chitosan carbon into tablets

Amine-grafted chitosan-derived mesoporous carbon powder (0.1 g) was added to a die having a diameter of 3 mm and then pressed using a commercial industrial tableting machine and held there for around 1 min.

Mechanical strength or friability tests

Crush strength measurements were performed on a ProLine materials testing machine (ZwickRoell). The tablets are put under pressure (laid flat) and the pressure at which the tablet breaks was recorded. Tablets were tested three times per sample, and the average crush strength was assessed.

Mechanical friability tests were performed on a digital rotator (IKA Loopster digital, Figure A2) with 2 mL SafeSeal microtube (PP). The speed was set at 50 rpm and the weight loss was measured after 500 cycles.



Figure A221: Picture of the attrition instrument that will be used in the future to assess the robustness of the structured adsorbents.

Cycling studies:

A TGA/DSC (thermogravimetric analyzer/differential scanning calorimeter, Figure A3) combo instrument was purchased in the project from Linseis (Germany). This instrument was dedicated to the measurement of the enthalpy of a CO_2 adsorption and regeneration and assessment of materials lifetimes via continuous adsorption-desorption cycles inrelevant gas mixtures, with and without humidity. It allows us to do accelerated aging studies of the adsorbents (e.g., varying O_2 content in the gas stream).

The specifications of the new TGA/DSC combo include the following:

- Simultaneous measurement of weight changes and heats of adsorption under relevant post combustion gas mixtures (CO_2, N_2, O_2) with controllable humid levels.
- Cycling testing for long-term stability asessments of the adsorbents.
- TSA and VSA operation modes.
- Liquid N_2 dewar to faster cool down the furnace.
- 4 MFCs allowing gas mixing under dry or humid conditions or flowing premixed gas compositions from cylinders.
- Measurements under varying temperatures ranging from -150 °C to 1000 °C.
- Two different humidity generators:

    1. A bubbler system that allows one to saturate gas mixtures with water vapor at room temperature for measurements under VSA or TSA conditions. For the former, there is a check valve that is meant to inhibit water from the bubbler to reach the furnace under vacuum conditions.

    2. There is also a commercial humidity generator with a heated transfer line that allows for precisely tuning the humidity in the gas streams at various temperatures. This commerical system is intended for operationa only under TSA cycling conditions.

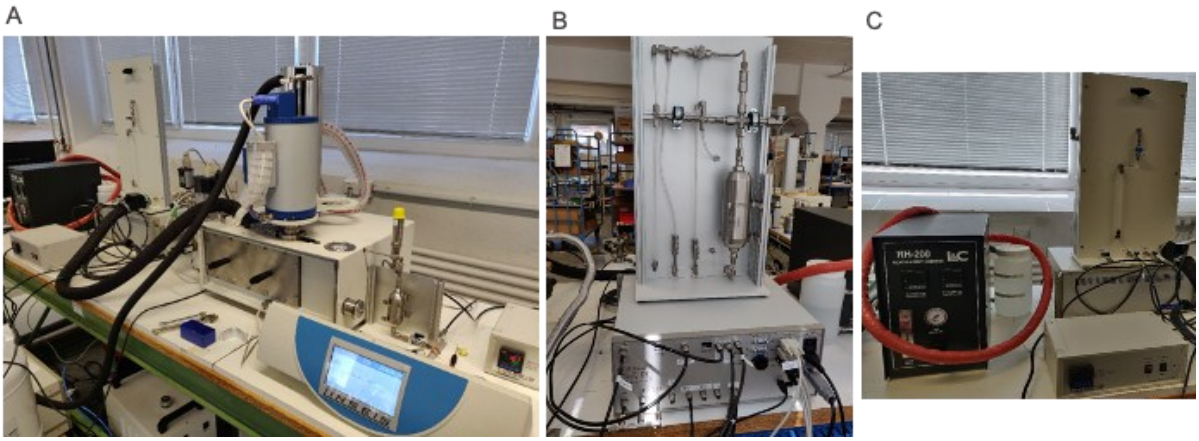


Figure A3: (A) Image of the TGA/DSC combo instrument that allowa the measurements of mass changes during adsorption and desorption and enthalpies associated with CO_2 adsorption/release during realistic cycles. (B) Water bubbler to saturate gas mixtures with water vapor at room temperature that allows for working under TSA and VSA conditions. (C) Controllable humidity generator that allows for setting precise humidity levels in the gas stream and is able to work under TSA conditions.

6.2 WP3 Technoeconomic assessment to investigate for the viability of CO2 capture process

Reference flow equations used in LCA assessment for zeolite 13X

In the following equations, mCO_2 is the amount of captured CO_2, expressed in the functional unit: FU = 1 [kg] mCO_2

Equation for the energy reference flow:

$$RF_E = \frac{X_i \cdot P_i}{m_{CO_2}} \cdot \frac{1\ kW}{1000\ W} \cdot 3.6\ \frac{MJ}{1\ kWh} = \frac{E}{m_{CO_2}}$$
$$RF_E = \frac{[h] \cdot [W]}{FU} \cdot \frac{[kW]}{[W]} \cdot \frac{[MJ]}{[kWh]} = \frac{[MJ]}{FU}$$

Equation for the infrastructure reference flow:

$$RF_{inf} = \frac{X_i}{m_{CO_2}} \cdot \frac{1\ day}{H} \cdot \frac{1\ year}{D} \cdot \frac{1\ inf}{Y} = \frac{inf}{m_{CO_2}}$$
$$RF_{inf} = \frac{[h]}{FU} \cdot \frac{[day]}{[h]} \cdot \frac{[year]}{[days]} \cdot \frac{[p]}{[years]} = \frac{[p]}{FU}$$

Equation for the end-of-life reference flow:

$$RF_{EoL} = \frac{inf}{m_{CO_2}} \cdot \eta_{EoL}$$
$$RF_{EoL} = \frac{[p]}{FU} \cdot [-] = \frac{[p]}{FU}$$

Table A1: TSA flows for the specific unit processes, their respective values, and the corresponding ecoinvent 3.6 processes use

Unit processes	Flow type	Flow	Quantity	Unit	Ecoinvent 3.6 process or created process	Comment
Captured CO2	Final demand flow - Output	Captured CO2	1.00	kg	Captured CO2, TSA | Cutoff, U, MABOR	
	Reference flows - Inputs	Energy	6.76	MJ	Energy, TSA | Cutoff, U, MABOR	Energy consumption from [19]
		Infrastructure	2.70E-05	Item(s)	Infrastructure production, TSA - CH | Cutoff, U, MABOR	Calculated with an infrastructure operating for 330 days per year, 12 hours a day and with a lifetime of 20 years.
		EoL - Infrastructure	2.70E-05	Item(s)	EoL of infrastructure, TSA - CH | Cutoff, U, MABOR	The infrastructure is assumed to be 100% landfilled or incinerated at the end of its lifetime.
Infrastructure production	Reference flow - Output	Infrastructure	1.00	Item(s)	Infrastructure production, TSA - CH | Cutoff, U, MABOR	
	Intermediary flows - Inputs	Zeolite	14.70	kg	market for zeolite, powder | zeolite, powder | Cutoff, U - GLO	This ecoinvent process is assumed to be similar as the NaX composition from the studies used.
		Heat exchanger	1.00	Item(s)	market for blower and heat exchange unit, decentralized, 180-250 m3/h | blower and heat exchange unit, decentralized, 180-250 m3/h | Cutoff, U - GLO	A substitute for the heat exchanger needed for the technology.
		Column production	4.00	Item(s)	Column production, TSA | Cutoff, U, MABOR	The technology is assumed to need 4 columns.
		Column transport	6.01E+03	kgkm	market for transport, freight, lorry, unspecified | transport, freight, lorry, unspecified | Cutoff, U - RER	Estimated 111 km transport from producer in Sierre to the facility in Lausanne. The unspecified transport process is used because of lack of data about the specific vehicle.
TSA technology	Reference flow - Output	Energy	1.00	MJ	Energy, TSA | Cutoff, U, MABOR	
	Intermediary flows - Inputs	Electricity	1.00	MJ	electricity, high voltage, production mix | electricity, high voltage | Cutoff, U - CH	The technology is assumed to consist of this ecoinvent average energy mix.
EoL of Infrastructure	Reference flow - Output	EoL infrastructure	1.00	Item(s)	EoL of infrastructure, TSA - CH | Cutoff, U, MABOR	
	Intermediary flows - Outputs	Waste zeolite	14.70	kg	market for waste zeolite | waste zeolite | Cutoff, U - CH	The zeolite is assumed to be 100% landfilled.
		Scrap steel	267.00	kg	market for scrap steel | scrap steel | Cutoff, U - CH	A sum of steel inputs with the highest share of the different processes in the Infrastructure process
		Waste aluminium	15.40	kg	market for waste aluminium | waste aluminium | Cutoff, U - GLO	A sum of aluminium inputs with the highest share of the different processes in the Infrastructure process.
		Waste polystyrene	7.20	kg	market for waste polystyrene | waste polystyrene | Cutoff, U - CH	A sum of polystyrene inputs with the highest share of the different processes in the Infrastructure process.
	Intermediary flows - Inputs	Waste transport	1.22E+04	kgkm	market for transport, freight, lorry, unspecified | transport, freight, lorry, unspecified | Cutoff, U - RER	Estimated 40 km transport of waste from the facility in Lausanne to a recycling facility in Montreux. The unspecified transport process is used because of lack of data about the specific vehicle.
Column production	Intermediary flow - Output	Column	1.00	Item(s)	Column production, TSA | Cutoff, U, MABOR	
	Intermediary flows - Inputs	Steel production	13.50	kg	market for steel, chromium steel 18/8 | steel, chromium steel 18/8 | Cutoff, U - GLO	Substitute for the column material.

Table A2: TVSA flows for the specific unit processes, their respective values, and the corresponding ecoinvent 3.6 processes used

Unit processes	Flow type	Flow	Quantity	Unit	Ecoinvent 3.6 process or created process	Comment
Captured CO2	Final demand flow - Output	Captured CO2	1.00	kg	Captured CO2, TVSA | Cutoff, U, MABOR	
	Reference flows - Inputs	Energy	3.22	MJ	Energy, TVSA | Cutoff, U, MABOR	Energy consumption from [19]
		Infrastructure	1.20E-05	Item(s)	Infrastructure production, TVSA - CH | Cutoff, U, MABOR	Calculated with an infrastructure operating for 330 days per year, 12 hours a day and with a lifetime of 20 years.
		EoL - Infrastructure	1.20E-05	Item(s)	EoL of infrastructure, TVSA - CH | Cutoff, U, MABOR	The infrastructure is assumed to be 100% landfilled or incinerated at the end of its lifetime.
Infrastructure production	Reference flow - Output	Infrastructure	1.00	Item(s)	Infrastructure production, TVSA - CH | Cutoff, U, MABOR	
	Intermediary flows - Inputs	Zeolite	14.70	kg	market for zeolite, powder | zeolite, powder | Cutoff, U - GLO	This ecoinvent process is assumed to be similar as the NaX composition from the studies used.
		Heat exchanger	1.00	Item(s)	market for blower and heat exchange unit, decentralized, 180-250 m3/h | blower and heat exchange unit, decentralized, 180-250 m3/h | Cutoff, U - GLO	A substitute for the heat exchanger needed for the technology.
		Column production	4.00	Item(s)	Column production, TVSA | Cutoff, U, MABOR	The technology is assumed to need 4 columns.
		Vacuum pump prod.	1.00	Item(s)	pump production, 40W | pump, 40W | Cutoff, U - CH	Substitute for the vacuum pump
		Column transport	6.01E+03	kgkm	market for transport, freight, lorry, unspecified | transport, freight, lorry, unspecified | Cutoff, U - RER	Estimated 111 km transport from producer in Sierre to the facility in Lausanne. The unspecified transport process is used because of lack of data about the specific vehicle.
TVSA technology	Reference flow - Output	Energy	1.00	MJ	Energy, TVSA | Cutoff, U, MABOR	
	Intermediary flows - Inputs	Electricity	1.00	MJ	electricity, high voltage, production mix | electricity, high voltage | Cutoff, U - CH	The technology is assumed to consist of this ecoinvent average energy mix.
EoL of Infrastructure	Reference flow - Output	EoL infrastructure	1.00	Item(s)	EoL of infrastructure, TVSA - CH | Cutoff, U, MABOR	
	Intermediary flows - Outputs	Waste zeolite	14.70	kg	market for waste zeolite | waste zeolite | Cutoff, U - CH	The zeolite is assumed to be 100% landfilled.
		Scrap steel	267.00	kg	market for scrap steel | scrap steel | Cutoff, U - CH	A sum of steel inputs with the highest share of the different processes in the Infrastructure process
		Waste aluminium	15.40	kg	market for waste aluminium | waste aluminium | Cutoff, U - GLO	A sum of aluminium inputs with the highest share of the different processes in the Infrastructure process.
		Waste polystyrene	7.20	kg	market for waste polystyrene | waste polystyrene | Cutoff, U - CH	A sum of polystyrene inputs with the highest share of the different processes in the Infrastructure process.
		Waste bulk iron	1.20	kg	market for waste bulk iron, excluding reinforcement | waste bulk iron, excluding reinforcement | Cutoff, U - CH	A sum of bulk iron inputs with the highest share of the different processes in the Infrastructure process.
	Intermediary flows - Inputs	Waste transport	1.22E+04	kgkm	market for transport, freight, lorry, unspecified | transport, freight, lorry, unspecified | Cutoff, U - RER	Estimated 40 km transport of waste from the facility in Lausanne to a recycling facility in Montreux. The unspecified transport process is used because of lack of data about the specific vehicle.
Column production	Intermediary flow - Output	Column	1.00	Item(s)	Column production, TVSA | Cutoff, U, MABOR	
	Intermediary flows - Inputs	Steel production	13.50	kg	market for steel, chromium steel 18/8 | steel, chromium steel 18/8 | Cutoff, U - GLO	Substitute for the column material.

Table A3: SA-TSA flows for the specific unit processes, their respective values, and the corresponding ecoinvent 3.6 processes used.

Unit processes	Flow type	Flow	Quantity	Unit	Ecoinvent 3.6 process or created process	Comment
Captured CO2	Final demand flow - Output	Captured CO2	1.00	kg	Captured CO2, SA-TSA | Cutoff, U, MABOR	
	Reference flows - Inputs	Energy	10.20	MJ	Energy, SA-TSA | Cutoff, U, MABOR	Energy consumption from [20]
		Infrastructure	1.60E-05	Item(s)	Infrastructure production, SA-TSA - CH | Cutoff, U, MABOR	Calculated with an infrastructure operating for 330 days per year, 12 hours a day and with a lifetime of 20 years.
		EoL - Infrastructure	1.60E-05	Item(s)	EoL of infrastructure, SA-TSA - CH | Cutoff, U, MABOR	The infrastructure is assumed to be 100% landfilled or incinerated at the end of its lifetime.
Infrastructure production	Reference flow - Output	Infrastructure	1.00	Item(s)	Infrastructure production, SA-TSA - CH | Cutoff, U, MABOR	
	Intermediary flows - Inputs	Zeolite	13.30	kg	market for zeolite, powder | zeolite, powder | Cutoff, U - GLO	This ecoinvent process is assumed to be similar as the NaX composition from the studies used.
		Heat exchanger	1.00	Item(s)	market for blower and heat exchange unit, decentralized, 180-250 m3/h | blower and heat exchange unit, decentralized, 180-250 m3/h | Cutoff, U - GLO	A substitute for the heat exchanger needed for the technology.
		Column production	3.00	Item(s)	Column production, SA-TSA | Cutoff, U, MABOR	The technology is assumed to need 3 columns.
		Steam boiler prod.	1.00	Item(s)	market for gas boiler | gas boiler | Cutoff, U - GLO	The steam boiler is assumed to consist of the same material as this gas boiler ecoinvent process.
		Column transport	5.44E+03	kgkm	market for transport, freight, lorry, unspecified | transport, freight, lorry, unspecified | Cutoff, U - RER	Estimated 111 km transport from producer in Sierre to the facility in Lausanne. The unspecified transport process is used because of lack of data about the specific vehicle.
SA-TSA technology	Reference flow - Output	Energy	1.00	MJ	Energy, SA-TSA | Cutoff, U, MABOR	
	Intermediary flows - Inputs	Electricity	0.25	MJ	electricity, high voltage, production mix | electricity, high voltage | Cutoff, U - CH	The technology is assumed to consist of this ecoinvent average energy mix.
		Heat	0.75	MJ	market for heat, from steam, in chemical industry | heat, from steam, in chemical industry | Cutoff, U - RER	This ecoinvent market for heat process from steam is a substitute for the steam needed for the technology.
EoL of Infrastructure	Reference flow - Output	EoL infrastructure	1.00	Item(s)	EoL of infrastructure, SA-TSA - CH | Cutoff, U, MABOR	
	Intermediary flows - Outputs	Waste zeolite	13.30	kg	market for waste zeolite | waste zeolite | Cutoff, U - CH	The zeolite is assumed to be 100% landfilled.
		Scrap steel	73.00	kg	market for scrap steel | scrap steel | Cutoff, U - CH	A sum of steel inputs with the highest share of the different processes in the Infrastructure process
		Waste aluminium	15.40	kg	market for waste aluminium | waste aluminium | Cutoff, U - GLO	A sum of aluminium inputs with the highest share of the different processes in the Infrastructure process.
		Waste polystyrene	7.20	kg	market for waste polystyrene | waste polystyrene | Cutoff, U - CH	A sum of polystyrene inputs with the highest share of the different processes in the Infrastructure process.
	Intermediary flows - Inputs	Waste transport	4.35E+03	kgkm	market for transport, freight, lorry, unspecified | transport, freight, lorry, unspecified | Cutoff, U - RER	Estimated 40 km transport of waste from the facility in Lausanne to a recycling facility in Montreux. The unspecified transport process is used because of lack of data about the specific vehicle.
Column production	Intermediary flow - Output	Column	1.00	Item(s)	Column production, SA-TSA | Cutoff, U, MABOR	
	Intermediary flows - Inputs	Steel production	16.30	kg	market for steel, chromium steel 18/8 | steel, chromium steel 18/8 | Cutoff, U - GLO	Substitute for the column material.

Column Scheduling

Table A4. Scheduling equations for the TVSA process, describing the number of columns, vacuum pumps, idle time, number of trains/modules, and flue gas flow rate per train.[24]

Parameter	Formula	Note
Number of columns	$N = \text{ceiling}(\sum_{i=\text{steps}} t_i / t_{ads})$	t_{ads} is the time between the start of successive adsorption steps. This value determines how many columns are required in rotation to ensure continuous operation.
Number of vacuum pumps	$N_{v,j} = \text{ceiling}(t_j / t_{ads})$ j = blowdown/evacuation	If the duration of the blowdown or evacuation step (t_j) exceeds tads, multiple pumps must operate in parallel to complete desorption within the cycle time.
Idle time	$t_{idle} = N \cdot t_{ads} - \sum_{i=\text{steps}} t_i$	Accounts for any mismatch between the total cycle time and the product of the number of columns and t_{ads}. Idle time ensures cycle synchronization and smooth operation.
Number of trains/modules	$M = \text{ceiling}(\dot{F}_{flue} / \dot{F}_{train})$	Represents how many parallel process trains are needed to handle the total flue gas flow. Calculated by dividing the total feed flow by the maximum capacity of a single train.
Flue gas flow rate per train	$\dot{F}_{train} = (1/t_{ads}) \int_0^{t_{ads}} \dot{F}\, dt$	Average molar flow of flue gas handled by one train during the adsorption step. The integral over the adsorption time captures variations in flow and pressure, giving a representative mean value.

Techno-economic analysis framework

The principal cost items include:

Adsorption columns, sized according to column volume using

$$\log(PC_{column}) = 3.4974 + 0.4485 * \log(Volume) + 0.1074 * [\log(Volume)]^2$$

where volume is expressed in m³ and PC_{column} represents the purchase cost.

The compressor cost correlation is based on power consumption:

$$\log(PC_{compressor}) = 2.2897 + 1.3604 * \log(Power)) + 0.1074 * [\log(Power)]^2$$

Power of the compressor is calculated by

$$\text{Power} = \frac{\varepsilon\, A\, \gamma\, v_0}{\eta\, (\gamma - 1)} \int P_{feed} * \left(\frac{P_{feed}}{P_{atm}}\right)^{\frac{\gamma-1}{\gamma}} - 1\ dt$$

where, ε is the bed void fraction, A is the column cross-sectional area (m²), η =0.7 is the compressor efficiency, γ =1.4 is the adiabatic constant, v_0 is the interstitial velocity of the gas (m/s), P_{atm} = 1 atm and power is in kW.

The motor drive cost is calculated separately:

$$\log(PC_{motor}) = 2.1206 + 0.9545 * \log(Power) - 0.0661 * [\log(Power)]^2$$

For the air-cooled heat exchangers required in TVSA operation:

$$\log(PC_{cooler}) = 3.2138 + 0.2688 * \log(Area) + 0.07961 * [\log(Area)]^2$$

where Area represents the heat transfer area in m². The overall heat transfer coefficient is assumed to be 20 W/(m²·°C) for cooling system design.

The cost of the vacuum system was established primarily through vendor communications, since no reliable literature data are available for equipment of this scale. In discussions with suppliers such as NASH, it was indicated that a large liquid-ring vacuum pump (LRVP) with a suction pressure in the range of 0.1–0.15 bar and a volumetric capacity of ~37,000 m³/h is priced at approximately 200,000 CHF per unit. Based on this input, two LRVPs in parallel were included in the design to cover the blowdown requirement.

During these vendor exchanges it was also noted that LRVPs alone cannot reliably achieve the low-pressure levels (below 0.1 bar) required for regeneration. To extend the operating range, an additional mechanical booster (roots blower) stage in series with the LRVPs was recommended by suppliers (e.g., Aerzen, Howden). Standard industrial roots blowers of smaller scale (~10,000 m³/h) are commercially available in the 10,000 to 50,000 CHF price range. By applying cost-scaling to the larger capacities required in this study (tens of thousands of m³/h per unit), and supported by vendor quotations, the expected cost for industrial-scale booster blowers falls in the range of 100,000 to 150,000 CHF per unit. Large-capacity roots blowers of this scale are indeed commercially available, with manufacturers such as Roots Blower offering rotary lobe blowers up to 120,000 m³/h.

Bare module costs and annualized capital expenses

The bare module cost (BMC) represents the installed cost of a single piece of equipment, which includes the purchase price of the equipment itself as well as all direct installation expenses such as foundations, piping, instrumentation, insulation, and electrical connections. It does not, however, include indirect costs such as engineering, contingency, or project overheads.

In cost-estimation practice, the bare module cost is obtained by applying an installation (module) factor to the purchase cost of the equipment. This approach provides a more realistic estimate of the capital investment required to install the equipment in an operating plant. The correlations used in this work follow those reported by Farooq et al.[23]

For adsorption columns, the bare module cost is calculated as:

$$BMC_{column} = \frac{4.65 * M * N * PC_{column}}{397}$$

where PC_{column} = purchase cost of a single column, M = number of modules, N = number of columns per module, 397 = base CEPCI index for normalization, 4.65 = installation factor that accounts for piping, instrumentation, and other direct installation costs.

For other equiments including cooler, compressor and vacuum pump the following correlations have been used.

$$BMC_{cooler} = \frac{3.3 * PC_{cooler}}{397}$$

$$BMC_{compressor} = \frac{2.5 * (PC_{compressor} + P_{motor\ drive})}{397}$$

$$BMC_{pump} = 2.5 * M * PC_{pump}$$

$$TBMC = 1.43 * (BMC_{column} + BMC_{cooler} + BMC_{compressor} + BMC_{pump})$$

The total bare-module cost (TBMC) incorporates additional factors for spares and contingencies:

The factor 1.43 accounts for:

10% allowance for spare equipment and components

30% contingency for unforeseen costs and design modifications

Integration and commissioning expenses

The TBMC is the sum of all equipment bare-module costs (columns, compressors, coolers, vacuum pumps, etc.) and represents the installed direct capital cost of the capture plant. To obtain the total plant cost (TPC), a multiplier of 1.2 is applied to account for balance-of-plant items such as site preparation, utilities, and auxiliary systems.[23]

$$TPC = 1.2 \times TBMC$$

Finally, to express the capital investment as an annual expense, the total bare-module cost (TBMC) is multiplied by a capital charge factor. This factor accounts for plant lifetime, interest rate, and financing assumptions. Following Farooq et al. (2015), a plant life of 15 years and an annual interest rate of 5% with a 1:1 debt-to-equity ratio were assumed, which yields a capital charge factor of 0.0815.

Accordingly, the annualized capital cost is calculated as:

$$ACC = 0.0815 \times TBMC$$

Annualized operating expenses and CO_2 capture cost

Energy represents a significant operational expense for TVSA systems due to heating, cooling and vacuum requirements. The annual energy cost is the energy that is required for thermal to heat column and the electricity required

$C_{energy} = E_{thermal} + E_{mechanical}$

The thermal energy requirement is associated with heating the adsorption column during desorption. This includes heating of the column wall and the adsorbent bed, which is given by

$Q_{wall} = C_{p,wall} \cdot \rho_{wall} \cdot V_{wall} \cdot (T_{des} - T_{ads})$

$Q_{ads} = C_{p,ads} \cdot \rho_{ads} \cdot V_{ads} \cdot (T_{des} - T_{ads})$

where Q_{wall} and Q_{ads} represent the sensible heat required to raise the temperature of the column wall and adsorbent material, respectively. Here, $C_{p,wall}$ and $C_{p,ads}$ denote the specific heat capacities of the wall and adsorbent, while ρ_{wall} and ρ_{ads} refers to their corresponding densities. T_{des} is the desorption temperature, T_{ads} is the adsorption temperature. The mechanical energy requirement arises from the operation of blowers and vacuum pumps used during blowdown and evacuation.

The annual adsorbent cost accounts for periodic replacement:

$\mathrm{C_{adsorbent}} = rf_{ads} * \rho_{\mathrm{ads}} * (1 - \varepsilon) * M * N * V * unit_{cost}$

where ρ_{ads} is the adsorbent bulk density, ε is the bed voidage, M denotes the number of modules, N denotes the number of columns, V is the column volume, and rf_{ads} accounts for the replacement frequency. Zeolite 13X adsorbent replacement is assumed to be replaced for every 3 years.

Annualized operating cost is given by the following equation,

$AOC = C_{adsorbent} + 1.1 * C_{labor} + 0.055 * \mathrm{TPC} + 0.15 * (1.1 * C_{labor} + 0.05 * TPC) + C_{energy}$

In the above formula,

$C_{adsorbent}$ is the cost of the adsorbent

$1.1 * C_{labor}$ = Labor cost + Direct supervisory and clerical labor (10% of labor)

$0.055 * \mathrm{TPC}$ = Maintenance and repairs (5.5% of TPC) + Operating supplies (10% of maintenance)

$0.15 * (1.1 * C_{labor} + 0.05 * TPC)$ = Administration and plant overheads (15% of combined labor and maintenance costs)

$\mathrm{C_{labour}} = 8760 * \text{operators required} * hourly\ rate$

The total annualized cost (TAC) combines capital and operating expenses:

$TAC = ACC + AOC$

Cost per tonne CO_2 captured:

$$Cost\ captured\left(\frac{CHF}{ton_{captured}}\right) = \frac{Annualized\ capital\ expenses + Anuualized\ operating\ expenses}{Annual\ CO_2\ captured}$$

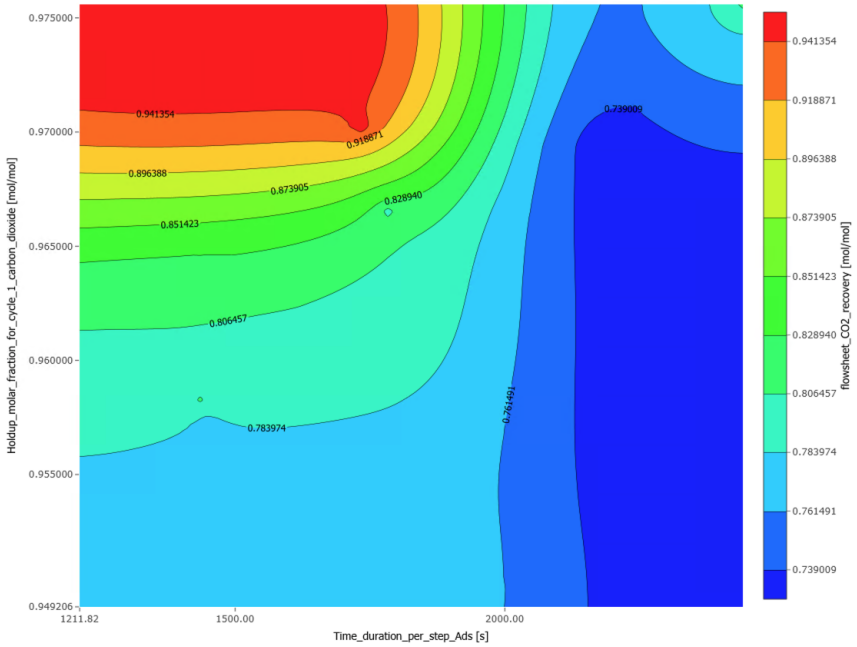


Figure A4: Contour plot of CO_2 recovery as a function of adsorption duration and CO_2 molar fraction after reaching cyclic steady state.

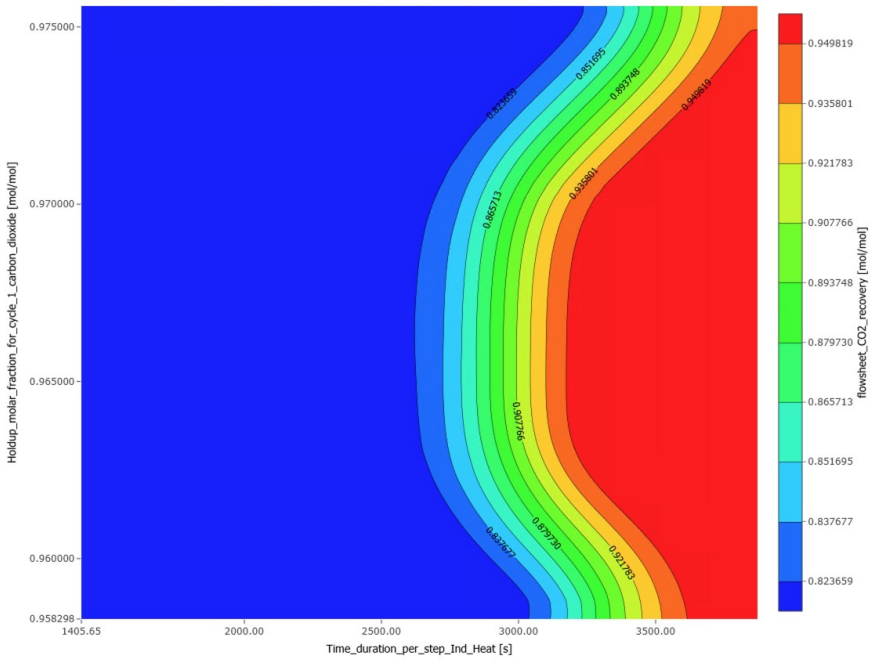


Figure A5: CO_2 recovery as a function of desorption (heating) time and CO_2 molar fraction after reaching cyclic steady state

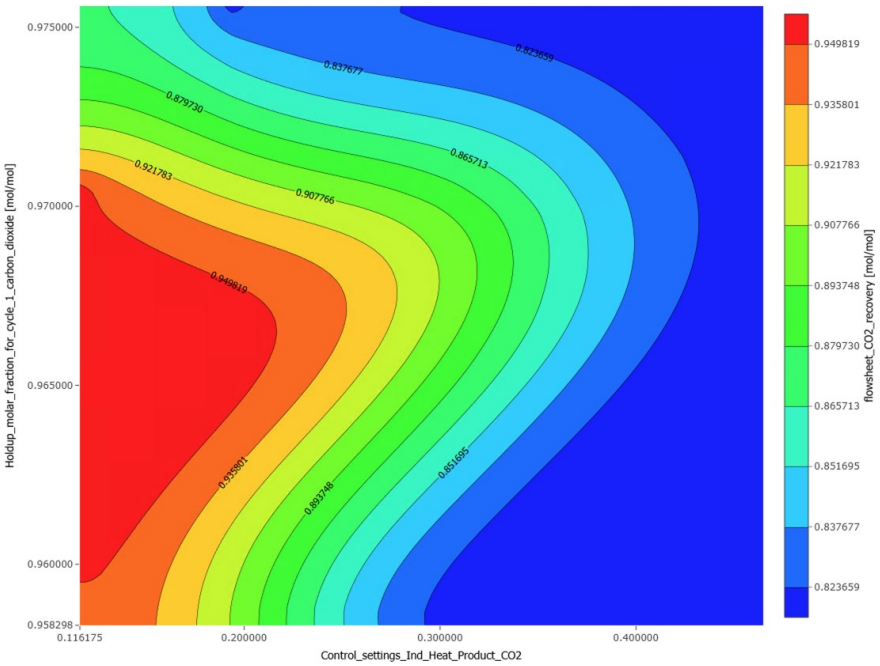


Figure A6: Contour plot showing the effect of vacuum pressure during desorption and CO_2 molar hold-up in the adsorbent bed on overall CO_2 recovery.

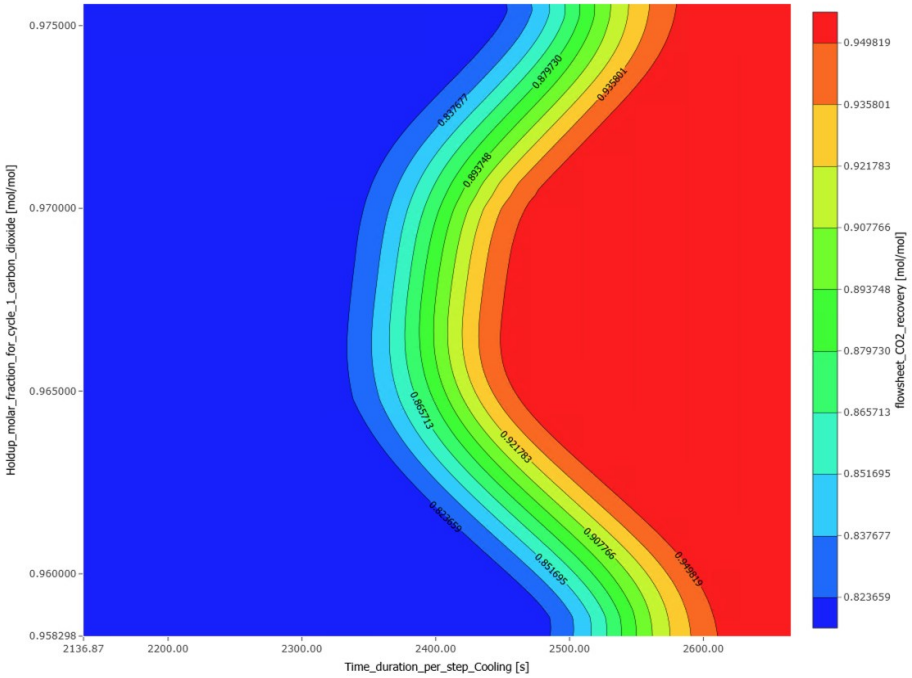


Figure A7: Contour plot showing the effect of cooling time and CO_2 molar hold-up on overall CO_2 recovery in the TVSA process.

Cr-BDC synthesis

In a 1 L Teflon-lined stainless steel autoclave, 52.8 g of chromium(III) nitrate nonahydrate ($Cr(NO_3)_3 \cdot 9H_2O$, 0.132 mol), and 18.0 g of terephthalic acid (H_2BDC, 0.108 mol) were dispersed in 660 mL of deionized water. To this, 8.56 mL of 69% nitric acid (0.132 mol, equimolar to Cr) was added. The mixture was stirred for 30 minutes at room temperature to ensure homogeneity. The autoclave was then transferred to a preheated oven and maintained at 200°C for 16 hours. Upon completion, the system was allowed to cool down naturally within the oven for an additional 12 hours. The supernatent was decanted, and subsequently divided into six 50 mL Falcon tubes for centrifugation at 7800 rpm for 10 minutes. The supernatant was discarded, and each tube was washed with 35 mL of dimethylformamide (DMF), followed by shaking for 10 minutes. The washed solids were transferred into a 500 mL glass jar containing 200 mL of fresh DMF and stirred at 700 rpm for 6 hours. This DMF washing procedure was repeated three more times to ensure the removal of unreacted species. A similar solvent exchange protocol was then performed using ethanol: 200 mL of fresh ethanol was added to the solid, stirred at 700 rpm for 6 hours, and this step was repeated three times. Finally, the purified Cr-BDC product was vacuum dried at room temperature for 24 hours to yield the activated as-synthesized material for subsequent modification and characterization.

MOF functionalization protocol

In this method, 5.5 g of as-synthesized Cr-BDC was dispersed in 200 mL of methanol (MeOH), and 52.5 mL of tetraethylenepentamine (TEPA) was added directly to the suspension in a 1 L round-bottom flask. Separately, 25.6 mL of trimethylolpropane triglycidyl ether (TMPTE) was dissolved in 200 mL of MeOH and subsequently introduced into the original mixture. The suspension was stirred at 298 K for 3 h. After reaction, the mixture was centrifuged at 7800 rpm for 5 min, and the supernatant was discarded. The resulting solid was vacuum dried at room temperature for 24 h. Finally, the material was

cured by heating to 393 K over 1 h and maintained at that temperature under vacuum for 12 h prior to adsorption measurements. This process yielded 8 g of functionalized Cr-BDC.

Sorbent synthesis inventory

Table A5. Energy requirement for MOF synthesis

Process Step	Equipment	Power (W)	Duration (h)	Energy (kWh)	Notes
Synthesis (200°C)	Oven	250	16	4.03	Heating at 200°C
Cooling in oven	Oven	63	12	0.76	25% power during cooling
Centrifugation (initial)	Centrifuge	350	1.0	0.35	6 tubes × 10 min
DMF washing (shaking)	Shaker	20	0.17	0.003	10 min shaking
DMF washing (stirring)	Magnetic stirrer	30	24	0.72	4 cycles × 6h
Ethanol washing (stirring)	Magnetic stirrer	30	18	0.54	3 cycles × 6h
Centrifugation (during multiple washes)	Centrifuge	350	1.75	0.61	7 more wash cycles
Vacuum drying	Vacuum oven	500	24	12.00	Room temperature
Total energy for synthesis				**19.02**	**1.06 kWh/g**

The energy consumption values for each process step were estimated using a combination of manufacturer specifications, laboratory instrumentation data, and published literature. The synthesis and cooling steps were carried out using a Thermo Scientific Heratherm oven, which typically consumes between 170–275 W depending on gravity or mechanical convection modes at 150–200 °C. For our calculations, we used a value of 250 W for synthesis and 63 W for cooling, which represents ~25% of synthesis power during the temperature maintenance phase.

Table A6. Energy requirements for MOF functionalization

Process Step	Equipment	Power (W)	Duration (h)	Energy (kWh)	Notes
Main reaction	Magnetic stirrer	30	3	0.09	3 hours at 298K
Centrifugation	Centrifuge	500	0.08	0.04	5 minutes at 7800 rpm
Vacuum drying	Vacuum oven	500	24	12.00	At 298K for 24h
Heating to 393K	Vacuum oven	700	1	0.70	Higher to 393K
Activation at 393K	Vacuum oven	500	12	6.00	Maintating at 393K
Total energy for functionalization				**18.83**	**2.35 kWh/g**

Centrifugation was modeled at 350 W, falling within the range of 130–750 W reported for lab scale centifuges scuh Sorvall ST8 centrifuges. For magnetic stirring, we adopted a conservative value of 30 W, which is taken from external references such as the Corning Scholar 171 stirrer (rated at 30 W) and also falls within the adjustable range of 5–20 W reported for Thermo Scientific's Cimarec Power Direct stirrers. Orbital shaking was estimated at 20 W, based on typical small-scale benchtop orbital shakers. For example, the Marshall Select MS-OS200 orbital shaker (40–200 rpm) draws 20 W of input power.Although high-capacity incubated shakers (e.g., the MaxQ 4000) may consume up to 625 W, our 20 W estimate is appropriate and conservative for small-scale, ambient-temperature shaking. Finally, the vacuum drying step was modeled at 500 W, supported by the Thermo Lab-Line 3606-DB (600 W) and Precision Model 29 (1,000 W) vacuum ovens.

Estimation methods for chemicals not in database

Chromium(III) nitrate nonahydrate production

$$Cr(OH)_3 + 3HNO_3 \rightarrow Cr(NO_3)_3 + 3H_2O$$

To produce 52.8 g of chromium nitrate nonahydrate required for MOF synthesis, approximately 13.59 g of $Cr(OH)_3$ and 24.94 g of HNO_3 were modeled as inputs.

Tetraethylenepentamine (TEPA) production modeling

TEPA is produced as part of a mixture of ethyleneamines (EDA, DETA, TETA, TEPA...) via a nucleophilic substitution reaction between[33]:

- Ethylene dichloride (EDC) → $C_2H_4Cl_2$
- Ammonia (NH_3) → in large excess
- High temperature (180–250 °C) and pressure, in the presence of a catalyst (e.g., nickel or cobalt)

The resulting mixture is then fractionally distilled to isolate TEPA.

$$4\ C_2H_4Cl_2 + 5\ NH_3 \rightarrow TEPA + 8\ HCl$$

Material requirements for TEPA production were estimated at 2.62 kg of ethylene dichloride and 0.56 kg of ammonia per kilogram of TEPA produced. Energy consumption for TEPA production was estimated at 3.5-6.0 MJ/kg using the scale-up framework of Piccinno et al. (2016) for chemical processes, incorporating reaction heating requirements for nucleophilic substitution at 180-250°C and energy for distillation separation of ethyleneamine mixtures based on Capello et al. (2005) industrial data for organic solvent separation. For this analysis, a conservative estimate of 3.5 MJ/kg was adopted, representing optimized industrial conditions with effective heat integration, waste heat recovery, and modern process efficiency measures that are typically implemented in large-scale chemical manufacturing facilities to minimize energy consumption and operational costs.

Trimethylolpropane Triglycidyl Ether (TMPGTE) production modeling

TMPTGE is synthesized through a two-step reaction process. The first step involves etherification, where trimethylolpropane (TMP) reacts with epichlorohydrin in the presence of a Lewis acid catalyst to form a halohydrin intermediate. The second step is dehydrochlorination, in which the halohydrin intermediate is treated with sodium hydroxide (NaOH) to yield TMPTGE and sodium chloride as a by-product[34].
The overall stoichiometric reaction can be represented as:

$$TMP + 3\ Epichlorohydrin + 3\ NaOH \rightarrow TMPTGE + 3\ NaCl + 3\ H_2O$$

Based on stoichiometric calculations, the production of 1 kg TMPTGE requires 0.493 kg TMP, 1.020 kg epichlorohydrin, and 0.442 kg NaOH as the primary chemical inputs, following the 1:3:3 molar ratio established by the reaction stoichiometry.

6.3 Technology Roadmap

6.3.1. Outline

This roadmap defines the strategic pathway for transitioning the CO_2 capture technology, developed at LFIM using solid adsorbents into the market. The focus is on scaling beyond the pilot plant stage, addressing industrial needs, ensuring IP protection, and preparing for real-world implementation. The goal is to establish this technology as a commercially viable CO_2 capture in diverse fields.

Unlike solvent-based approaches, this technology offers the advantages of lower regeneration energy demand, reduced solvent waste, and modular adaptability to diverse industrial systems. The immediate priority is scaling beyond the pilot plant stage while ensuring intellectual property protection, industrial validation, and techno-economic competitiveness.

The roadmap sets the following milestones: achieving tonne-scale sorbent production, demonstrating energy efficiency improvements in temperature/ temperature-vacuum swing adsorption (TSA/TVSA) cycles, and securing industrial validation of the process. In particular, Swiss industrial partners will play a central role by independently validating the techno-economic (TEA) and life cycle (LCA) assessments, ensuring that the technology is both cost-effective and environmentally beneficial under real operating conditions.

By leveraging Switzerland's strong industrial ecosystem and regulatory commitment to net-zero by 2050, this project positions itself as a commercially viable and sustainable CO_2 capture solution for deployment across power generation, waste incineration, steelmaking, and chemical industries.

6.3.2. Involvement of industrial partners

Collaboration with industrial partners is critical to successful market introduction. The pathway from laboratory to full market deployment of sorbent-based CO_2 capture requires a staged involvement of different industrial partners. Each stage calls for a specific type of partner, and the timing of their participation is critical to ensure that the technology matures efficiently and is adopted where it is most relevant.

Phase 1: Material scale-up (years 0–2)

In the earliest stage, the key requirement is to establish reliable and scalable production of sorbents. Academic laboratories can only supply kilogram quantities, but for industrial demonstration, tonne-scale production is essential. This step requires industrial adsorbent manufacturers who already have experience in producing materials such as zeolites, activated carbons, or silica at commercial scale. Companies such as Zeochem (Switzerland), BASF Schweiz AG, and Clariant represent realistic partners, as they operate large production facilities and have the expertise to adapt manufacturing lines to new sorbents. Working with industrial suppliers ensures not only that enough material can be produced, but also that every tonne of sorbent meets the same standards of strength, stability, and performance required for reliable industrial operation.

Phase 2: Industrial demonstration (year 2-5)

Once materials are available at larger scale, the next stage is to demonstrate process feasibility under real flue gas conditions. This requires the engagement of several types of partners. First, equipment and reactor manufacturers must design and construct adsorption columns and auxiliary equipment such as vacuum pumps, blowers, and compressors. A company like Casale SA, with its strong background in process engineering, can serve as a lead partner for this task. Complementary firms such as

Burckhardt Compression can provide advanced gas-handling solutions. At the same time, system integrators and process engineering companies are needed to retrofit capture units into existing facilities and ensure that cycles such as temperature or pressure swing processes are matched to the site-specific conditions. Engineering firms like Casale will again play a central role - providing engineering expertise and validating the integration

The most important players at this stage, however, are the validation partners, the industrial end-users who host industrial demonstration plants. These partners provide real operating conditions and generate data that can confirm the assumptions made in techno-economic and life cycle analyses. Municipal Waste Incineration (MSWI) facilities such as Satom SA in Monthey and Enevi in Sion are particularly attractive, since their flue gases typically contain 10 to 15% CO_2[1]. Our TEA for a representative Swiss MSWI case indicates capture costs around 50 CHF t^{-1} CO_2 when desorption energy is fully provided by waste heat, with thermal energy contributing about 90% of the total demand. These conditions make TVSA well-suited to incineration facilities, where reliable access to low-grade heat enables competitive and energy-efficient capture.

Beyond incineration, other end-users such as Alpiq, one of Switzerland's largest power producers, operates natural gas combined cycle plants where CO_2 concentrations fall in the 3 to 4% range. In these facilities, PSA or VPSA systems may be preferable, depending on the availability of waste heat. The Swiss Steel Group in Lucerne, operating electric arc furnaces with CO_2 in their flue gases, represents another hard-to-abate sector where early capture projects could have strong impact. n the chemical industry, major companies such as Lonza, Syngenta, BASF Schweiz, EMS Chemie, Firmenich and Givaudan generate process- or utility-off-gases whose CO_2 concentrations fall within ranges frequently targeted for post-combustion technologies (on the order of ~5-15 vol % CO_2). Prtnering with these companies would provide diverse test cases and confirm the adaptability of the technology across industrial contexts.

Phase 3: Commercial rollout (years 5 and beyond)

With successful pilots and demonstrations in place, the final stage involves preparing for widespread market adoption. Here, infrastructure and energy providers become central. GAZNAT SA, for example, could play a vital role in providing infrastructure link between capture units and downstream CO_2 handling networks, enabling compression, transport, and eventual storage or utilization. Such integration becomes essential such that captured CO_2 has a clear pathway to either permanent sequestration or valorisation.

At this stage, the market enablers also come into play. EPFL's Technology Transfer Office[3] will coordinate licensing agreements, while distributors and engineering contractors will package the capture units for a broader set of industrial customers. This is the point where the technology must be marketed effectively to end-users across sectors, highlighting not only environmental benefits but also compliance with regulatory frameworks and potential revenue from carbon credits or CO_2 utilization.

The first large-scale adopters are expected in waste incineration, due to favourable flue gas composition and available heat, but once proven, the same post-combustion capture technology can be applied to other sectors with comparable conditions. Power plants, steelmaking, and chemical manufacturing, natural gas are all viable markets where CO_2 concentrations in the range of 3-15%[4] align with the design of sorbent-based capture systems.

6.3.3. Identification of potential application fields

To maximize market potential, the CO_2 capture technology will be tailored for various application fields. The following outlines the applications and the key Swiss companies active in these sectors, which could be a potential market for the technology developed.

The suitability of sorbent-based CO_2 capture varies across industrial sectors, depending on CO_2 concentration, flue gas composition, and the availability of low-grade heat. According to the International Energy Agency, capture costs decline with increasing CO_2 concentration: around USD 15-25 per tonne CO_2 for high-purity sources such as ethanol production and natural-gas processing, rising to USD 40-120 per tonne CO_2 for lower-concentration post-combustion streams from sectors such as power and cement.[5]. Our own techno-economic analysis, focusing on Swiss municipal solid-waste incineration, shows a capture cost of roughly 72 CHF/tCO_2 (capturing from dry flue gas) when 30% of the desorption energy demand is supplied by waste heat. This cost falls to approximately 50-65 CHF/tCO_2 if a majority (70-90%) of the desorption energy is provided from waste heat. While the IEA values represent global averages, our analysis highlights the strong impact of local conditions and energy integration strategies on capture costs.

To maximize market potential, sorbent-based CO_2 capture can be tailored to different application fields. In Switzerland, this includes waste-to-energy plants, cement and lime production, biogas upgrading, and other point sources where low-grade heat is available. Several Swiss companies are active in these sectors, representing potential early adopters of the technology under development.

Waste incineration

Municipal solid waste incineration plants typically emit flue gases containing 6 to 12% CO_2[1], making them highly suitable for TVSA processes. At this concentration, capture is efficient, and the availability of low-grade heat further improves performance. With 30% waste heat integration, costs of around 72 CHF/tCO_2 are achievable. Given their continuous operation and established role in Swiss energy recovery, incineration facilities represent the most attractive first deployment sites. Examples of Swiss operators include Satom SA (Monthey) and Enevi (Sion).

Power generation

Natural gas combined-cycle plants emit flue gases with 3 to 4% CO_2[6], while biomass combustion plants operate at somewhat higher levels. Biomass-based CO_2 capture costs typically fall in the 40 to 120 USD/tCO_2 range[7], depending on waste heat availability and plant configuration. Where low-grade heat or steam is present, TVSA is advantageous; otherwise, pressure/vacuum-pressure swing (PSA/VPSA) configurations are more suitable.

Steelmaking

In the steelmaking sector (particularly in facilities such as electric-arc furnaces), flue gases can contain relatively low to moderate concentrations of CO_2 (often estimated in the ~3-27 % range[8]). According to the IEA and IEAGHG, capture costs for such industrial point sources can fall in the range of around USD 40-100 per tonne CO_2[1], depending heavily on CO_2 concentration, heat integration and site-specifics. Steelmaking remains a hard-to-abate sector where CO_2 capture is one of the few viable decarbonisation pathways. In Switzerland, companies such as the Swiss Steel Group could play a pioneering role.

Emerging opportunities

Other sectors also present attractive conditions:

- Biogas plants (25-50% CO_2 in raw biogas[9]) can achieve low capture costs (15–40 USD/tCO_2[10]) when integrated with upgrading to biomethane.

- WWTPs generate CO_2-rich streams from sludge digestion and biogas upgrading, offering decentralized opportunities for capture and utilization. Current studies highlight that integration with carbon capture remains at early development stages (TRL 3–4) and faces high-cost and scale-up challenges[11].
- Bioethanol fermentation provides nearly pure CO_2, representing the global benchmark for lowest-cost capture (25-35 USD/tCO_2[5]).
  -

Flue gas quality

Regardless of sector, contaminants such as SO_x, NO_x, and acid gases must be removed upstream, and humidity carefully managed, to protect sorbent performance and ensure long service life.

Overall perspective

The most favorable opportunities lie in sectors with ≥10% CO_2 concentration and access to low-grade heat, particularly waste incineration and biogas upgrading. Power, steel, and chemicals remain technically feasible but involve higher costs. By matching the process configuration to site conditions, the technology can be flexibly deployed across Switzerland's industrial landscape, with companies such as Satom, Enevi, Alpiq, Swiss Steel, Lonza, and Syngenta representing early candidates for implementation.

6.3.4. IP protection and licensing

Safeguarding the intellectual property generated in this project will be a crucial step in preparing the technology for industrial deployment. The primary focus of IP protection will be on the synthesis, amine impregnation methods used to develop sorbents, modification strategies used to enhance adsorption capacity, recyclability, and scalability, and structuring methods that which eases the handling.

A dedicated licensing framework will be established to ensure that technology transfer to industry is carried out in a controlled and strategic manner. The framework will define rights related to manufacturing, operational use, and geographical application, while ensuring broad dissemination to maximize impact. Within EPFL, the Technology Transfer Office (TTO) will managing this process, drawing on its experience in structuring agreements and supporting commercialization pathways.

In parallel, collaboration with engineering partners will allow the validation of protected processes under real operating conditions, ensuring that licensed technologies are not only protected on paper but also proven in practice. This combination of strong IP protection and targeted licensing will create a clear pathway from laboratory innovation to industrial adoption, while also strengthening the position of the technology in global CO_2 capture markets.

6.3.5. Remaining technical challenges

Although substantial progress has been made in under this project, there are obstacles that must be resolved before the technology can move from pilot demonstrations to full scale deployment.

A first challenge lies in **material scalability and cost**. Zeolite 13X is already produced at industrial volumes, but its cost effectiveness depends strongly on shaping and structuring methods that preserve adsorption capacity and the need to scrub water out of the flue gas, which reduces performance otherwise. Unlike zeolites, MOF-amine and silica-amine based sorbents, reliable production beyond laboratory scale has not yet been demonstrated. How these materials will perform, both technically and economically, when manufactured at tonne scale remains uncertain.

A second challenge concerns **energy efficiency and capture cost**. Modeling has shown that capture costs are highly dependent on waste heat availability. For municipal solid waste incineration, TVSA can achieve around 50 CHF per tonne when waste heat fully meets desorption requirements, about 72 CHF per tonne when only 30 percent waste heat is available, and above 100 CHF per tonne when no waste heat is integrated. Such sensitivity makes facilities without sufficient heat integration particularly challenging for cost effective operation.

A third challenge is the **environmental footprint** of adsorbent materials. Zeolite 13X performs well in TVSA configurations, with capture efficiencies close to 90 percent. By contrast, MOF based systems are still dominated by energy and solvent intensive synthesis steps, which account for the majority of their environmental burden. Although LCA studies indicate that major improvements are possible, whether these can be reproduced at scale remains unresolved.

Durability and impurity resistance represent further hurdles. Zeolite 13X shows stability in clean, dry gas mixtures but suffers performance losses in the presence of humidity or acid gases such as SO_x and NO_x. MOF composites meanwhile have not yet been systematically tested for long term stability under real flue gas conditions. Laboratory studies indicate that improvements are possible, but reproducibility at industrial scale remains to be proven.

Finally, **system integration and retrofitting** remain to be validated. Industrial facilities differ widely in flue gas composition, operating conditions, and waste heat availability. While pilot tests demonstrate technical feasibility, it has not yet been shown that capture units can be reliably retrofitted into diverse industrial processes without disrupting core operations.

Together, these issues highlight the most important technical barriers that must be overcome before the technology can achieve industrial readiness.

6.3.6. Required research and development activities

The transition from laboratory breakthroughs to market-ready CO_2 capture technologies requires a coordinated series of research and development steps. Building on the progress achieved in Year 3, the following activities define the critical path forward.

Material scaling and structuring

1) Develop tonne-scale production routes for advanced sorbents such as MOF amine composites (Cr-MOF–TEPA–TMPTE) and amine-appended silicas (KIT-6/PEI).
2) Refine shaping methods to ensure mechanical strength without compromising adsorption capacity.
3) Adapt MOF and silica synthesis protocols for larger batch reactors, incorporating solvent recovery and energy-efficient drying.
4) Validate reproducibility and quality at industrial scale in collaboration with material suppliers such as Zeochem, BASF, and Clariant.

-

Process optimization and modeling

1) Understand how best to handle water present in systems containing zeolites to gain more accurate estimates of energy and cost of capture.
2) Extend validated TSA and TVSA models to multi-column industrial geometries.
3) Investigate PSA and PVSA as alternative routes for facilities with limited or no waste-heat integration.
4) Develop process-specific models for MOF composites, capturing their unique adsorption–desorption behavior, energy penalties, and humidity sensitivity.

5) Integrate TEA and LCA metrics into modeling to identify the most sustainable and cost-effective process configurations.
6) Engage engineering partners to provide industrial design expertise and validate model outcomes.

-

Pilot-to-demonstration scale-up

1) Construct demonstration units capable of treating tens to hundreds of Nm^3/h of flue gas under continuous operation.
2) Deploy first at waste incineration plants (e.g. Satom in Monthey, enevi in Sion), where 10-15 percent CO_2 flue gas and waste-heat availability provide favorable conditions.
3) Use extended demonstration campaigns to generate operational data for validation of TEA and LCA.
4) Expand to more sites such as natural gas combined-cycle plants (e.g. Alpiq) and steel furnaces (e.g. Swiss Steel Group), enabling application to other sectors.

-

Integrate environmental and economic assessments

1) Combine operational data from demonstration units with updated TEA and LCA to confirm that capture costs can remain competitive (below 60–70 CHF per tonne where waste heat is available).
2) Quantify the impact of MOF process improvements such as solvent recovery and air drying, which can reduce material footprints by up to 80 percent.
3) Benchmark performance directly against amine scrubbing to position sorbent-based capture relative to the commercial state of the art.

Durability and impurity resistance

1) Conduct long-term testing of sorbents over more than 1,000 cycles under real flue gas conditions.
2) Assess the long-term stability of zeolite 13X and MOF composites under humid and impure flue gas conditions, including exposure to SO_x, NO_x, and water vapor.
3) Define the pre-treatment requirements or develop improved formulations needed to ensure sorbent lifetimes of multiple years in industrial operation.

Together, the current system has reached TRL 5-6, corresponding to pilot-scale validation in a relevant environment. Over the next five years, the objective is to advance to TRL 7 through a fully integrated prototype demonstration at an industrial site, such as a municipal solid waste incinerator or biogas plant, achieving > 1,000 stable adsorption-desorption cycles and a specific capture cost below 60-70 CHF t^{-1} CO_2 when utilizing available waste heat.

In the following phase (5-10 years), efforts will focus on reaching TRL 8-9, targeting full-scale deployment and commercial licensing. Key gating steps toward a near 1:1 industrial separation unit include:

i). verifying long-term sorbent durability beyond 1,000 cycles;

ii). confirming cost competitiveness (< 60-70 CHF t^{-1} CO_2 with waste-heat recovery);

iii). validating seamless integration under real industrial flue-gas conditions.

Industrial participation will scale progressively with these milestones: materials suppliers ensure reproducible sorbent manufacturing, utility operators provide authentic flue-gas environments for pilot validation, and infrastructure partners enable downstream integration with compression, transport, and storage or utilization networks.

6.3.7. Validation by industrial partners

Validation of the technology by industrial partners is a critical step in ensuring its practical relevance and accelerating the pathway to market. Independent benchmarking of the capture process against industry standards, together with real-world simulations and field trials, will confirm whether performance targets derived from laboratory and pilot studies can be met under operating conditions. Industrial partners including engineering firms, utilities, waste incineration operators, and chemical producers, will play a central role in hosting demonstration units, generating operational data, and verifying techno-economic and life-cycle assessments. The feedback loop created through this validation will provide essential insights into cost, energy use, durability, and integration requirements, and will directly inform further optimization of both materials and processes.

Taken together, this validation phase ensures that the roadmap extends beyond pilot-scale demonstration to industrially credible deployment. By aligning technical progress with market requirements, the CO_2 capture technology will be positioned as a sustainable and economically viable solution for emission reductions across multiple hard-to-abate sectors.

6.3.8. References

1. CCS on Waste to Energy. *IEAGHG* https://ieaghg.org/publications/ccs-on-waste-to-energy/.
2. U.S. Department of Energy, National Energy Technology Laboratory. *9.2 Carbon Dioxide Capture Approaches*. Retrieved from https://netl.doe.gov/research/carbon-management/energy-systems/gasification/gasifipedia/capture-approaches
3. Ecole polytechnique fédérale de Lausanne. *From Lab to Market – Technology Transfer Office*. Retrieved from https://www.epfl.ch/research/technology-transfer/
4. Thambimuthu K., Soltanieh M., Abanades J.C. (2005). "Capture of CO_2."In: IPCC Special Report on Carbon Dioxide Capture and Storage (SRCCS), Chapter 3, pp. 105–178. Intergovernmental Panel on Climate Change, Cambridge University Press, Cambridge and New York. ISBN 92-9169-119-4.
5. Baylin-Stern A., Berghout N., "Is carbon capture too expensive?", International Energy Agency, February 17 2021. Available at: https://www.iea.org/commentaries/is-carbon-capture-too-expensive
6. Du, Y., Gao, T., Rochelle, G. T. & Bhown, A. S. Zero- and negative-emissions fossil-fired power plants using CO2 capture by conventional aqueous amines. *International Journal of Greenhouse Gas Control* **111**, 103473 (2021).
7. Sher, F. *et al.* Bioenergy with carbon capture and storage technology to achieve net zero emissions–A review. *Renewable and Sustainable Energy Reviews* **210**, 115229 (2025).

8. Yun, S., Jang, M.-G. & Kim, J.-K. Techno-economic assessment and comparison of absorption and membrane CO2 capture processes for iron and steel industry. *Energy* **229**, 120778 (2021).
9. Li, Y. *et al.* Composition and Toxicity of Biogas Produced from Different Feedstocks in California. *Environ Sci Technol* **53**, 11569–11579 (2019).
10. International Energy Agency, *Assessing the Sustainable Potential and Cost of Feedstocks for Biogas and Biomethane*, in *Outlook for Biogas and Biomethane: Prospects for Organic Growth*, 2020. Available at: https://www.iea.org/reports/outlook-for-biogas-and-biomethane/assessing-the-sustainable-potential-and-cost-of-feedstocks-for-biogas-and-biomethane
11. Zhou, R., Ren, Y., Jiang, C. & Lu, Q. Wastewater as a resource for carbon capture: A comprehensive overview and perspective. *Journal of Environmental Management* **377**, 124608 (2025).